

Annual Report 2021

MLZ is a cooperation between:

Bavarian State Ministry of
Science and the Arts



SPONSORED BY THE



Federal Ministry
of Education
and Research

The Heinz Maier-Leibnitz Zentrum (MLZ):

The Heinz Maier-Leibnitz Zentrum is a leading centre for cutting-edge research with neutrons and positrons. Operating as a user facility, the MLZ offers a unique suite of high-performance neutron scattering instruments. This cooperation involves the Technische Universität München, the Forschungszentrum Jülich GmbH and the Helmholtz-Zentrum hereon GmbH. The MLZ is funded by the German Federal Ministry of Education and Research, together with the Bavarian State Ministry of Science and the Arts and the partners of the cooperation.

The Forschungs-Neutronenquelle Heinz-Maier-Leibnitz (FRM II):

The Forschungs-Neutronenquelle Heinz-Maier-Leibnitz provides neutron beams for the scientific experiments at the MLZ. The FRM II is operated by the Technische Universität München and is funded by the Bavarian State Ministry of Science and the Arts.

Joint Annual Report 2021
of the MLZ and FRM II

208
science-
related
media
articles



360
scientific
journal
articles

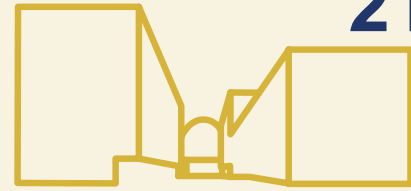
467



posts in
social media

57

news
articles
on the
web pages



2180 m²
of new
space

255
people
moved
in total



3500
moving
boxes
required



PUBLICATIONS AND COMMUNICATION

WORKING SPACE AT THE MLZ AREA

2021 IN NUMBERS

SCIENTIFIC EVENTS

EVENTS FOR THE PUBLIC

211
participants
at the MLZ
Conference



„Neutrons for
Life Sciences“



374

participants
at the MLZ
User Meeting



46

participants
at the
Heraeus-Seminar

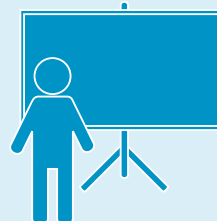


70 children at
the „Open-
Door-Day with
the Mouse“



807
visitors

despite challenges due to
COVID 19 pandemic



200

live-stream-viewers
at the „Science for
Everyone“ lecture
(by Deutsches Museum)

Mission restart 7

Scientific Highlights

Engineered disorder	10
A charged topic: batteries under observation	11
Positrons detect defects in solar cell material	12
What happens to mRNA therapeutics in the body?	13
To the tumor via magnets	14
Dancing on dry land: how proteins stay active without water	15
Revolution in imaging using neutrons	16
50-year-old physics mystery unraveled	17
Breakthrough in magnonics?	18
The signature of the ideal glass	19

Industry & Medicine

Neutrons “see” internal stresses in components from 3D printing	22
Pressure and heat: testing alloys for gas turbines	23
Conjuring colors out of cylinders	24
Using antimatter to improve wastewater cleaning	25
Strong weld joints for aerospace applications	26
Neutrons detect clogs in pipelines	27
Coping with fouling in drinking water production	28
Optimization of mRNA containing nanoparticles	29
A better understanding of multiple sclerosis	30
Making the gray cells happy	31

Scientific Reports

Materials Science	34
Quantum Phenomena	42
Soft Matter	49
Structure Research	61
Neutron Methods	69

Reactor & Development

No neutrons delivered, but challenging tasks completed	78
Update from reactor physics: progress towards conversion	80

Facts & Figures

The year in pictures	84
Workshops, Conferences and Schools	91
Science in place of crisis	92
Another virtual year at the User Office	94
Organization, Staff and Budget	96
Publications & Theses	100
Cover pages	102
Committees	103
Partner institutions	108
Imprint	112



Mission restart

If you are wondering what a neutron source without neutrons can possibly do, you will be surprised to learn just how busy it can get. And so it was in 2021.

Originally, the plan was to restart the reactor in early 2021, but we unfortunately faced a technical issue with the cold source of the FRM II during the restart. Careful analysis showed that the in-pile part of the cold source would have to be removed, which was successfully accomplished by the end of 2021, and replaced with a new one. Bad luck struck again soon afterwards, when a tiny leak was detected on the light water side of the central channel. The only remedy: Exchange it for a new one (see page 78).

After restarting the FRM II without the cold source - the new one will still be at the manufacturing stage - the neutron spectrum available at the MLZ will be shifted towards thermal and hot neutrons. However, most of the instruments normally optimized for cold neutrons will even be able to measure using thermal neutrons, as detailed simulations of the flux show. Thus, we are on the path back to a user operation with the MLZ's full neutron and instrument portfolio.

Meanwhile, the instrument scientists are not only preparing for the "thermal intermezzo", but have also refurbished their instruments, invented new services and can offer remote access during an ongoing pandemic. Robotic arms, deuteration services and new sample environments or improved software are only a few examples highlighting the diversity and versatility of the MLZ's services.

Also, on the peripheries of the reactor, the MLZ staff have been busy preparing for the advent of neutrons. In the neutron guide hall east, construction is progressing. A prominent example of newly installed instrumentation is the 12 meter long magnet for the experiment PERC, which was transported via three cranes into the guide hall (see photo on the left).

Large funding projects assure the future of neutron science and the smooth exchange of data. The German Research Foundation (DFG) will support the project "DATA from PHoton and Neutron Experiments" (DAPHNE4NFDI) for five years as part of the National Research Data Infrastructure to make research data more accessible and sustainable. The three MLZ partners, Technical University of Munich, Forschungszentrum Jülich and Helmholtz-Zentrum Hereon, are responsible for networking, training and public relations within the consortium.

The Heinz Maier-Leibnitz Zentrum will receive € 3.3 million of funding for the Global Neutron Scientists (GNeuS) program. The project, funded by the European Union within Marie Skłodowska-Curie Actions, offers 45 fellowships to train a new generation of high-caliber neutron researchers.

One big achievement in 2021, for which the MLZ is very thankful, is the prolongation of the cooperation agreement. The German Federal Ministry for Education and Research will continue to fund the cooperation partners of the MLZ for the next five years.

Furthermore, there is good news concerning fuel enrichment. The Federal and State Ministries of Science have agreed on a new timeline to convert to lower enrichment of U-235 in the fuel element: 2023 will be the year to decide on one out of three fuel types, which will make it possible to run the neutron source below 50% U-235.

On a personal note, we would like to welcome Prof. Dr. Martin Müller, head of the Institute of Materials Physics at Helmholtz-Zentrum Hereon. He succeeds Prof. Dr. Stephan Förster, whom we wish to thank for his three-year term as MLZ director. Now, Martin Müller represents the Helmholtz partners Forschungszentrum Jülich and Hereon on the Scientific Directorate of the MLZ.

We are all looking forward to welcoming back users for the first reactor cycle after this long shut-down. This is our mission.



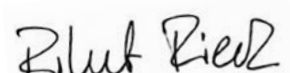
Peter Müller-Buschbaum



Martin Müller



Axel Pichlmaier

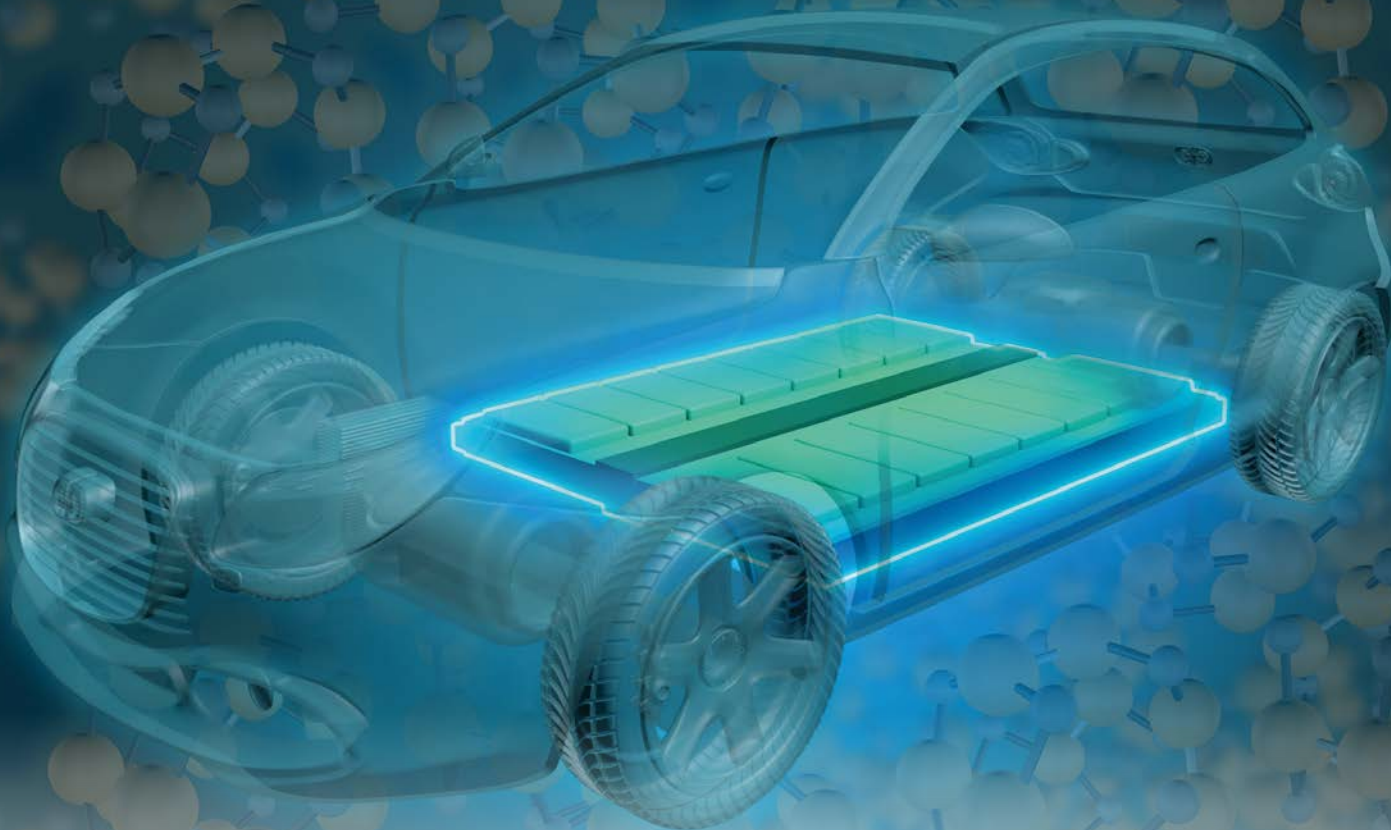


Robert Rieck



Scientific Highlights





ENGINEERED DISORDER

New solid-state batteries promise to deliver higher energy than their conventionally used counterparts that feature liquid electrolytes. A study involving neutrons at the MLZ proposes engineering a solid electrolyte – a core component of this type of battery – without changing the composition of the material itself.

Recently, lithium thiophosphates as a material for solid-state batteries have gained attention since they are mechanically soft and thus easy to process. They exhibit high ionic conductivity, which means that the lithium exchange and transfer are promoted in such systems.

Jumping between lithium cages

Their ionic conductivity is highly influenced by the structural disorder of anions. However, it is not entirely clear if and how this affects the distribution of lithium and how it relates to transport, which is critical for improving conductivity. The site disorder increases with temperature and can be frozen in. Previous studies on this phenomenon involved changes in chemical composition, which could also have influenced the structure. New quenching techniques have made it possible to decouple chemical makeup and site-disorder.

Researchers used neutron diffraction on the newly engineered material at the MLZ to show that the phenomenon

of site disorder affects the lithium subsystem. “The positively charged lithium ions jump between so-called cages of clustered lithium ions. When disordered, the jump distances decrease, expansion creates more way for Li diffusion and increases ionic conductivity”, explains Dr. Anatoliy Senyshyn, instrument scientist at the MLZ powder diffractometer SPODI.

Higher disorder increases conductivity

The changing local charges affect the lithium distribution. The higher the site-disorder, the more spatially lithium is distributed and the shorter the distances between the positively charged lithium ions. This can lead to a fourfold increase in ionic conductivity. And higher conductivity means improved performance, lower internal resistance and less operational stress over the entire battery.

*A. Gautam, M. Sadowski, M. Ghidui, N. Minafra, A. Senyshyn, K. Albe, W. G. Zeier, Engineering the Site-Disorder and Lithium Distribution in the Lithium Superionic Argyrodite $\text{Li}_6\text{PS}_5\text{Br}$, Adv. Energy Mater., 11, 2003369 (2021)
DOI: 10.1002/aenm.202003369*

The experiments were carried out at SPODI.

A CHARGED TOPIC: BATTERIES UNDER OBSERVATION

Batteries are getting smaller, cheaper, and more powerful. To achieve this, researchers at the Heinz Maier-Leibnitz Zentrum took a close look inside a battery, both while it was charged and discharged.

Who has not experienced it? 20 minutes before leaving, one realizes that the cell phone battery is almost empty and hopes to charge it at the last minute. The fast charging of lithium-ion batteries is becoming crucial, even more so for e-mobility.

What happens during charging?

Researchers at the MLZ attempted to tackle the problem using neutron scattering. The inner structure of a battery and how lithium and electrolytes are distributed is well known for the end states, when the battery is charged or discharged. However, the researchers went one step further and for the first time visualized the lithium distribution in the graphite anode of a running high-power battery during charging and discharging. As the battery is charging, lithium is extracted from the cathode and intercalated into the anode; the reverse happens upon discharging. The scientists saw that the lithium is heterogeneously distributed throughout the entire cycling process. This is attributed to an uneven load of the battery components due to a non-uniform current distribution.

The researchers' major advance was to capture lithium inhomogeneities in the battery at a higher resolution. In the neutron experiment, they achieved a millimeter-sized spatial resolution. Further measurements with synchrotron radiation achieved a spatial resolution down to micrometer.

Charging time vs. driving range

In the longer perspective, the control and optimization of lithium gradients in high-power batteries is crucial for developing fast charging for e-cars. Car acceleration is directly linked to a high power density. On the other hand, a high energy density ensures a long driving range. According to Dr. Anatoliy Senyshyn, instrument scientist at SPODI, "these requirements are antagonists. But if we can get a handle on lithium distribution, we can significantly improve battery performance." And then it will be possible to charge the cell phone shortly before an appointment!

*D. Petz, M. J. Mühlbauer, V. Baran, A. Schökel, V. Kochetov, M. Hofmann, V. Dyadkin, P. Staron, G. Vaughan, U. Lienert, P. Müller-Buschbaum, A. Senyshyn, Lithium distribution and transfer in high-power 18650-type Li-ion cells at multiple length scales, Energy Storage Mater., 41, 546 (2021)
DOI: 10.1016/j.ensm.2021.06.028*

The experiments were carried out at STRESS-SPEC and SPODI.



POSITRONS DETECT DEFECTS IN SOLAR CELL MATERIAL

How can the efficiency of photovoltaic plants be increased? Positron lifetime studies helped to understand new solar cell material and characterize defects.

Metal halide perovskites facilitate a new photovoltaic solar cell technology: They show a high absorption coefficient, are cheap to produce and simple to manufacture. In addition, they have the potential to achieve higher efficiencies than silicon-based solar cells.

Defects in crystals influence performance

However, researchers are still trying to understand why the photovoltaic conversion of metal halide perovskites is so high. Atomic scale point defects in the crystal structure normally reduce the efficiency of solar photovoltaic devices. Therefore, it is necessary to identify and confirm different defect types, in order to design manufacturing processes for optimum performance.

Until recently, researchers have only been able to gain insight into the probable point defects using theoretical calculations alone. Now, British and Swedish have performed positron annihilation lifetime spectroscopy at the MLZ's positron source NEPOMUC to detect these defects and identify respective defect types and their probable charge states.

Positrons provide information on type of defect

Positrons annihilate with electrons after implantation, which leads to the emission of radiation after a certain time. Dr. Marcel Dickmann of the Universität der Bundeswehr München measured this radiation using the Pulsed Low-Energy Positron System (PLEPS) at the MLZ: "We can determine the type and concentration of the defects in the crystal by measuring the positrons' lifetime using the emitted radiation."

Positrons are trapped inside crystal vacancy defects. Since their lifetime is a measure of the local electron density, measuring the time between implantation and annihilation can be used to characterize specific vacancy defect types. Using a pulsed, monoenergetic beam, positron lifetime measurements permit the depth-profiling of vacancy-related defects from the near-surface down to depths of a few micrometers. Theoretical calculations of positron lifetimes were compared to measurements and enabled the missing atom site to be identified.

D. J. Keeble, J. Wiktor, S. K. Pathak, L. J. Phillips, M. Dickmann, K. Durose, H. J. Snaith, W. Egger, Identification of lead vacancy defects in lead halide perovskites, Nat. Commun. 12, 5566 (2021)

DOI: 10.1038/s41467-021-25937-1

The experiments were carried out at the instrument PLEPS of the NEPOMUC positron source.

WHAT HAPPENS TO mRNA THERAPEUTICS IN THE BODY?

International researchers led by the Malmö University collaborated with the global biopharmaceutical company AstraZeneca to understand how mRNA is transported and released once administered into the bloodstream.

Messenger RNA (mRNA) is the blueprint for the production of proteins that a cell can read and implement. Researchers want to make use of this principle in the form of mRNA therapeutics, with mRNA that specifically contains the blueprint for the required proteins. It has many potential applications, from vaccines and cancer to chronic diseases such as heart failure.

Test under real conditions

For their work, the researchers investigated how the mRNA-containing lipid nanoparticles (LNPs) bind to proteins in a patient's blood in a model system, how they are transported to the right place and how they release the mRNA there. The focus was set on apolipoprotein E as the binding partner.

To investigate the exact structure of the LNPs and the distribution of the individual components in the complex, the scientists used the small-angle scattering instrument KWS-2. The environment of the LNP's closely resembled that in the human body.

Neutrons make interfering lipids invisible

The LNPs consist of three different fat molecules in different proportions. They all have different scattering properties. By deliberately exchanging hydrogen atoms for heavier deuteri-

um atoms in individual fats, the researchers made them invisible. They thus saw exactly where the individual molecules were located in the structure.

They found that the structure of the LNPs changes significantly as soon as they bind to apolipoprotein E in the blood. This leads to a redistribution of the lipid molecules on the surface and in the nucleus, which in turn influences the properties of the LNPs, for example how easily they can release the bound mRNA again.

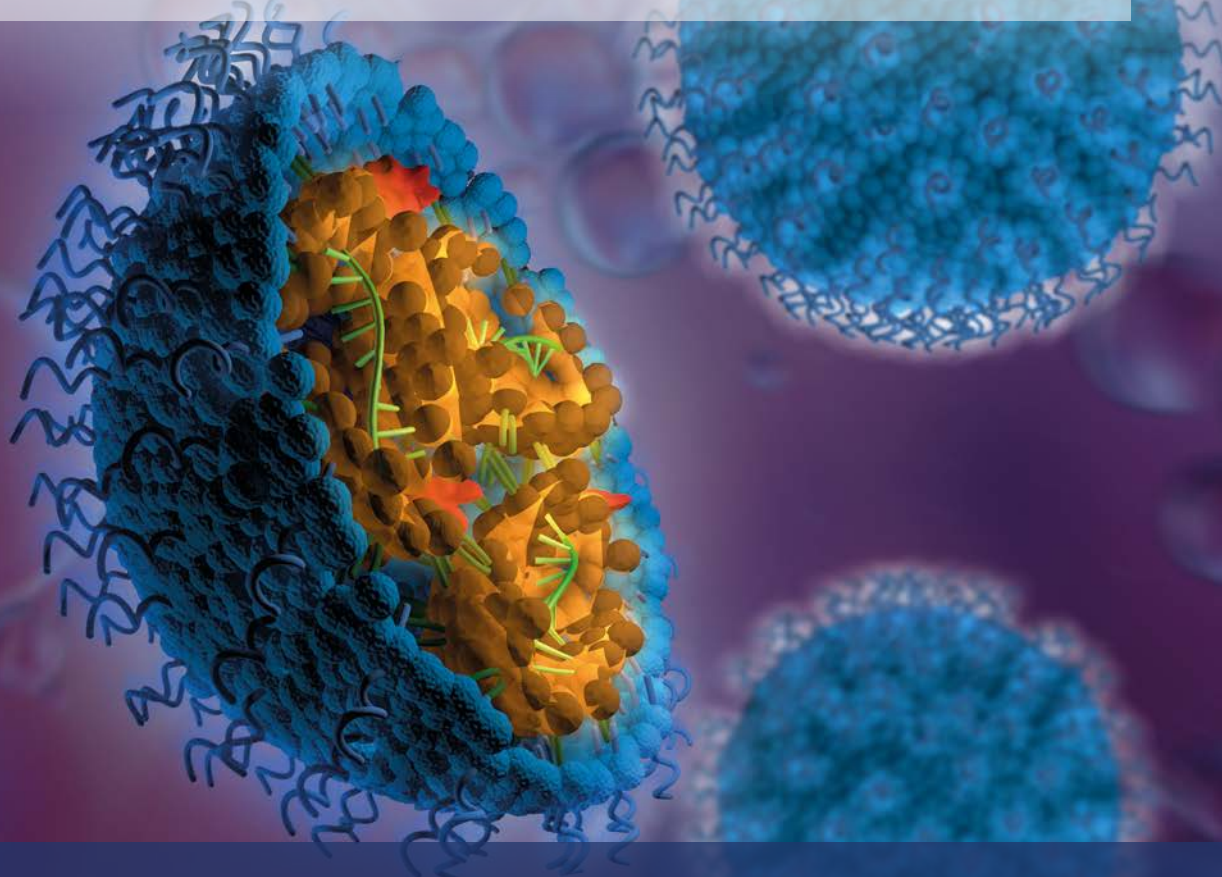
More precise drug design possible

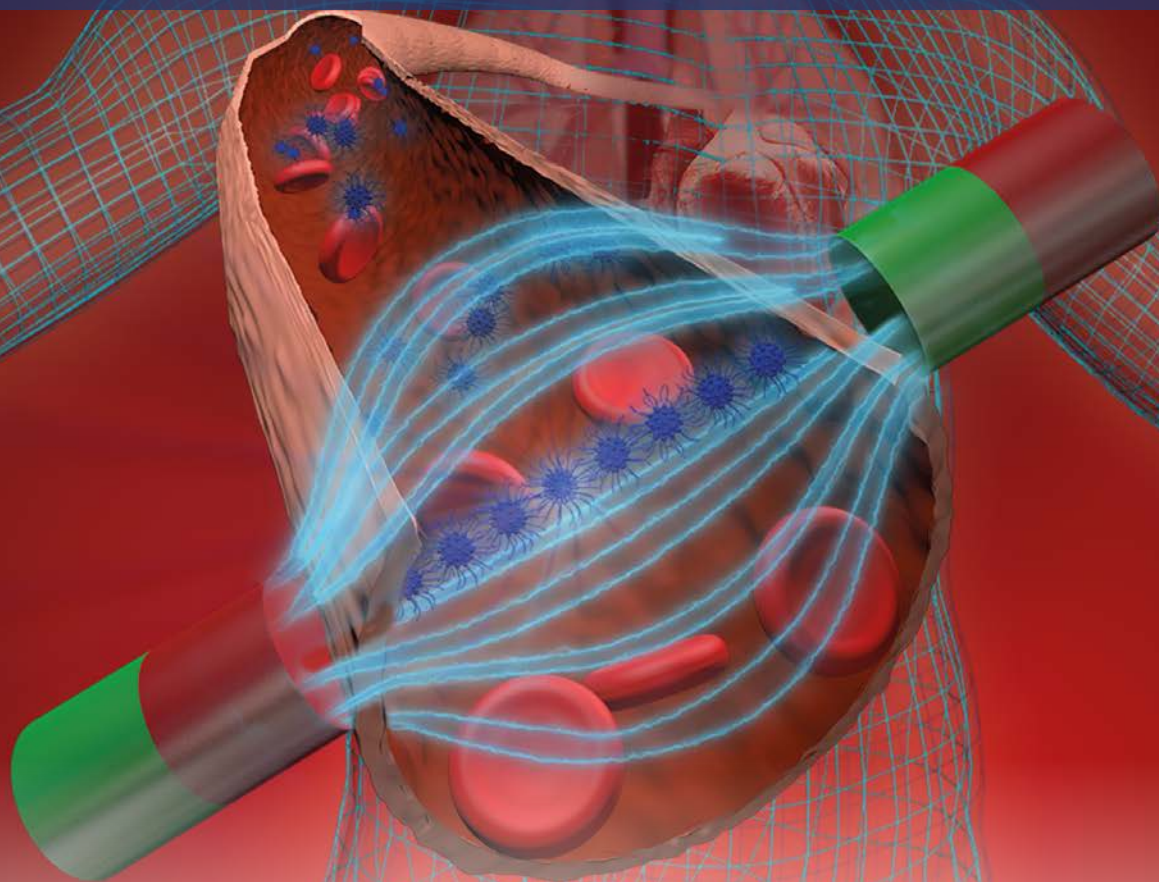
The results have the potential to optimize the development of mRNA therapeutics. For example, it is now known that some of the LNPs are initially bound tightly in the liver. Knowing what proportion of the mRNA eventually reaches the target cells of the therapy will make the fate of the mRNA-LNPs in the body clearer.

F. Sebastiani, M. Yanez Arteta, M. Lerche, L. Porcar, C. Lang, R.A. Bragg, C. S. Elmore, V.R. Krishnamurthy, R. A. Russell, T. Darvish, H. Pichler, S. Waldie, M. Moulin, M. Haertlein, V. T. Forsyth, L. Lindfors, M. Cárdenas, Apolipoprotein E binding drives structural and compositional rearrangement of mRNA-containing lipid nanoparticles, ACS Nano, 15, 6709 (2021)

DOI: 10.1021/acsnano.0c10064

The experiments were carried out at KWS-2.





TO THE TUMOR VIA MAGNETS

Biocompatible iron oxide nanoparticles (IONPs) offer great potential for biomedical applications. Rapid progress in researching IONPs now looks promising thanks to a new method combination developed by a team at the Forschungszentrum Jülich using neutrons at the MLZ.

Killing cancer cells without side effects

Magnetic nanoparticles could be used as therapeutics in tumor tissues: Magnetic particles are able to kill cancer cells if they are set rotating using magnetic fields, thus generating heat. If transported to specific sites in the body, they can release active substances precisely where they are needed, again activated by magnetic fields. Both methods can keep side effects to a minimum due to accurate targeting.

Chains move better in blood vessels

One challenge in medical applications is the transport of the particles to the location. One option is to manoeuvre the nanoparticles using a magnetic field. Aggregates of the particles are better suited for this than individual nanoparticles because their magnetic moment is greater, which means they can be controlled by smaller magnetic fields. At the same time, thread-like aggregates can move more easily through long, thin blood vessels.

The nanoparticles can self-assemble into thread-like chains when conditions are suitable. If there is no spatial boundary acting on the particles, certain parameters such as the strength of the applied magnetic field determine the

self-organization. However, current methods of visualizing the chains in real space are somewhat limited to the area of analysis and cannot directly map the position of chains in a solvent carrier.

Neutrons make the nanoparticles visible

Now researchers present a new approach that makes the chains and their formation directly visible in the solvent without spatial limitation. To do this, they combined experimental studies using small-angle neutron scattering at the instrument KWS-1 with simulations. Small-angle scattering enables high-resolution structural analysis of IONPs dispersed in an environment suitable for biomedical applications. Simulation of this data provides a method to directly image chains in real space and their evolution with an applied magnetic field.

N. Nandakumaran, L. Barnsley, A. Feoktystov, S. A. Ivanov, D. L. Huber, L. S. Fruhner, V. Leffler, S. Ehlert, E. Kentzinger, A. Qdemat, T. Bhatnagar-Schöffmann, U. Rücker, M. T. Wharmby, A. Cervellino, R. E. Dunin-Borkowski, T. Brückel, M. Feygenson, Unravelling Magnetic Nanochain Formation in Dispersion for In Vivo Applications, Adv. Mater. 33, 2008683 (2021)

DOI: 10.1002/adma.202008683

The experiments were carried out at KWS-1.

DANCING ON DRY LAND: HOW PROTEINS STAY ACTIVE WITHOUT WATER

Taking a close look with the aid of neutrons, researchers have observed that proteins can also perform their function without water. They have shown how the oxygen-transporting muscle protein myoglobin moves in that case.

It used to be an unwritten law that proteins need water. Without the liquid element as a lubricant, they cannot move, and thus cannot become active, according to this doctrine. However, in 2010 researchers found that multichain molecules, known as polymers, also breathe life into proteins. This is interesting for applications in medicine and cosmetics.

Film in picosecond resolution

Now, an international team of researchers led by Dr. Martin Weik of the University of Grenoble, France, have used neutrons at the MLZ to see exactly how proteins with polymers move as compared to in an aqueous solution. For measurements on the protein myoglobin, they followed the movements of the myoglobin and polymers, which are distinctly labeled, down to a time scale of picoseconds. That is because neutrons reveal the motion of hydrogen atoms more clearly than those of the heavier deuterium, which is used as a marker. The team also measured high-resolution spectra to observe various motion processes directly at the molecular level.

Polymer mimics movement of water

“With the results, we make a concrete suggestion on what to improve in the polymer to make the protein even more

active,” says Martin Weik. “Surprisingly, we found that the polymer mimics the movements of water.” This keeps the dry protein biologically active, but certain movements are suppressed. This helps the researchers explain why the protein is less active when the water is replaced by polymers. With a little fine-tuning, however, it is possible to make the protein more active.

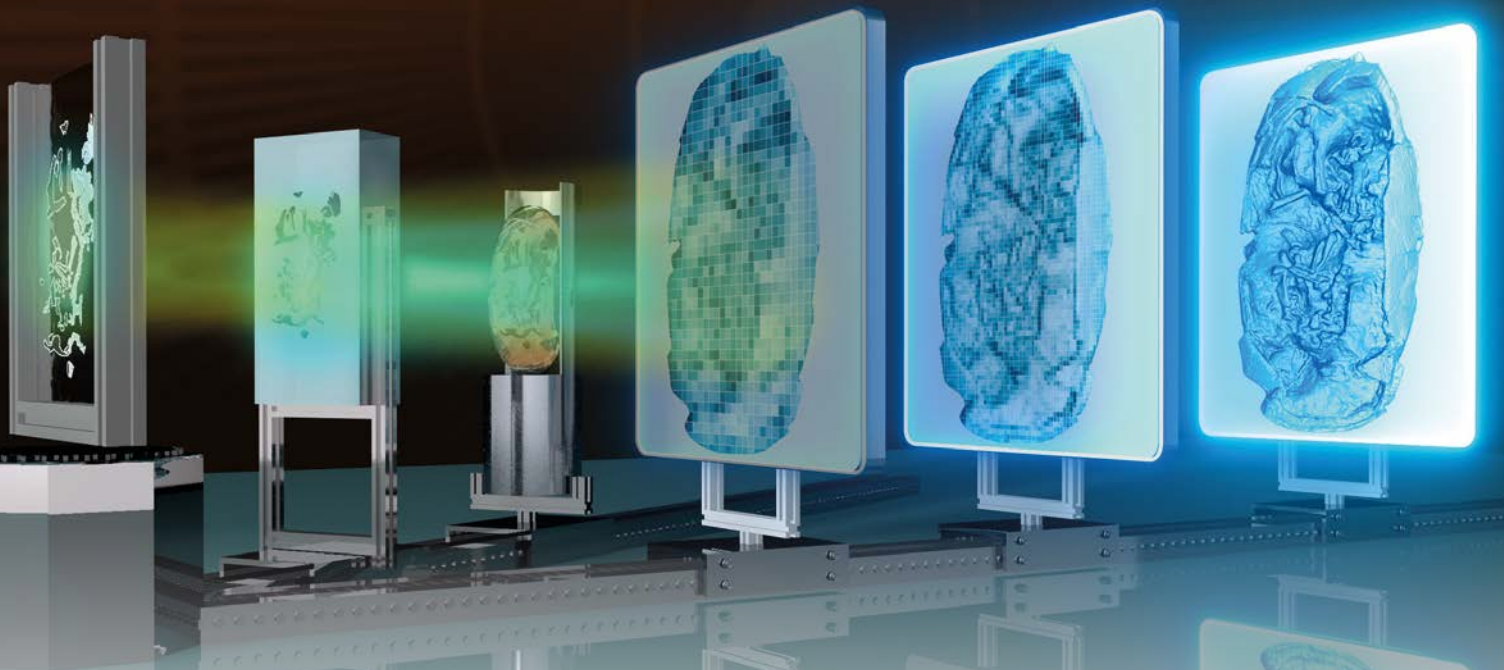
Heart patients benefit

This new insight is useful for the development of next-generation cell therapies for treating cancer or regeneration after heart attacks. The aim of the scientists is to use protein-polymer hybrids in cell therapies, e.g., to help heart attack patients recover by regenerating healthy heart tissue. The advantage of the waterless protein-polymer compounds is that they prolong the survival of the patient and promote the settlement of the transplanted cells.

G. Schirò, Y. Fichou, A. P. S. Brogan, R. Sessions, W. Lohstroh, M. Zamponi, G. J. Schneider, F.-X. Gallat, A. Paciaroni, D. J. Tobias, A. Perriman, M. Weik, Diffusive-like motions in a solvent free protein-polymer hybrid, Phys. Rev. Lett., 126 (2021)

DOI: 10.1103/PhysRevLett.126.088102

The experiments were carried out at SPHERES and TOFTOF.



REVOLUTION IN IMAGING USING NEUTRONS

Researchers have developed a new imaging technology which could not only vastly improve the resolution of neutron measurements, but also reduce the radiation dose for medical X-ray imaging.

Modern cameras still rely on the same principle they used 200 years ago: An image sensor is exposed for a period of time. Any desired, but also undesired, contributions to the image are recorded. For long exposure times, this can produce high levels of noise.

The new imaging method of Dr. Adrian Losko of the Technical University of Munich together with colleagues measures individual photons on a time-resolved and spatially-resolved basis. This makes it possible to separate neutrons from noise, reducing the unwanted contributions in radiographs.

Measuring individual photons

Neutron researchers use scintillators for imaging to detect neutrons, for example in examining fossilized dinosaur specimens. When the scintillator absorbs a neutron, photons are generated which are measured using optical cameras.

Until now, all these cameras have collected light during the entire exposure time, whereby the image sharpness is strongly dependent on the thickness of the scintillator. The new concept detects each individual photon generated by a neutron, making it possible to reconstruct a more precise origin for each individual neutron interaction.

Recording relevant events only

Since the absorption of a neutron in the detector generates many photons, the new system makes use of the coincidence of several photons to determine individual neutrons. "We record only those events which are relevant for the final image", explains Adrian Losko.

The new concept is a dramatic improvement since it already provides three times better spatial resolution and reduces the amount of noise by more than a factor of seven.

Lower radiation dose and more details in hard X-rays

The new system could also help in medicine: When X-raying a broken bone for example. Hairline fractures would be more easily detectable and, at the same time, the patient's exposure to radiation could be reduced.

And perhaps this will also revolutionize everyday cameras: Images made in the dark would be greatly improved and noise could be practically eliminated.

*A. Losko, Y. Han, B. Schillinger, A. Tartaglione, M. Morgano, M. M. Strobl, J. Long, A. Tremsin, M. Schulz, New Perspectives for Neutron Imaging through Advanced Event-Mode Data Acquisition, Sci Rep. 11, 21360 (2021)
DOI: 10.1038/s41598-021-00822-5*

The experiments were carried out at the Paul Scherrer Institute, Switzerland.

50-YEAR-OLD PHYSICS MYSTERY UNRAVELED

More than 50 years ago, researchers discovered a pronounced phase transition in strontium iron oxide. However, what exactly happens during this process at the atomic level has been unclear ever since. Using high-resolution neutron and resonant elastic X-ray measurements, a research team from the Max Planck Institute for Solid State Research has now been able to solve this old mystery.

Phase transitions in solids are phenomena in which order emerges from disorder. Macroscopically, they show up through anomalies, such as a sharp increase in magnetism or a sudden drop in resistance. In strontium iron oxide ($\text{Sr}_3\text{Fe}_2\text{O}_7$), which the scientists studied in more detail, the phase transition was evident in the thermal properties: The specific heat suddenly changes upon cooling.

Mössbauer spectroscopy identified this phase transition 50 years ago. “We wanted to understand what happens at the atomic level,” explains Dr. Thomas Keller, instrument scientist at the TRISP three-axis spin echo spectrometer at the MLZ. Researchers called the phenomenon “hidden order”.

Solution in the checkerboard

“In very simple terms, the iron atoms are normally arranged on a square lattice. These, in turn, are stacked in layers,” says Keller. In the individual square layers, the two valence states of the iron produce a simple checkerboard pattern.

However, the stacking of the successive layers is random. Using uniquely high-resolution Larmor diffraction made it possible to measure the spacing of the atoms and see that they were minimally distorted by charge. The research team combined the MLZ measurements with high-resolution X-ray measurements at the German Electron Synchrotron DESY, which made the stacking visible.

New concepts for data storage

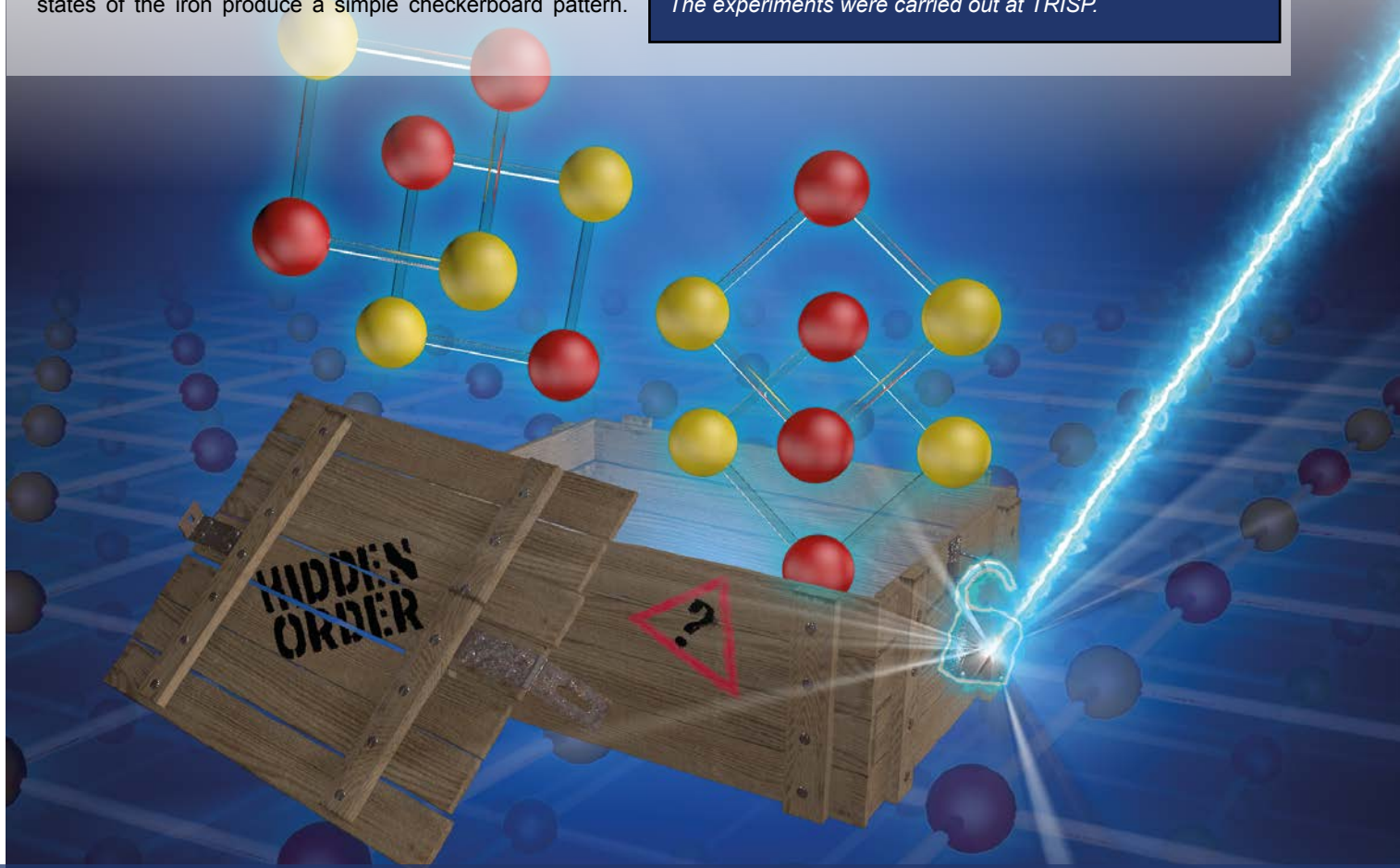
$\text{Sr}_3\text{Fe}_2\text{O}_7$ is a candidate for a new type of data memory called “phase change memory”. If it were possible to manipulate the randomly stacked “checkerboards” of the individual layers and bring the stacking into an order, two “ordered” and “disordered” types of states would result. This can be transferred into the data bits 0 and 1.

A small distortion on the atomic level might therefore have greater future significance.

J.-H. Kim, D. C. Peets, M. Reehuis, P. Adler, A. Maljuk, T. Ritschel, M. C. Allison, J. Geck, J. R. L. Mardegan, P. J. Bereciarua Perez, S. Francoual, A. C. Walters, T. Keller, P. M. Abdala, P. Pattinson, P. Dosanjh, B. Keimer, Hidden Charge Order in an Iron Oxide Square-Lattice Compound, Phys. Rev. Lett. 9, 127 (2021)

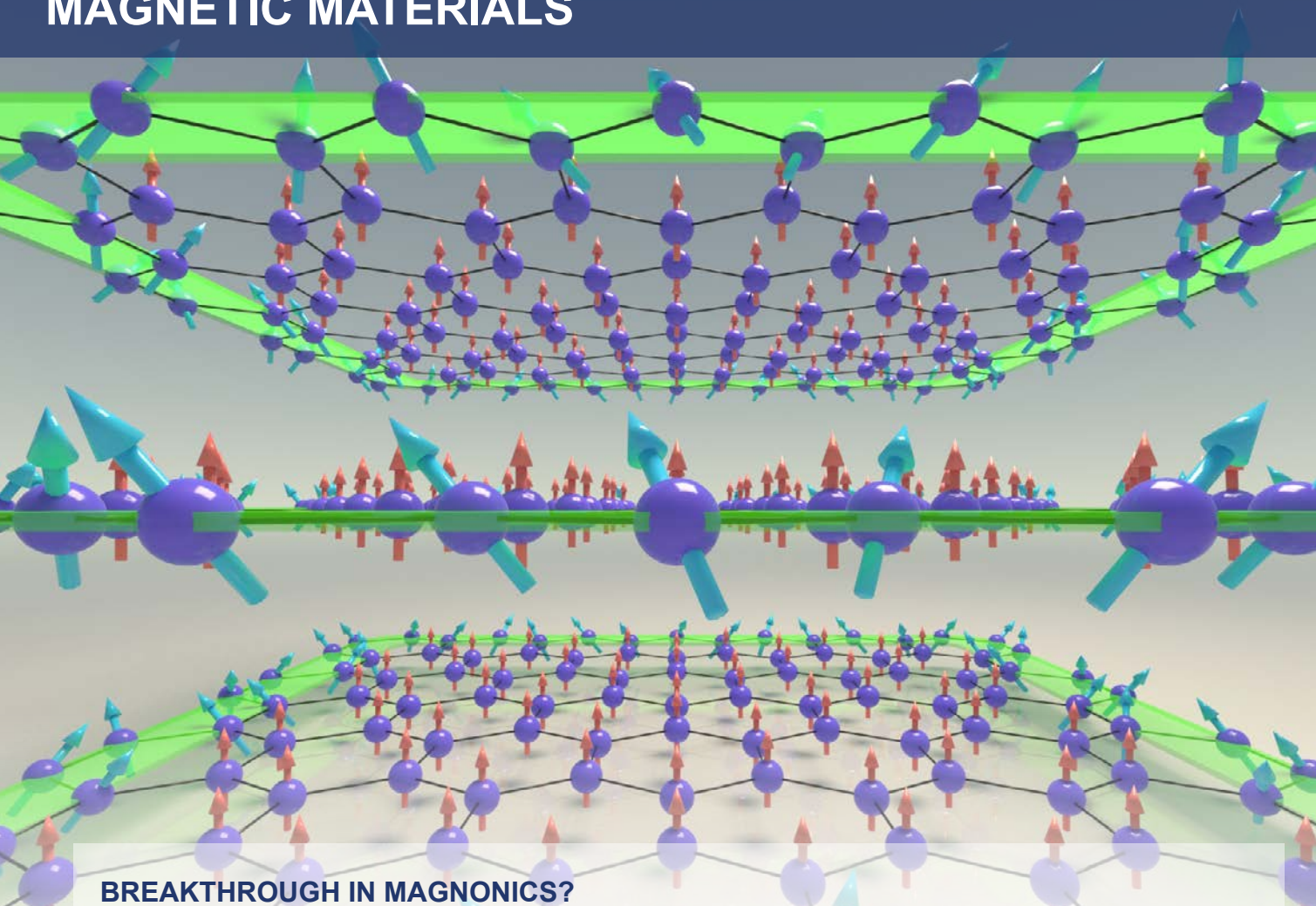
DOI: 10.1103/PhysRevLett.127.097203

The experiments were carried out at TRISP.



MAGNETIC MATERIALS

MAGNETIC MATERIALS



BREAKTHROUGH IN MAGNONICS?

Electronic devices as thin as a sheet of paper, flexible, transparent and with low energy consumption but fast computing power and enormous storage capacity – what was once science fiction is now coming within our grasp. With the so-called “two-dimensional (2D) van der Waals materials”, it is now possible to implement many of the electronic properties that we use in today’s electronic devices, where typically semiconductors and electrical insulators have been used.

Exotic new properties

These 2D quantum materials often manifest properties that the same materials do not exhibit as solid crystals, because quantum mechanical effects cause the electrons to behave in a different way. The name “van der Waals” reflects the fact that, although the atoms within a 2D layer are firmly connected to each other, the chemical bond between layers only occurs via weak, so-called “van der Waals forces”. This differentiates 2D van der Waals materials from other thin-film systems.

Depending on the material composition and the lattice symmetry of the 2D systems, exotic properties can also emerge. Scientists have now demonstrated a completely new property: The materials studied are actually topological insulators for magnons, analogous to the known topological insulators for electric currents that are electrical insulators, but conduct electricity with almost no resistance along their edges. Mag-

nons are collective excitations in magnetic systems whose energy is quantized. They can be thought of as waves that pass through the material, just as a stone thrown into water generates ripples. The magnetic moments in the material remain in place – only their orientation changes.

Ten times less energy consumption

These topologically protected magnonic states are stable against perturbations, and do not involve the dissipation of energy. They can be ideally used for faster switching and more energy-saving devices in future information and quantum technologies. “As no electrical charge has to be transported when transmitting information using magnons, we expect energy consumption to be around ten times lower compared to using modern semiconductor chips. This is why magnonic devices are suitable for integration into mobile IT applications,” explains Prof. Yuriy Mokrousov from the Peter Grünberg Institute.

*F. Zhu, L. Zhang, X. Wang, F. José dos Santos, J. Song, T. Mueller, K. Schmalzl, W. F. Schmidt, A. Ivanov, J. T. Park, J. Xu, J. Ma, S. Lounis, S. Blügel, Y. Mokrousov, Y. Su, T. Brückel, Topological magnon insulators in two-dimensional van der Waals ferromagnets CrSiTe₃ and CrGeTe₃: Toward intrinsic gap-tunability, Sci. Adv. 7, eabi7532 (2021)
DOI: 10.1126/sciadv.abi7532*

The experiments were carried out at DNS and PUMA.

THE SIGNATURE OF THE IDEAL GLASS

It has been long debated whether the ideal glass exists. Now, physicists have succeeded in producing the ideal glass and relating it to observations using neutron scattering.

What is the difference between a crystal and a glass? A crystal has the most ordered state possible. Its internal structure will not change, no matter how long it is left standing. The situation is quite different with glass: When cooling rapidly, the molecules solidify in the same disordered state as in the liquid form. Unbalanced forces between the molecules allow the glass to change its structure slightly in order to reach a more stable internal structure. However, it will never reach the state of a crystal, because to do so it would have to break the stable bonds already formed between molecules by investing energy which it does not have.

Can a glass be more ordered than a crystal?

The degree of order is quantified by the entropy. The lower the entropy, the higher the order. Through structural changes, a glass strives to approach a more ordered state. Calculations predict that the glass entropy should fall below that of an ordered crystal. By definition, this is not possible because the greatest order, and the lowest entropy, is possessed by the crystal structure, unattainable for a glass. To solve this so-called Kauzmann paradox, it has long been hypothesized

that a glass undergoes a phase transition to an ideal glass before reaching the entropy of its corresponding crystal. In this state, it will have the minimal entropy that it can reach as a glass while still lying above that of a crystal.

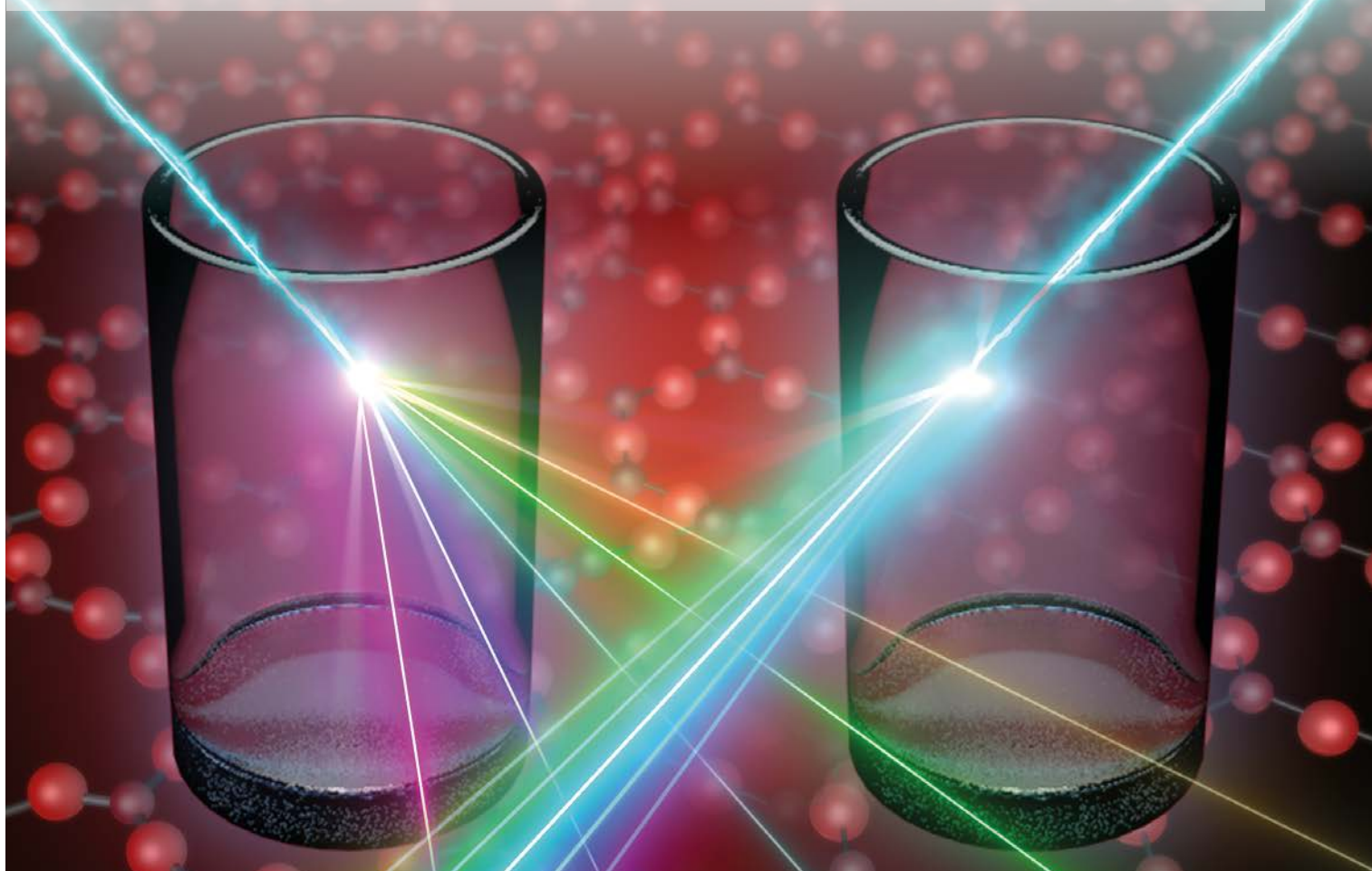
TOFTOF reveals the ideal glass for the first time

Using the TOFTOF time-of-flight spectrometer at the MLZ, researchers from the University of the Basque Country have not only demonstrated the existence of the ideal glass, but also linked it for the first time to observations in inelastic neutron scattering. Glasses, because of their higher disorder, are able to absorb the energy of incident neutrons better than an ideal glass. This energy absorption by an ideal glass should become apparent by a certain disappearing intensity at the maximum of the scattering spectrum, providing a unique signature of ideal glass.

X. Monnier, J. Colmenero, M. Wolf, D. Cangialosi, Reaching the Ideal Glass in Polymer Spheres: Thermodynamics and Vibrational Density of States, Phys. Rev. Lett. 126, 118004 (2021)

DOI: 10.1103/PhysRevLett.126.118004

The experiments were carried out at TOFTOF.



BASIC RESEARCH



Industry & Medicine



Neutrons “see” internal stresses in components from 3D printing

3D printing has opened up a completely new range of possibilities, including the production of turbine blades. However, the 3D printing process often induces internal stress in these components, which can in the worst case lead to cracks. Now, a research team, including the gas turbine manufacturer Siemens Energy, has used neutrons for non-destructive detection of this internal stress – a key achievement for the improvement of the production processes.

Gas turbine blades have to withstand extreme conditions: They are exposed to tremendous centrifugal forces under high pressure and at high temperatures. In order to further maximize energy yields, the blades have to withstand temperatures, which are actually higher than the melting point of the material. This is made possible by using hollow turbine blades, which are air-cooled from the inside.

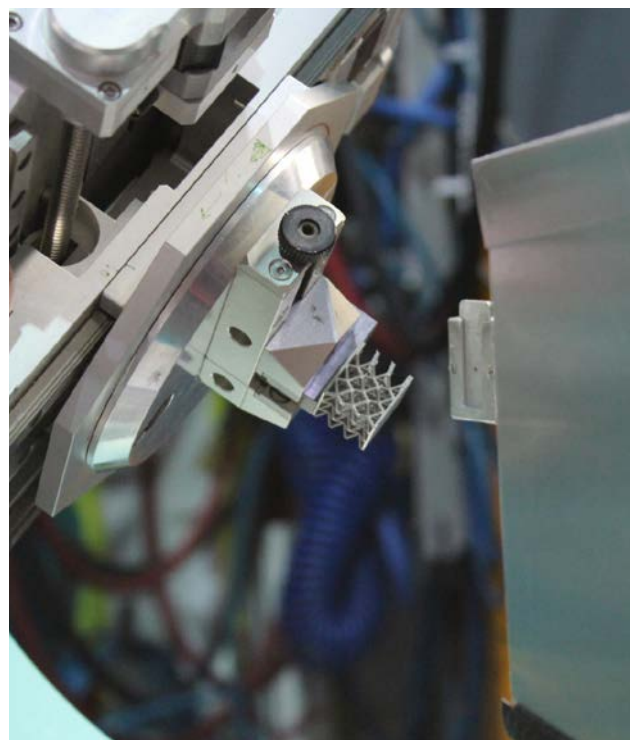
These turbine blades can be made using Laser Powder Bed Fusion, an additive manufacturing technology: Here, the starter material in powder form is built up layer by layer by selective melting with a laser.

Manufacturing creates internal stress

“Complex components with such intricate structures would be impossible to make using conventional manufacturing methods like casting or milling”, says Dr. Tobias Fritsch of the German Federal Institute for Materials Research and Testing (BAM).

But the highly localized heat input of the laser and the rapid cooling of the melt pool lead to residual stress in the material. Manufacturers usually eliminate such stress in a downstream heat-treatment step, which however takes time and thus costs money. What is more, these stresses can unfortunately cause damage to the components even during the production process and up until post-processing takes place. “The stress can in the worst cases lead to cracks”, says Fritsch.

Therefore, he investigated a future gas turbine component for internal stress using neutrons at the instrument STRESS-SPEC. The component was made using additive production processes by the gas turbine manufacturer Sie-



The gas turbine component is in measuring position at the STRESS-SPEC instrument.

mens Energy. They printed a lattice structure only a few millimeters in size using a nickel-chrome alloy typically used for gas turbine components. The usual heat-treatment for stress relieve after production was intentionally omitted.

Even distribution of heat during printing

The team has succeeded in detecting the internal stress within the component. The next step is to reduce this destructive stress during 3D printing. The crucial factor is the heat input over time when building up the individual layers. The more localized the heat application is during the melting process, the more internal stress results.

For as long as the printer’s laser is aimed at a given point, the heat of the point rises relative to adjacent areas. This results in temperature gradients that lead to irregularities in the atomic lattice. “So we have to distribute the heat as evenly as possible during printing”, says Fritsch.

*T. Fritsch, M. Sprengel, A. Evans, L. Farahbod-Sternahl, R. Saliwan-Neumann, M. Hofmann, G. Bruno, On the determination of residual stresses in additively manufactured lattice structures, J. Appl. Crystallogr. 54, 228 (2021)
DOI: 10.1107/S1600576720015344*

Pressure and heat: testing alloys for gas turbines

Gas turbines have to endure extreme conditions like high forces at temperatures above 600°C. Thus, gas turbine materials must be sufficiently robust, and as such they are under constant development. Together with the Friedrich-Alexander-Universität Erlangen-Nürnberg (FAU), VDM Metals tested its improved VDM® Alloy 780 using a specially developed testing machine at the FRM II.

The new nickel VDM® Alloy 780 is resistant to high temperatures and corrosion, making it ideally suited for gas turbines. “It can manage temperatures 50 - 100 °C higher than conventional alloys”, adds Dr. Frank Kümmel from the MLZ’s Advanced Materials Group. The nickel alloy is not the only innovation: The researchers have developed a testing apparatus specifically for investigating this alloy.

Neutrons help in the study of the mechanical properties of the alloy. The researchers mount the sample in the testing apparatus, which creates the desired environmental conditions and maintains or changes them throughout the investigation. While these extreme forces are applied to the sample, the scientists study the changes in the alloy using neutrons on the STRESS-SPEC instrument. Before and after loading, the sample can additionally be checked for pores and cracks at ANTARES. The SANS-1 instrument then illuminates nanoscale structures. The results help to understand the properties of the alloy: They provide information on how the alloy is structured and what influence high temperatures and forces have on the alloy. VDM Metals thus knows how to adapt the manufacturing process.

1200°C in the testing apparatus

To replicate the extreme conditions of a gas turbine, a special sample environment is necessary. The new testing machinery generates temperatures of up to 1200°C, and recreates a vacuum or an air environment similar to a gas turbine. During the investigations, the testing system also generates forces such as tension or compression on the sample, simulating the large centrifugal forces of a gas turbine in operation.

“With our tests, we wanted to investigate two questions: Does our testing machine work, as it should? And what are the mechanical properties of the new VDM® Alloy 780?”, Frank Kümmel explains.

The results: the testing apparatus meets all expectations and works perfectly. The researchers are still automating the operation of the machine so that visiting scientists can also use it easily.

Upgrade planned

The next step is to upgrade the testing apparatus so that it can generate even more complex test conditions, such as rapid sample cooling from high temperatures, cyclic loads, or other gas environments. So, in the future, extreme conditions even closer to those in the aircraft turbine will be featured in the testing apparatus.

F. Kümmel, A. Kirchmayer, C. Solís, M. Hofmann, S. Neumeier, R. Gilles, Deformation Mechanisms in Ni-Based Superalloys at Room and Elevated Temperatures Studied by In Situ Neutron Diffraction and Electron Microscopy, Metals 11, 719 (2021)

DOI: 10.3390/met11050719



Dr. Frank Kümmel inserts a sample into the testing apparatus.

Conjuring colors out of cylinders

Nanoparticles can be found in pharmaceuticals, catalysts, and even TVs. Researchers at the chemical company Merck, the Friedrich-Alexander-Universität Erlangen-Nürnberg (FAU), and the University of Duisburg-Essen (UDE) used neutrons at the MLZ to study colloidal nanoparticles. They are particularly well suited for converting electrical signals into light or, vice versa, light into electricity.

Green nanorods promise a rich pallet of applications: For example, they are already used in the screens of modern QLED TVs. They consist of cadmium selenide with cylindrical protective shells, where the outermost stabilization layer is organic and whose hydrocarbon chains reach outward like tiny hairs. The nanoparticles owe their name to their strongly pronounced green glow. "The advantage of such nanoparticles is that their optical properties, and thus the color of the glow, can be tuned by their size. Moreover, unlike their organic counterparts, inorganic particles cannot fade", says Prof. Dr. Tobias Unruh from the Institute for Crystallography and Structural Physics of the FAU.

Shells preserve the properties

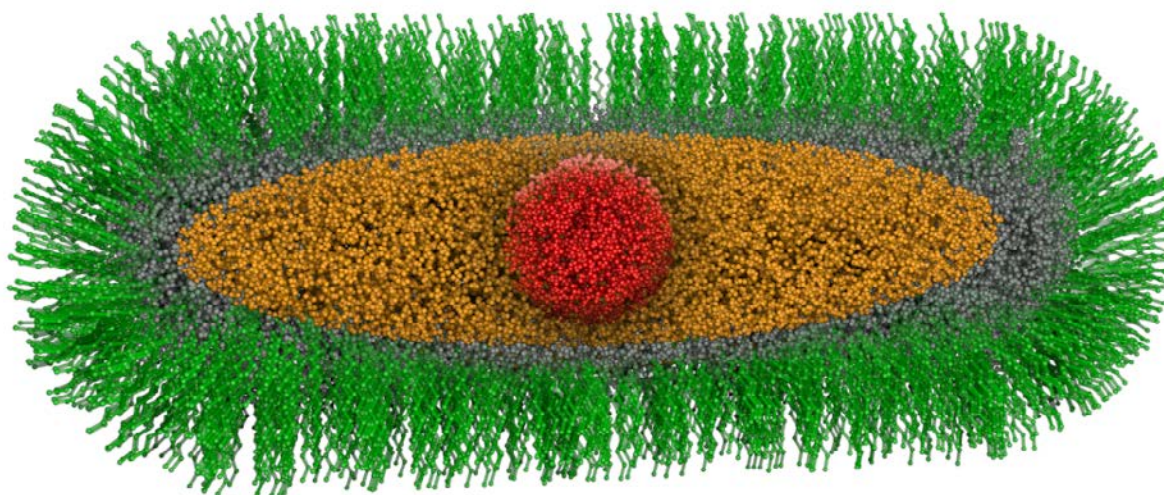
Researchers can tune the special properties of nanoparticles by changing not only their chemical composition and structure but also their size, shape, and interfacial properties. The problem is that nanoparticles lose some or all of their special properties when they encounter molecules in their environment. The protective shells should prevent this and at the same time control the contact between them.

However, there is currently a lack of methods and models to predict the production of such complex nanoparticles with tailored properties. To this end, the research team has closely examined the structure of already known nanoparticles.

Neutrons show stability

Organic molecules are added during the production of the nanoparticles, some of which are required for the nanoparticle synthesis while others are incorporated into the shell itself. In the end, the remnants of the organic molecules must be washed out without removing the shell itself. Until now, it was unclear how much the shell would suffer under the washing. "With the help of neutrons, we were able to take a closer look at the organic shell", says Dr. Sebastian Busch, instrument scientist at the MLZ's SANS-1 instrument, where these nanoparticles were studied. Neutrons are ideally suited for this study because, when hydrogen is replaced with deuterium in the solvent, it is quite easy to distinguish the shell from its surroundings. The researchers used the neutron measurements to show that the washing process not only leaves the shell undamaged, but also actually strengthens it.

*W. Lin, C. Greve, S. Härtner, K. Götz, J. Walter, M. Wu, S. Rechberger, E. Spiecker, S. Busch, T. Schmutzler, Y. Avad-hut, M. Hartmann, T. Unruh, W. Peukert, D. Segets, Unraveling Complexity: A Strategy for the Characterization of Anisotropic Core Multishell Nanoparticles, Part. Part. Syst. Charact. 37, 2000145 (2020)
DOI: 10.1002/ppsc.202000145*



Schematic structure of the "green nanorods": the spherical core of cadmium selenide (red) is surrounded by a crystalline ellipsoidal cadmium sulfide (orange) and a crystalline cylindrical zinc sulfide layer (gray). This complex "core-shell-shell" particle is stabilized by an organic ligand shell (green).

Using antimatter to improve wastewater cleaning

Who would want to drink the residues of detergents or medicines? Researchers from Belgium and the Netherlands used positrons, the antiparticles of electrons, at the Heinz Maier-Leibnitz Zentrum to study membranes designed to filter precisely such micropollutants from wastewater.

Clean drinking water is a precious resource, especially in southern hemisphere countries. When there is not enough fresh water, water treatment plants purify wastewater so that it is drinkable. Huge plants filter wastewater through a partially permeable membrane that traps dirt particles and salt. “One risk with these membranes is that organic micro- and nano-pollutants slip through during filtration”, says Dr. Marcel Dickmann from the Universität der Bundeswehr München. These are synthetically produced substances, such as residues from detergents or medication. “For example, organic micropollutants include the well-known painkiller paracetamol”, Dickmann explains.

Marcel Dickmann operates the so-called positron annihilation lifetime spectroscopy instrument at the positron source NEPOMUC. This is the first time Dickmann has used positrons to examine a wastewater filter membrane for its ability to filter out organic micropollutants. They are thumbnail-sized rectangular platelets that look a bit like coffee filter paper.

Pore size studied at micrometer level

Researchers from the Netherlands and Belgium developed this membrane. Earlier studies had tested the general permeability of the membrane. It quickly became clear that the smaller the pores in the membrane, the more likely it was that micro-pollutants would stick. In the new study, the researchers sharpened their focus: “We went down to the micro and nanometer level and looked at the individual pores of the membrane”, says Dickmann. To do this, the team of scientists brought membranes with different pore sizes, different thicknesses, and from different manufacturing processes to the positron source.

Non-destructive measurement with positrons

Dickmann bombarded the membranes with positrons. As soon as a positron interacts with an electron, it forms positronium, which emits radiation after a certain time. The smaller the pore in the membrane, the faster the positro-



Dr. Marcel Dickmann places the membrane on a sample plate to study it using positron annihilation lifetime spectroscopy.

nium emits the radiation. The pore size of the membrane can thus be determined via the lifetime of the positronium. “No other method can determine the pore size so precisely without destroying the membrane”, Dickmann says. The researchers needed the size of the pores for their studies. In this way, they were able to draw conclusions as to which manufacturing processes provide the appropriate pore sizes. Another result surprised the researchers: The thicker the membrane, the more permeable it was to pollutants.

Marcel Dickmann is certain: “The study will help improve the design of wastewater filters.” After all, residues of medicines or detergents have no place in drinking water.

M. Roman, P. Roman, R. Verbeke, L. Gutierrez, M. Vanoppen, M. Dickmann, W. Egger, I. Vankelecom, J. Post, E. Cornelissen, K. Keesman, A. Verliefde, Non-steady diffusion and adsorption of organic micropollutants in ion-exchange membranes: effect of the membrane thickness, ISCIENCE 24, 102095 (2021)

DOI: 10.1016/j.isci.2021.102095

Strong weld joints for aerospace applications

When a rocket is launched, the weld seams on the enormous fuel tanks have to withstand immense forces. To produce joints with the necessary strength, a process known as “friction stir welding” is used. Scientists at the Technical University of Munich (TUM) are working to make this process more efficient. They are using positrons generated by the positron source NEPOMUC at the MLZ to precisely localize “atomic holes” in the material.

The friction stir welding process is increasingly common in applications requiring particularly strong and leakproof joints such as aircraft fuselages or rocket fuel tanks. In contrast to other welding processes, friction stir welding requires no additional filler metal and temperatures generally remain below the melting point of the workpieces. Consequently, the process is especially suitable for heat-sensitive materials such as aluminum.

Material mixed without melting

Once the workpieces are clamped in place, the rapidly rotating welding pin is moved along the joint between the materials. The pin softens the material through frictional heat without melting it. While moving forward, the pin intermixes



Dr. Andreas Bachmann (left) watches through safety glass as the robot welds two metal plates together with the rapidly rotating welding pin.

the two materials at the joint, producing a strong joint after cooling.

The problem with this process, invented just 30 years ago, is a lack of empirical data. With every new component and material, the equipment setup needs to be redefined through trial and error. An automatic control system capable of selecting and adjusting the settings itself would enormously improve the efficiency of the process. With that goal in mind, Dr. Andreas Bachmann has developed a control concept in his research work at the TUM.

Positrons detect “holes” in metals

Bachmann began by working with a special aluminum alloy used in aerospace applications to analyze the influence of temperature and welding speed on the process. To do so, he used NEPOMUC, the world’s most intense positron source, at the FRM II and found flaws in the metal in and near the weld nugget.

In the CDBS method, the researchers fire positrons into the metallic sample. There they are repelled by positively charged atomic nuclei and find their way into atomic vacancies (“holes”) where they meet their antiparticle, the electron. This results in electron-positron annihilation and the creation of high-energy photons. The coincident detection of these annihilation photons provides valuable information on the position, concentration and chemical surrounding of atomic vacancies.

Defects are linked to temperature

Fewer defects at higher welding temperatures of around 500°C were detected. “That shows: A lower welding temperature is naturally better for these temperature-sensitive materials. But if it is too low, however, it has a negative impact on the strength of the weld”, says Bachmann. The ideal welding temperature may differ for other materials and must be determined on a case by case basis. Bachmann has used these insights to develop a control for setting the optimal temperature, which produced 1.5 times stronger weld joints than without the control.

*A. Bachmann, T. Gigl, C. P. Hugenschmidt, M. F. Zaeh, Characterization of the microstructure in friction stir welds of EN AW-2219 using coincident Doppler-broadening spectroscopy, Mater. Charact. 149, 143 (2019)
DOI: 10.1016/j.matchar.2019.01.016*

Neutrons detect clogs in pipelines

Industry and private consumers alike depend on oil and gas pipelines that stretch thousands of kilometers underwater. It is not uncommon for these pipelines to become clogged with deposits. Until now, there have been no means of identifying the formation of plugs in-situ and non-destructively. Measurements at the FRM II now show that neutrons may provide the solution of choice.

For a clog to be remediated in-situ, the affected section of the pipeline must first be found. Localizing clogs from the outside is challenging, since they can form anywhere along the length of the pipeline.

To date, thermal imaging cameras and gamma rays have been used to detect the clogs. However, neither of these methods works underwater. Ultrasound, on the other hand, has no problem penetrating water, but the hydrate blocks can only be detected in close contact from outside the pipeline wall and only explore 50 mm inside a pipeline of 300 mm inside-diameter.

This constraint poses practical difficulties because underwater pipelines are laid at depths of up to 2000 meters and are often covered by seabed materials like sand or silt. Another technical challenge associated with acoustic methods arises from the lack of a clear difference between the acoustic impedances of the hydrate phase and other phases of the crude oil mixture, which makes discrimination difficult.

Neutrons – the perfect probe

TechnipFMC, a company that specializes in subsea pipelines, was “looking for a more efficient method to find the plugs in a non-contact, non-destructive and reliable way despite thick walls”, says Dr. Xavier Sebastian, project manager at the company.

As suggested by Dr. Sophie Bouat, CEO of Science-S.A.V.E.D., “neutrons are the perfect probe for the task at hand. Using prompt gamma neutron activation analysis, light atoms and hydrogen in particular can be detected very precisely.” Since the hydrogen content of hydrates and normal oil or gas is considerably different, it should be possible to detect blockages by measuring the hydrogen concentration.

Feasibility study at FRM II

Using PGAA, the researchers established that this approach can be used to differentiate between oil and gas and the blockage. At the NECTAR radiography and tomography facility and the FaNGAS (fast neutron-induced gamma ray spectroscopy) instrument, they showed that a sufficiently large number of neutrons penetrate the metal walls and the insulating polypropylene layers of the pipelines to facilitate the respective measurement, and that the measurement also works well underwater.

A small neutron source detects plugs

Moreover, “our experiments have shown that we can even distinguish an incipient blockage from a fully developed one”, says Dr. Ralph Gilles, industry coordinator at the FRM II. “That’s very beneficial, because then one can even preventatively heat a pipe segment to melt the blockage before it fully develops.”

In practice, a mobile detector with a small neutron source will move back and forth along the pipeline to look for plugs. “We are very pleased that we have now found an efficient method that will make it much easier to detect these plugs in the future”, says Dr. Xavier Sebastian.

S. Bouat, L. Pinier, X. Sebastian, A. Losko, R. Schütz, M. Schulz, Z. Revay, Z. Ilic, E. Mauerhofer, T. Brückel, R. Gilles, Detection of hydrate plugs inside submarine pipelines using neutrons, Nondestruct. Test. Eval. (2021) DOI: 10.1080/10589759.2021.1990284



In particular, when a pipeline is idle for a longer time at low temperatures, hydrate plugs can form, similar to the methane hydrate core shown here.

Coping with fouling in drinking water production

Wastewater treatment plants are becoming increasingly important in arid regions to resolve the worldwide water shortage. In order to bring the treated water to a level adequate for secure and unlimited use, membrane technologies such as reverse osmosis and electrodialysis are used. However, fouling of the membranes significantly increases operational costs due to decreased water fluxes and higher maintenance expenses. Israeli and German researchers have studied this fouling process using neutrons. This broadens the understanding of fouling, could improve the treatment processes and lower costs.

Filters are clogged

Water is a precious resource, especially in countries of the southern hemisphere. When there is not enough fresh water available, water treatment plants purify brackish groundwater as well as wastewater to make it drinkable. Huge plants filter the pre-treated water through selective membranes, which remove unwanted organic materials, colloidal particles and salt from water.

However, these membrane filters often get clogged by minerals, such as silica particles. This reduces the amount of water which can be cleaned by the membrane. Thus, the membranes become fouled and less effective. Therefore, the membranes have to be replaced more frequently or washed with special agents, which in turn leads to higher costs.

Neutrons examine a model of membranes

Israeli and German researchers have now built a special cell for these membranes to simulate the scaling process which causes the clogging and fouling. This cell fits the requirements for conducting filtration experiments with in-situ small-angle neutron scattering measurements at the KWS-3 and KWS-1 instruments of the FRM II. This method provides the means of analyzing fouling from the mesoscopic down to the molecular level.

“We could simulate and follow the whole process as it is in reality”, says Dr. Dietmar Schwahn from the Forschungszentrum Jülich. “Neutrons show us non-destructively, how the silica particles accumulate in front of the membrane.” In many cases, the particles form a “cake-layer” on the mem-



Clean drinking water is scarce. In arid regions, wastewater treatment plants have to pre-treat brackish water to make it drinkable.

brane surface, in which they are ordered as a dense silica crystal. Using neutron scattering, the researchers were able to determine the distance of the silica particles from each other within this layer. Surprisingly, cake formation led to slightly enhanced water flux determined in parallel to the neutron measurements.

Cost-effective substances to prevent fouling

Neutrons showed what happens on mesoscopic down to sub-microscopic levels at membrane surfaces in wastewater treatment plants. “The engineers know the water flux through the membranes”, says Dr. Schwahn. “We now helped to explain the effect of silica accumulation on the water flux through the membrane.”

The results can be used to develop cost-effective substances that prevent the fouling of the membranes.

V. Pipich, T. Starc, J. Buitenhuis, R. Kasher, W. Petry, Y. Oren, D. Schwahn, Silica Fouling in Reverse Osmosis Systems—Operando Small-Angle Neutron Scattering Studies, Membranes 11, 413 (2021)

DOI: 10.3390/membranes11060413

Optimization of mRNA containing nanoparticles

Neutrons play an important role in the investigation of mRNA nanoparticles similar to those used in the Covid-19 vaccines from the vendors BioNTech and Pfizer. Researchers used the high neutron flux to characterize various formulations for the mRNA vaccine, and thus to lay the groundwork for improving the vaccine's efficacy.

The messenger RNA (mRNA) contains the specific blueprint for proteins, which are then synthesized by the cell. In the case of the Covid-19 vaccine, these are the proteins of the characteristic spikes on the surface of the Corona virus. The proteins are presented on the surface of immune cells; then, the human immune system triggers defenses against these foreign proteins and hence against the Corona virus. The mRNA itself is completely broken down after only a few hours, which is advantageous for the safety of these vaccines.

The road to the best packaging

The mRNA has to be packaged appropriately in order to keep it from being broken down on the way to the cell in the human body. This is done using nanoparticles, which can consist of a mixture of lipids or polymers. The lipids are fat molecules similar to the molecules of the cell membrane and help deposit the mRNA in the interior of the cell. The lipids and biopolymers are then broken down or excreted by the body. BioNTech developed formulations in which the nanoparticles consisted of various mixtures of lipids and biopolymers already proven in pharmaceuticals.

In order to compare the properties of the nanoparticles with one another, the researchers used neutrons at the instrument KWS-2 among others. The neutrons are scattered in



Scientist Dr. Aurel Radulescu at the instrument KWS-2.

the interior of the nanoparticles on the hydrogen nuclei and are deflected from their paths in a characteristic way. This is the basis for the conclusions regarding their distribution. If the hydrogen atoms of certain components – for example of the lipids only – are exchanged with heavy hydrogen, the chemical properties and the pharmaceutical efficacy do not change, but the scattering pattern of the neutrons does. “This method makes it possible to selectively highlight parts of a complex multi-component morphology without changing the physical chemistry of the sample”, says Dr. Aurel Radulescu of the Jülich Centre for Neutron Science and instrument scientist at KWS-2.

The right degree of order

In these analyses, the research team was interested in how efficiently the various formulations were able to transmit the mRNA into the cell, referred to as transfection. The researchers thus found out that the highest transfection rates were achieved with nanoparticles that are characterized by a certain type of internal arrangement.

“High levels of biological activity were registered whenever ordered and less ordered areas alternated in the interior of the nanoparticles in a characteristic manner. This could be a generally valid concept of structure-activity relationship which can be applied independently of the systems investigated here”, Dr. Heinrich Haas of BioNTech points out.

Such a system could be obtained by a single step protocol starting with a lipid and polymer mixture for nanoparticle formation, a concept that can be taken into account in the development of new mRNA-based therapeutic agents.

C. D. Siewert, H. Haas, V. Cornet, S. S. Nogueira, T. Nawroth, L. Uebbing, A. Ziller, J. Al-Gousous, A. Radulescu, M. A. Schroer, C. E. Blanchet, D. I. Svergun, M. P. Radsak, U. Sahin, P. Langguth, Hybrid Biopolymer and Lipid Nanoparticles with Improved Transfection Efficacy for mRNA, Cells 9, 2034 (2020)
DOI: 10.3390/cells9092034

C. Siewert, H. Haas, T. Nawroth, A. Ziller, S. S. Nogueira, M. A. Schroer, C. E. Blanchet, D. I. Svergun, A. Radulescu, F. Bates, Y. Huesemann, M. P. Radsak, U. Sahin, P. Langguth, Investigation of charge ratio variation in mRNA – DEAE-dextran polyplex delivery systems, Biomaterials 192, 612 (2019)
DOI: 10.1016/j.biomaterials.2018.10.020

A better understanding of multiple sclerosis

The brain is the center of our nervous system – structural changes are often involved in neurological diseases and mental disorders. A research team has now developed a neutron-based method to examine brain slices and better understand these diseases.

The brain can be divided into gray matter and white matter. The white matter contains the axons that transmit stimuli. For faster transmission, the axons are wrapped in an insulating layer of myelin, similar to a cable where the rubber insulation ensures that no electricity is lost. Injury or loss of the myelin sheath leads to impaired brain and body functions. In multiple sclerosis, the insulating myelin layer is severely attacked. However, the exact causes of the disease are still unclear.

Researchers at the Forschungszentrum Jülich have developed a new imaging method at the small-angle scattering facility KWS-1 to map the density, structure and spatial orientation of nerve fibres and myelin.

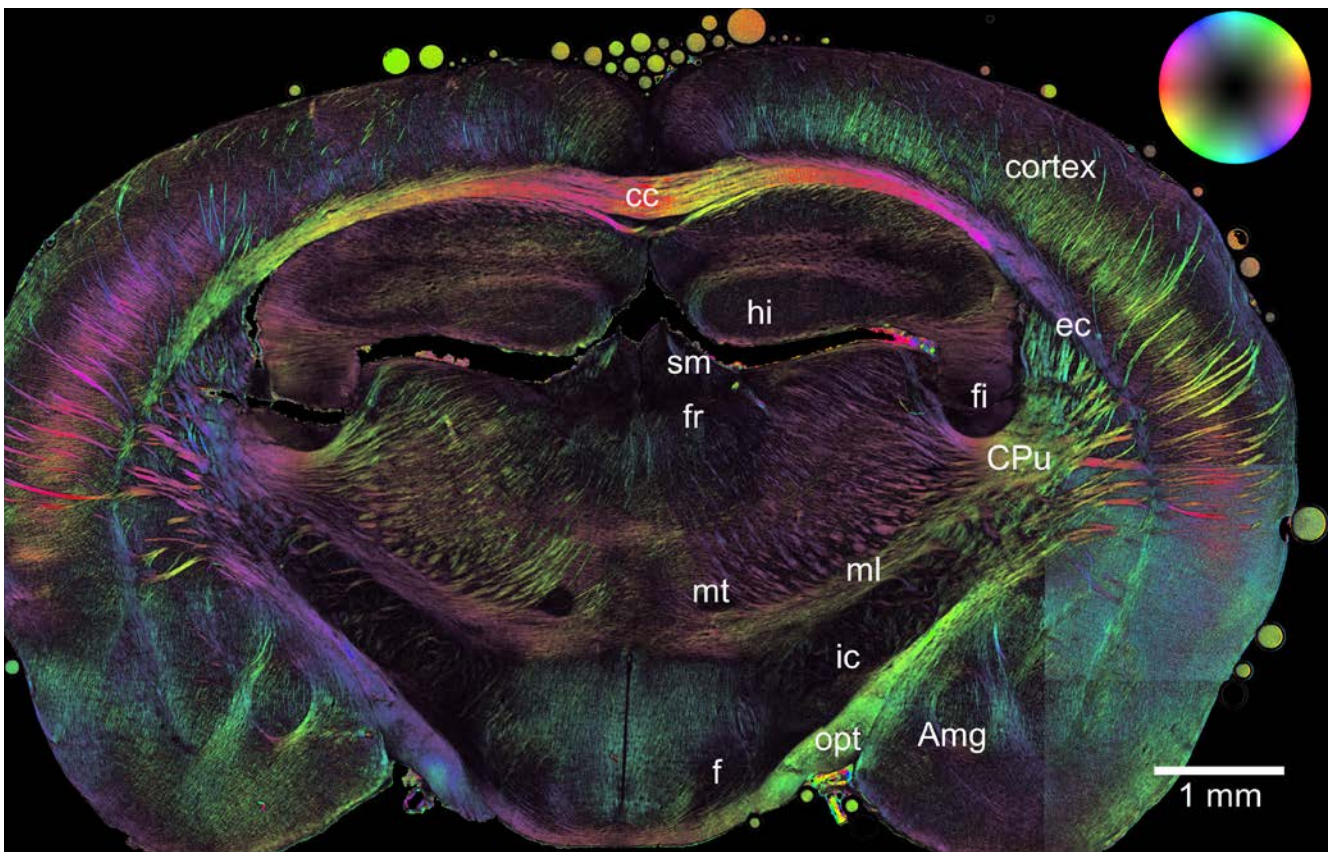
New method complements previous procedures

“The spatial orientation of nerve fibers in brain slices has long been able to be determined using polarization microscopy”, explains Dr. Henrich Frielinghaus of the Jülich Centre for Neutron Science, head of the KWS-1 group, “However, the exact structure and orientation of myelin on the molecular scale cannot be detected with light.” Using neutrons, the researchers can now determine both for the first time and correlate them with the measured polarization.

Application in medicine

From their new method, the researchers hope to better understand the causes of neurological diseases in the future. Although the resolution of the new method is still in the millimeter range, they expect that micrometer-precise measurements will be possible in the future.

*S. Maiti, H. Frielinghaus, D. Gräßel, M. Dulle, M. Axer, S. Förster, Distribution and orientation of nerve fibers and myelin assembly in a brain section retrieved by small-angle neutron scattering, Sci. Rep. 11, 17306 (2021)
DOI: 10.1038/s41598-021-92995-2*



3D Polarised Light Imaging scan of a mouse brain. The structural information about the orientation of the nerve fibres from this image served as a comparison for the new neutron measurements.

Making the gray cells happy

Depressive disorders are among the most frequent illnesses worldwide. The causes are complex and to date only partially understood. The trace element lithium appears to play a role. Using neutrons at the FRM II, a research team has now proved that the distribution of lithium in the brains of depressive people is different from the distribution found in healthy humans.

Lithium is familiar to many of us from rechargeable batteries. Most people ingest lithium on a daily basis in drinking water. International studies have shown that a higher natural lithium content in drinking water coincides with a lower suicide rate among the population. In much higher concentrations, lithium salts have been used for decades to treat mania and depressive disturbances. However, the exact role lithium plays in the brain is still unknown.

Scientists from the Technical University of Munich (TUM) joined medical experts at the Ludwig-Maximilians-University of Munich (LMU) and a team from the FRM II to develop a method, which can be used to precisely determine the distribution of lithium in the human brain. The team hopes to be able to draw conclusions for therapy, as well as to gain a better understanding of the physiological processes involved in depression.

Neutrons detect the slightest traces of lithium

The scientists investigated the brain of a suicidal patient and compared it with two control persons. The investigation focused on the ratio of the lithium concentration in the white brain matter to the concentration in the gray matter of the brain.

In order to determine how much lithium is present where in the brain, the researchers analyzed 150 samples from various brain regions – for example, those regions that are presumably responsible for processing feelings. At the FRM II Prompt Gamma-Ray Activation Analysis (PGAA) they irradiated thin brain sections with neutrons.

“One lithium isotope is especially good at capturing neutrons; it then decays into a helium atom and a tritium atom”, explains Dr. Roman Gernhäuser of the TUM Department of Physics. The two decay products are captured by detectors in front of and behind the sample and thus provide information on where exactly the lithium is located in the brain section.



Josef Lichtinger examines the lithium distribution in brain samples. In his hands, he holds the self-developed detector with the tissue sections.

Since the lithium concentration in the brain is usually very low, it is also very difficult to ascertain. “Until now it hasn’t been possible to detect such small traces of lithium in the brain in a spatially resolved manner”, says Dr. Jutta Schöpfer of the LMU Munich Institute for Forensic Medicine.

Significant difference between healthy and depressive patients

The researchers saw that there was significantly more lithium present in the white matter of a healthy person than in the gray matter. By contrast, the suicidal patient had a balanced distribution, without a measurable systematic difference.

“Our results are fairly groundbreaking, because we were able for the first time to ascertain the distribution of lithium under physiological conditions”, Schöpfer is glad to report. “Since we were able to ascertain trace quantities of the element in the brain without first administering medication and because the distribution is so clearly different, we assume that lithium indeed has an important function in the body.”

J. Schoepfer, R. Gernhäuser, S. Lichtinger, A. Stöver, M. Bendel, C. Delbridge, T. Widmann, S. Winkler, M. Graw, Position sensitive measurement of trace lithium in the brain with NIK (neutron-induced coincidence method) in suicide, Sci. Rep. 11, 6823 (2021)

DOI: 10.1038/s41598-021-86377-x





Scientific Reports



Migration kinetics of oxygen-ions in LaSrMnO_{3-δ} thin films during topotactic phase transitions

L. Cao^{1,2}, O. Petravic³, X.-K. Wei⁴, H. Zhang³, T. Duchoň⁵, F. Gunkel⁶, A. Koutsoubas⁷, K. Zhernenkov⁷, K. Z. Rushchanskii⁸, H. Hartmann⁹, M. Wilhelm⁵, Z. Li², Y. Xie², S. He^{3,6}, M. L. Weber⁶, K. Veltruská¹⁰, A. Stellhorn³, J. Mayer⁴, S. Zhou², T. Brückel^{3,7}

¹School of Advanced Materials, Peking University, Shenzhen Graduate School Shenzhen, China; ²Institute of Ion Beam Physics and Materials Research, Helmholtz-Zentrum Dresden-Rossendorf, Dresden, Germany; ³Jülich Centre for Neutron Science (JCNS-2) and Peter Grünberg Institute (PGI-4), JARA-FIT, Forschungszentrum Jülich GmbH, Jülich, Germany; ⁴Ernst Ruska Centre for Microscopy and Spectroscopy with Electrons, Forschungszentrum Jülich GmbH, Jülich, Germany; ⁵Peter Grünberg Institute (PGI-6), JARA-FIT, Forschungszentrum Jülich GmbH, Jülich, Germany; ⁶Peter Grünberg Institute (PGI-7), JARA-FIT, Forschungszentrum Jülich GmbH, Jülich, Germany; ⁷Jülich Centre for Neutron Science (JCNS) at MLZ, Forschungszentrum Jülich GmbH, Garching, Germany; ⁸Peter Grünberg Institute (PGI-1) and Institute for Advanced Simulation (IAS-1), Forschungszentrum Jülich GmbH, Jülich, Germany; ⁹Central Institute for Engineering, Electronics and Analytics (ZEA-3), Jülich, Germany; ¹⁰Department of Surface and Plasma Science, Faculty of Mathematics and Physics, Charles University, Prague, Czech Republic

Oxygen migration and surface exchange kinetics significantly govern the ionic, electronic, and catalytic properties of complex oxides. In this study, we report the first observation of a novel surface phase in La_{0.7}Sr_{0.3}MnO_{3-δ} (LSMO) epitaxial thin films during the topotactic transition from the perovskite (PV) to the brownmillerite (BM) phase. Real-time X-ray diffraction studies suggest a close correlation between structural evolution and oxygen migration kinetics. Using polarized neutron reflectometry on MARIA (MLZ), a direct depth profile of the oxygen gradient is achieved in the transformed state, facilitating a precise determination of the oxygen stoichiometry variation. The veracity of such an approach is supported by the visualization of the vacancy-induced structural change using high resolution electron microscopy. Given the anisotropic vacancy channels found in the surface phase, our studies will be of direct interest for the exploration of new candidates for solid-oxide fuel-cell materials and devices, as well as for a deeper understanding of oxide migration mechanisms.

Transition metal oxides have been at the core of cutting-edge information, energy, and environmental technologies owing to their versatile functionalities. Given the large flexibility of anion stoichiometry, the oxygen content plays a crucial role in determining their physical properties. However, a detailed characterization of the oxygen gradient throughout the film has remained elusive due to the difficulty in the imaging and quantification of local oxygen variations. In this regard, a

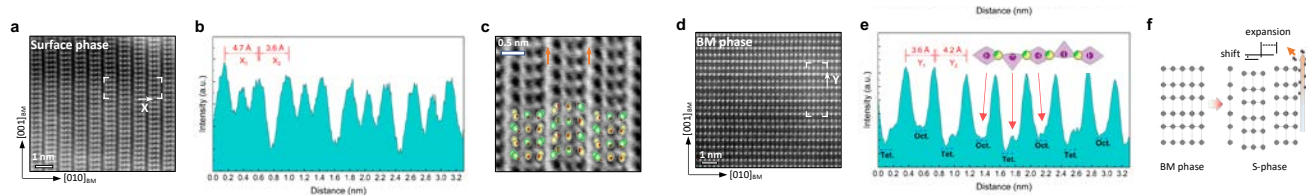
precise determination of the oxygen content and diffusion dynamics is highly sought after to address the interplay between local chemical evolution and physical phenomena.

Engineering oxygen defects

In our work, we perform a real-time study of the oxygen content evolution in La_{0.7}Sr_{0.3}MnO_{3-δ} (LSMO) epitaxial thin films by in-situ X-ray diffraction (XRD) and in-situ X-ray photoelectron spectroscopy. As shown in figure a, a topotactic transition from perovskite (PV) to brownmillerite (BM) is evidenced at elevated temperatures. The limiting cases of the transition are further investigated by polarized neutron reflectometry on MARIA at the MLZ, where the contrast in nuclear depth profiles eventually enables an accurate quantification of the oxygen content gradient for the topotactic phases (figure b). In particular, a novel phase is discovered at the near-surface region after the transition. In combination with scanning transmission electron microscopy (STEM), a highly anisotropic oxygen ion migration path is revealed for the first time, being essential for optimizing oxygen ion conductivity at moderate temperatures (figure c & d). Given the flexibility of manganese valence states and the anisotropic vacancy channels found in the surface phase, our studies will be of direct interest for the exploration of new candidates for solid-oxide fuel-cells.

[1] L. Cao et al., *Migration Kinetics of Surface Ions in Oxygen-Deficient Perovskite During Topotactic Transitions*, *Small* 17(51), 2104356 (2021)

DOI: 10.1002/smll.202104356



(a) In-situ XRD of LSMO thin film measured during vacuum annealing at 600°C; (b), (d) The measured non-spin-flip reflectivities (open symbols) for spin up - up (R^{++}) and spin down - down (R^{--}) polarized neutrons: (b) pristine PV phase; (d) transformed BM phase; (c) STEM image taken for the surface phase, with calculated atomistic structure overlaid as inset. The preferred oxygen diffusion paths along the vertical structural gaps are highlighted by arrows.

Stabilizing solid-electrolyte interphase with polyacrylamide for high-voltage aqueous lithium batteries

X. Hou¹, R. Wang², X. He^{1,3}, T. P. Pollard⁴, X. Ju¹, L. Du⁵, E. Paillard⁶, H. Frielinghaus², L. C. Barnsley^{2,7}, O. Borodin⁴, K. Xu⁴, M. Winter^{1,5}, J. Li^{1,6}

¹Helmholtz-Institute Münster (HI MS), IEK-12, Forschungszentrum Jülich GmbH, Münster, Germany; ²Jülich Centre for Neutron Science (JCNS) at MLZ, Forschungszentrum Jülich GmbH, Garching, Germany; ³School of Chemical Engineering, Sichuan University, Chengdu, China; ⁴Battery Science Branch, Sensor and Electron Devices Directorate, US Army Research Laboratory, Adelphi, USA; ⁵MEET Battery Research Center, Institute of Physical Chemistry, University of Münster, Münster, Germany; ⁶Department of Energy, Politecnico di Milano, Milano, Italy; ⁷Australian Synchrotron, ANSTO, Clayton, Australia

The introduction of the concept of a “water-in-salt” electrolyte (WiSE) opens up a new horizon for aqueous electro-chemistry in that it benefits from the formation of a solid-electrolyte interphase (SEI). Here, we report on a polymeric additive, polyacrylamide (PAM), that effectively stabilizes the interphase in WiSE. The formation mechanism of PAM-assisted SEI was investigated using in operando small angle neutron scattering at the KWS-1 instrument and density functional theory.

The case of the SEI

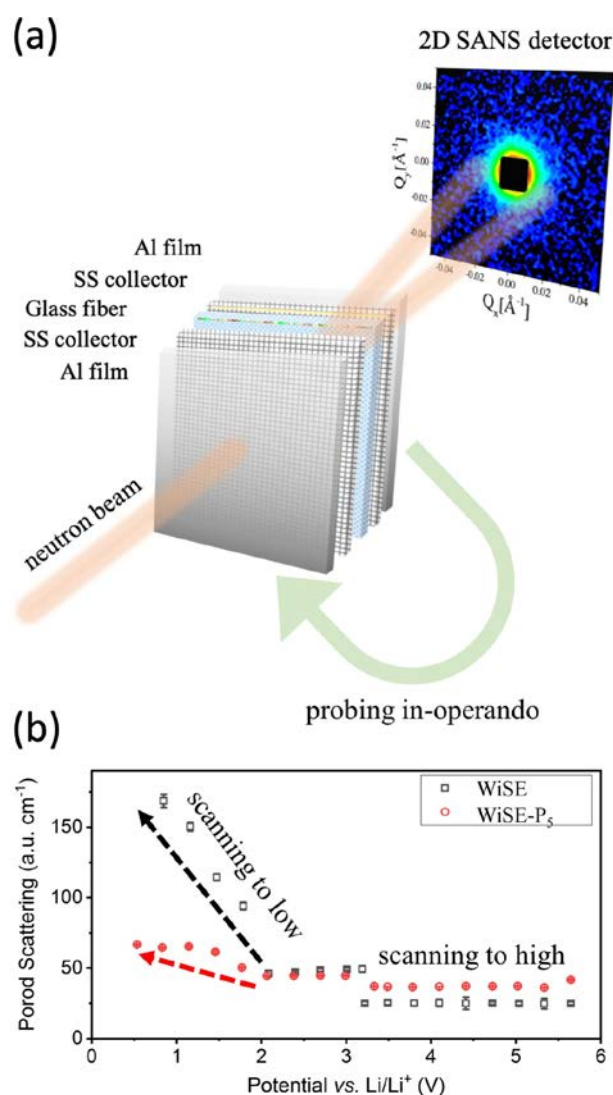
Aqueous lithium-ion batteries have generated intense interest due to their exceptional safety, low cost and low environmental impact, which make them attractive for various applications ranging from electronic devices to grid-scale storage systems. The new class of highly concentrated aqueous electrolytes, also known as WiSE, significantly expands the electrochemical stability window to ca. 3.0 V via the formation of a SEI. It has been found that the SEI formed at the anode/electrolyte interface in WiSE consists mainly of a combination of inorganic compounds (LiF, Li₂O and Li₂CO₃) originating from the reduction of dissolved gases (O₂ and CO₂) and the electrolyte salt anion TFSI. These insoluble salts suppress the H₂ evolution from the reductive decomposition of water. However, the “real life” SEI in WiSE-based cells is often inhomogeneous with a porous mosaic structure and is susceptible to dissolution, corrosion and mechanical cracking. Yet, chemically adsorbed PAM on metal surfaces can shield them against the attack from H⁺.

To understand the morphological evolution of SEI formation upon the addition of PAM, in operando SANS was applied (figure). The scattering obtained displays a strong Porod scattering that is evaluated further. When applying high potentials, Porod amplitudes are constant in both electrolytes. When applying low potentials, the behavior of these two electrolytes grows strongly. This indicates that below 2.0 V vs. Li|Li⁺ in WiSE, there is a continuous surface build-up due to sustained decomposition of the electrolyte, which is required to repair the SEI due to its constant dissolution. However, in the reference WiSE-P₅ (5 mol% of PAM of 21 kg/mol) electrolyte, morphological changes due to film formation are confined to a narrow potential range of

2.0 - 1.5 V vs. Li|Li⁺, beyond which the interphase stabilizes and the parasitic reactions are minimized. The steady scattering amplitude at lower potentials indicates that the anode/electrolyte interface shows an improved stabilization due to the addition of PAM.

[1] X. Hou et al., *Stabilizing the Solid-Electrolyte Interphase with Polyacrylamide for High-Voltage Aqueous Lithium-Ion Batteries*, *Angew. Chem. Int. Ed.* 60, 22812 (2021)

DOI: 10.1002/anie.202107252



(a) Schematic illustration of the in operando SANS experiments. The main focus of this study lies in the high intensity Porod scattering close to the center of the detector. (b) Porod scattering amplitudes of cells with WiSE and reference WiSE-P₅ when scanning to different potentials.

Dilatometer as a sample environment at STRESS-SPEC

X. H. Li¹, M. Hofmann¹, M. Landesberger¹, M. Reiberg², X. Zhang³, Y. D. Huang³, L. J. Wang¹, E. Werner², W. M. Gan⁴

¹Heinz Maier-Leibnitz Zentrum (MLZ), Technical University of Munich, Garching, Germany; ²Institute of Materials Science and Mechanics of Materials, Technical University of Munich, Garching, Germany; ³Institute of Metallic Biomaterials, Helmholtz-Zentrum hereon GmbH, Geesthacht, Germany; ⁴German Engineering Materials Science Centre (GEMS) at MLZ, Helmholtz-Zentrum hereon GmbH, Garching, Germany

A modified quenching and deformation dilatometer (TA instruments DIL 805A/D/T) is now in operation at the MLZ. It is customized for running neutron scattering measurements during the temperature/deformation treatment of the sample, in particular neutron diffraction (phase, texture, and lattice strain) and neutron small angle scattering.

A Unique Quenching and Deformation Dilatometer for Combined In Situ Neutron Diffraction Analysis of Engineering Materials

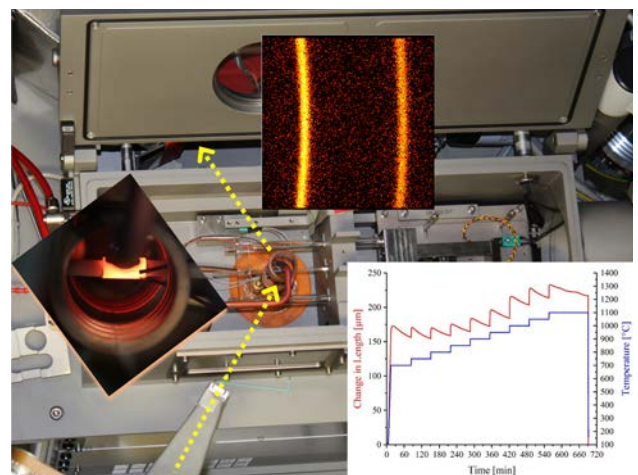
Thermal analysis (TA) and thermomechanical analysis (TMA) are standard techniques for studying the chemical and physical properties of materials as they change with temperature. For the development of new alloys and improvement of existing engineering materials, TA/TMA is essential to understanding material behavior under the influence of thermal loads, to predict its performance, and to optimize processing conditions. A dilatometer is a sufficiently precise piece of equipment that can be applied to perform TA as well as TMA experiments.

Initial results for the user experiments demonstrate in detail its powerful measurement capabilities after successfully combining with neutron diffraction in the phase transformation study of several materials [1]. The advantages can be summarized as follows: 1) The addition of the dilatometer compensates to a certain extent for the low time resolution of the in situ neutron diffraction measurement in the study of phase transformations. Some rapid phase transformation phenomena such as massive transformation in High Entropy Alloys and the related phase transformation temperature can be directly observed in the Time-Temperature-Length

(TTL) curves. 2) The high-resolution length change signal of the dilatometer exhibits a resolution much higher than that of neutron diffraction in quantitative phase analysis, providing additional accurate data for studying nucleation processes and slow precipitation. 3) The combination of dilatometry and neutron diffraction bundles various advantages into one in situ measurement such as high time resolution, high length change accuracy, precise temperature control, large gauge volume, microstructural analysis, and crystallographic insight. Several important parameters in phase transformation studies such as the start/end point of transformation, transformation-temperature/type/rate can thus be obtained within a single measurement setup.

[1] Xiaohu Li et al., *A Unique Quenching and Deformation Dilatometer for Combined In Situ Neutron Diffraction Analysis of Engineering Materials*, *Adv. Eng. Mater.*, (23) 2100163 (2021)

DOI: 10.1002/adem.202100163



The multi-component diagram shows the experimental signals during an in situ neutron diffraction experiment at STRESS-SPEC in combination with the dilatometer.

Non-destructive testing of additively manufactured specimens

C. G. Kolb¹, K. Zier², J.-C. Grager², A. Bachmann¹, T. Neuwirth³, S. Schmid², M. Haag⁴, M. Axtner⁴, F. Bayerlein¹, C. U. Grosse², M. F. Zaeh¹

¹Department of Mechanical Engineering, Institute for Machine Tools and Industrial Management, Technical University of Munich, Garching, Germany; ²Chair of Non-destructive Testing, Technical University of Munich, Munich, Germany; ³Heinz Maier-Leibnitz Zentrum (MLZ), Technical University of Munich, Garching, Germany; ⁴FIT Additive Manufacturing Group, Lupburg, Germany

The powder bed fusion of metals using a laser beam is a suitable additive manufacturing process which is increasingly used for the production of functional parts used in safety-relevant applications. To ensure that the demanding part specifications are achieved, comprehensive quality inspections are performed subsequent to the part fabrication. Empirical studies have revealed that the highest defect detection capability was achieved with neutron grating interferometry.

The powder bed fusion of metals using a laser beam (PBF-LB/M) is a leading additive manufacturing process for producing, e.g., turbine blades with internal cooling channels. During this process, metal powder is applied in layers and selectively melted by a focused laser beam. The PBF-LB/M process is subject to more than 100 influencing factors. Process instabilities caused by an unfavorable interaction of the process parameters can lead to the formation of defects. Typical defects are pores and cracks. Even a partial or total delamination of individual layers can occur.

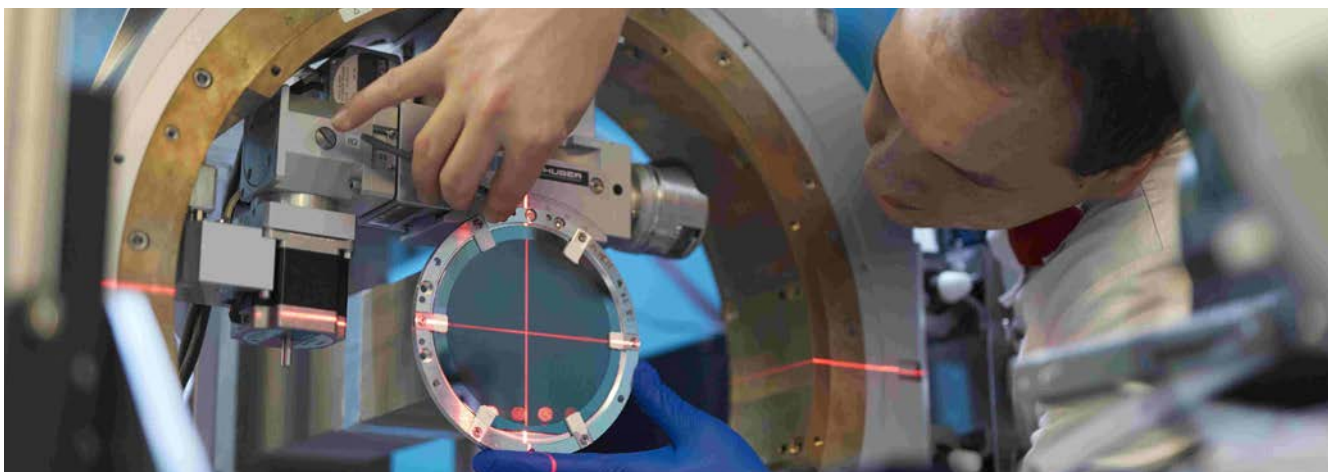
Defects in safety-critical components, such as turbine blades, can have serious consequences. To ensure that the sophisticated part specifications are achieved, 100% quality inspections are performed subsequent to the build-up process. However, knowledge about the detectability of defects in PBF-LB/M parts using non-destructive testing methods is limited.

Greater penetration and improved resolution using neutrons

Therefore, the researchers analyzed the suitability of non-destructive testing techniques, in particular active infrared thermography, neutron grating interferometry, X-ray computed tomography, and ultrasonic testing for the examination of PBF-LB/M parts made from the nickel-base alloy Inconel 718. At the research neutron source, the experiments were conducted at the ANTARES instrument (see figure). Based on a test specimen with artificially inserted defects of varying dimensions and depths, these non-destructive testing techniques were compared in terms of their attainable resolution and, thus, defect detection capability. The empirical studies revealed that the neutron grating interferometry shows the highest resolution capability. It was possible to detect defects with a diameter of 100 - 200 μm at a depth of 60 - 80 μm . The results contribute to a better understanding of the potential of non-destructive testing techniques and also assist stakeholders in additive manufacturing in evaluating the suitability of those techniques.

[1] C. G. Kolb et al., *An investigation on the suitability of modern nondestructive testing methods for the inspection of specimens manufactured by laser powder bed fusion*, *SN Appl. Sci.* 3, 713 (2021)

DOI: 10.1007/s42452-021-04685-3



Co-author Tobias Neuwirth adjusts the setup for the neutron grating interferometry at the ANTARES instrument of the research neutron source Heinz Maier-Leibnitz (FRM II) at the Technical University of Munich.

Comparison of 2D-ACAR and Compton scattering of Pd using a new 1D-to-2D reconstruction method

J. Ketels¹, D. Billington², S. B. Dugdale³, M. Leitner^{1,4}, C. Hugenschmidt^{1,4}

¹Physics Department, Technical University of Munich, Garching, Germany; ²School of Physics and Astronomy, Cardiff University, Cardiff, United Kingdom;

³H. H. Wills Physics Laboratory, University of Bristol, Bristol, United Kingdom; ⁴Heinz Maier-Leibnitz Zentrum (MLZ), Technical University of Munich, Garching, Germany

We determined the electron momentum density and the occupancy in the first Brillouin zone of Pd by measuring the 2D-ACAR and Compton scattering in order to point out the complementary nature of the two techniques. With the future upgrade of the 2D-ACAR spectrometer at NEPOMUC, we will enable depth resolved studies of the electronic structure and hence open up novel positron beam applications in solid-state physics.

The measurement of the angular correlation of electron-positron annihilation radiation (ACAR) and Compton scattering are two techniques which directly measure the electron momentum density (EMD) in the bulk. While Compton scattering delivers the 1D projection of the EMD, 2D-ACAR measures a 2D projection of the two-photon momentum density (TPMD) which is closely connected to the EMD, but includes the influence of the positron. Both have low demands on ambient conditions, meaning that they can easily access large regions of the phase diagram even across phase transitions. We performed measurements on Pd using both methods and compared them to first-principle calculations.

Direct Inversion Method

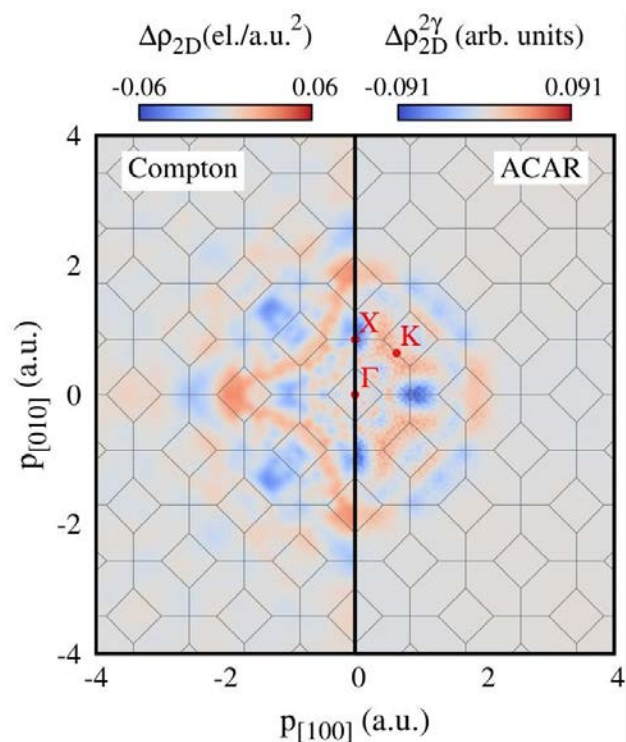
To recover the 2D information from multiple 1D Compton profiles, a new reconstruction algorithm was implemented. It employs linear matrices to model the experiment and the solution can be found by direct inversion. Thus, we call our method the Direct Inversion Method (DIM).

A comprehensive comparison between ACAR and Compton data from theoretical calculations and experimental measurements in 1D and 2D momentum space and in the first Brillouin zone clearly reveals the complementarity of both methods [1]. However, it also highlights the importance of positron probing effects in theoretical calculations of the TPMD. By way of example, the figure shows the experimental radial anisotropy obtained by ACAR and Compton measurements. The higher intensity of ACAR at low momenta originates from the large overlap of the positron wave function and the electrons close to the Fermi-surface.

In the future the 2D-ACAR spectrometer will be upgraded to use the monoenergetic positrons from the high intensity positron source NEPOMUC. Due to the well-defined penetration depth of monoenergetic positrons into solids, depth resolved studies of the electronic structure will be possible. This will enable us to follow the evolution of the electronic structure from surface to bulk or to investigate layered systems and hence open up novel positron beam applications in solid-state physics.

[1] J. Ketels et al., *Momentum density spectroscopy of Pd: Comparison of 2D-ACAR and Compton scattering using a 1D-to-2D reconstruction method*, *Phys. Rev. B* 104, 075160 (2021)

DOI: 10.1103/PhysRevB.104.075160



2D radial anisotropy of the EMD reconstructed by the DIM from ten 1D Compton spectra (left) and the corresponding 2D projection obtained by 2D-ACAR (right). Both spectra were normalized to the corresponding electron density of the EMD before calculating the radial anisotropy. The positions of the projected high-symmetry Γ , K , and X points are indicated.

Phase quantification using different neutron diffraction techniques

X. H. Li¹, S. Soria², W. M. Gan¹, M. Hofmann², M. Schulz², M. Hölzel², H.-G. Brokmeier³, W. Petry²

¹German Engineering Materials Science Centre (GEMS) at Heinz Maier-Leibnitz Zentrum (MLZ), Helmholtz-Zentrum hereon GmbH, Garching, Germany; ²Heinz Maier-Leibnitz Zentrum (MLZ), Technical University of Munich, Garching, Germany; ³Institute of Materials Science and Engineering, TU Clausthal, Germany

The content of strain-induced martensite in austempered ductile iron (ADI) has been quantitatively determined using three different kinds of neutron methods: (1) high-resolution powder diffraction with subsequent Rietveld refinement, (2) phase quantification using pole figure measurements and (3) Bragg edge neutron transmission (BET). A combination of these methods has been proven to be effective for dealing with problems like peak overlap in multiphase materials and texture formation after plastic deformation.

Multi-scale phase analyzes of strain-induced martensite in ADI

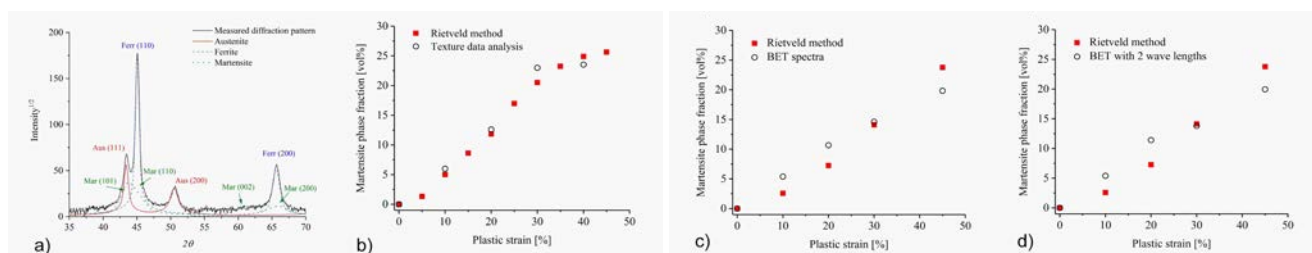
Rietveld refinement is a comprehensive and well-proven analysis method for phase quantification in all sorts of polycrystalline materials. Usually, no internal standard is needed with this methodology. However, the measurement, and especially the data analysis process, are relatively complex and time consuming. In the study of the mechanical properties of multi-phase metallic materials, peak overlap and texture always exist, making the quantitative phase analysis using the Rietveld method more difficult.

Such problems have been solved successfully upon combination of the different neutron techniques available at the instruments STRESS-SPEC and ANTARES. Figure a presents the neutron diffraction pattern of ADI after plastic deformation with a strain level of 35%. The peak shapes of each phase are marked with different colors. Peak overlap of peaks from austenite, ferrite and martensite can be easily seen in the diffraction pattern. Figures b, c and d compare the results obtained by the Rietveld method with those from texture data analysis and Bragg edge neutron transmission. Details of the experiments and data analysis process have been reported in [1].

Further, the results highlight the potential of using single peak pole figure data for quantitative phase analysis with high accuracy (figure b). The methods based on neutron diffraction and neutron transmission both show promising results for a quantification of the strain induced martensite in ADI and it is anticipated that they will become powerful tools for phase quantification in general.

[1] X. H. Li et al., *Multi-scale phase analyses of strain-induced martensite in austempered ductile iron (ADI) using neutron diffraction and transmission techniques*, *J. Mater. Sci.* 56, 5296 (2021)

DOI: 10.1007/s10853-020-05619-x



(a) Neutron diffraction pattern of ADI austempered at 350°C and compressed to 35% strain level as an example. (b) Comparison of the Rietveld method and texture data analysis in martensite phase quantification. The ADI samples with 0 wt.% Ni content and austempered at 350°C were compressed to different strain levels between 0% and 45%. (c) (d) Comparison of the Rietveld method and BET spectra analysis and BET imaging with 2 different wavelengths in martensite phase quantification using ADI samples with 1.5 wt.% Ni content.

Neutron depth profiling on silicon-graphite battery electrodes

E. Moyassari¹, L. Streck¹, N. Paul², M. Trunk², R. Neagu³, C.-C. Chang⁴, S.-C. Hou⁵, B. Märkisch³, R. Gilles², A. Jossen^{1,6}

¹Institute of Electrical Energy Storage Technology (EES), TUM School of Engineering and Design, Technical University of Munich, Munich, Germany; ²Heinz Maier-Leibnitz Zentrum (MLZ), Technical University of Munich, Garching, Germany; ³Physics Department, Technical University of Munich, Garching, Germany; ⁴Department of Greenery, National University of Tainan, Tainan, Taiwan; ⁵Department of Materials Science and Engineering, National Cheng Kung University, Tainan, Taiwan; ⁶Munich School of Engineering (MSE), Technical University of Munich, Garching, Germany

Neutron Depth Profiling (NDP) quantifies the lithium concentration over the depth of various material matrices. Here, the lithium profiles in silicon-graphite (SiG) electrodes with varying Si contents were studied. NDP shows the amount and the position of the lithium in the SiGs. The specific capacities and capacity losses increase with greater silicon content. In addition, NDP reveals a homogeneous lithium accumulation over the electrode depth.

Instrumental

The NDP instrument at the PGAA facility of the Heinz Maier-Leibnitz Zentrum allows for the non-destructive near-surface quantification of concentration profiles of light nuclides such as ³He, ⁶Li, ¹⁰B, ¹⁴N, ¹⁷O in various material matrices. Upon neutron capture, these nuclides emit charged particles that traverse through the host material. They lose energy on their pathway and so their depth of production can be determined with high resolution down to tens of nanometers, depending on the sample material. Since ⁶Li is naturally used in lithium-ion batteries, NDP allows for the quantification of the lithium concentration profile in the electrode, complementing electrochemical measurements on the performance of the whole battery.

Summary of results

In this work, the lithium accumulation in SiGs with varying Si contents was studied. The capacity losses ΔQ due to SEI formation for three different SiG compositions measured by the observed capacity reduction of the batteries show that the specific capacities increase with higher Si content. In addition, the measured capacity losses due to SEI formation for different SiGs increases. These results are complemented using NDP, which reveals not only the amount but also the position where the lithium is accumulated in the SiG

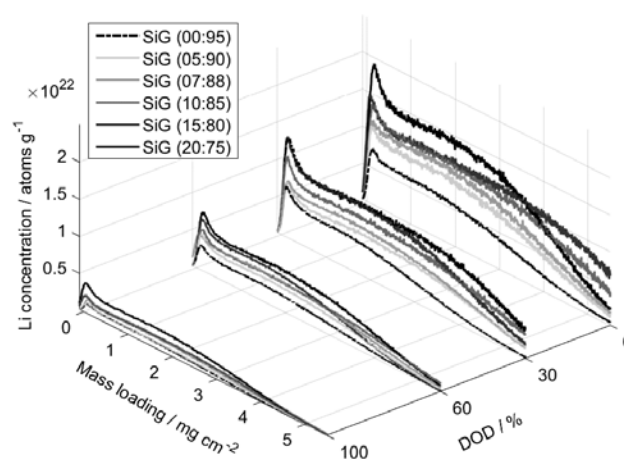
electrodes. In the figure measured depth profiles are shown for different Si contents and depths of discharge (DODs).

For the NDP measurement, a nominal 7.5- μm -thick Kapton[®] foil was placed in front of the detector. This foil is permeable for the ³H particles emitted by the ⁶Li(n, α)³H reaction but it blocks the α particle signal, which would otherwise superimpose on that of the ³H particles, making a quantitative analysis difficult. The concentration profiles reveal the incorporation of reversibly attached lithium together with lithium forming SEI in the electrodes and they agree well with the previously observed capacity losses.

This work is supported by BMBF with grant numbers: 03XP0138B, 03XP0255, 05K19WO8, 05K16WO1, and 03XP0224C.

[1] E. Moyassari et al., *Impact of Silicon Content within Silicon-Graphite Anodes on Performance and Li Concentration Profiles of Li-Ion Cells using Neutron Depth Profiling*, *J. Electrochem. Soc.* 168 (2), 020519 (2021)

DOI: 10.1149/1945-7111/abe1db



Lithium concentration profiles for different SiG electrode compositions at different DODs].

Supramolecular organization of antibacterial humic acid/TiO₂ nanomaterials for water remediationV. Venezia¹, J. Houston², G. Luciani¹, G. D'Errico^{3,4}, L. Paduano^{3,4}, G. Vitiello^{1,4}

¹Department of Chemical, Materials and Production Engineering, University of Naples Federico II, Naples, Italy; ²Jülich Centre for Neutron Science (JCNS) at MLZ, Forschungszentrum Jülich GmbH, Garching, Germany and European Spallation Source (ESS), Lund, Sweden; ³Department of Chemical Sciences, University of Naples Federico II, Naples, Italy; ⁴Center for Colloid and Surface Science (CSGI), Sesto Fiorentino (FI), Italy.

Humic acids (HAs) provide an important bio-source for redox-active materials. Their functional chemical groups are responsible for several properties, such as metal ion chelation, adsorption ability towards small molecules and antibacterial activity, through the generation of Reactive Oxygen Species (ROS). However, the poor selectivity and instability of HAs in solution hinder their application.

A waste-to-wealth strategy for biowaste valorization

A promising strategy for overcoming these disadvantages is a conjugation with an inorganic phase, which leads to more stable hybrid nanomaterials with tunable functionalities. In this study, we demonstrated that HAs/TiO₂ nanomaterials, prepared at different HAs:TiO₂ wt/wt ratios via *in situ* solvothermal strategy, displayed promising antibacterial activity against various pathogens and behave as selective sequestering agents of amoxicillin and tetracycline antibiotics [1].

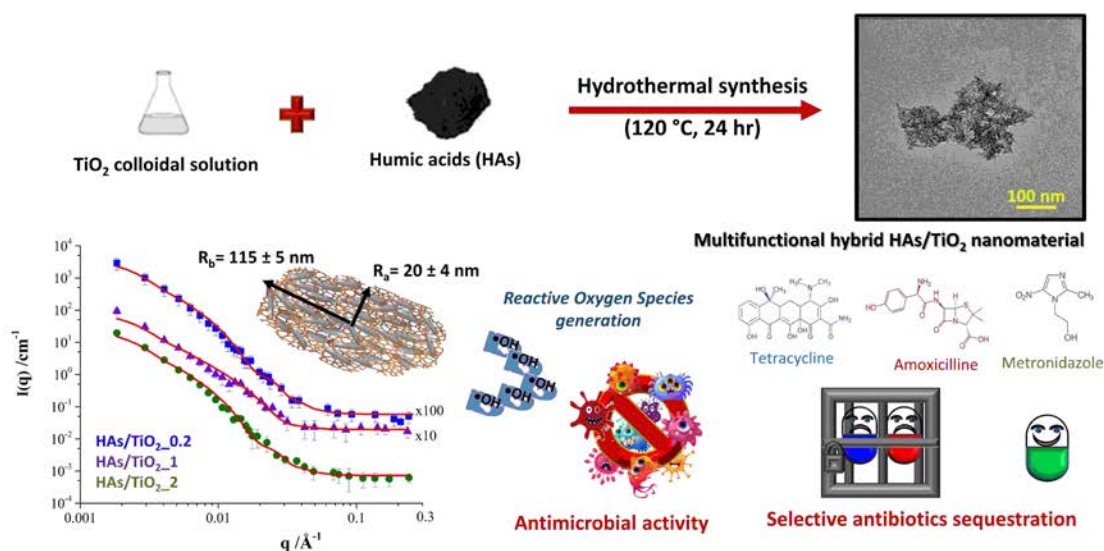
A wide physicochemical investigation shed light on the structure-property-function relationships (see figure) of these nanomaterials. TEM and BET indicated the formation of crystalline TiO₂-based nanoparticles of ~20 nm in size with a rod-like structure and pores of ~70 Å, while spectroscopic analysis confirmed the HAs presence and a close interconnection at the molecular scale with the metal oxide, thus leading to an enhanced ability to generate •OH radicals

in an aqueous environment with respect to bare TiO₂. DLS showed the presence of a single population with a mean size of about 85 ± 5 nm corresponding to stable clusters. In addition, SANS curves were recorded at 25°C on the KSW-2 instrument and modelled through a Feigin model, in which the form factor for an ellipsoid with uniform scattering length density was normalized by the particle volume. The results suggested the formation of ellipsoid nanostructures, with a radius along the rotational axis of the ellipsoid, $R_a = 20 \pm 4$ nm, and a radius perpendicular to the rotational axis of the ellipsoid, $R_b = 115 \pm 5$ nm. Hybrid nanostructures should be formed by small TiO₂ nanoparticles randomly assembled with HAs, as supported by the experimental ρ value ($\sim 2.0 \times 10^{-6} \text{ \AA}^{-2}$) obtained by best fitting and ranged between the ρ values of bare TiO₂ and HAs.

These results suggested that HAs played a key role in the hierarchical organization of HAs/TiO₂ hybrids, furnishing a technological path for the exploitation of biowaste in the design of multifunctional nanomaterials and, also addressing environmental and health problems related to water contamination.

[1] G. Vitiello et al., *Hybrid humic acid/titanium dioxide nanomaterials as highly effective antimicrobial agents against gram(-) pathogens and antibiotic contaminants in wastewater*, *Environ Res.* 193, 110562 (2021)

DOI: 10.1016/j.envres.2020.110562



Description of the synthetic scheme followed to realize multifunctional hybrid HAs/TiO₂ nanomaterial, whose morphological and structural features were confirmed by TEM and SANS analyses.

Frustration in a triangular-lattice artificial spin system studied by GISANS with polarization analysis

A. Glavic¹, P. Pip², K. Zhernenkov³

¹Laboratory for Neutron and Muon Instrumentation, Paul Scherrer Institute (PSI), Villigen, Switzerland; ²Laboratory for Multiscale materials eXperiments, Paul Scherrer Institute, (PSI) Villigen, Switzerland; ³Jülich Centre for Neutron Science at MLZ, Forschungszentrum Jülich GmbH, Garching, Germany

We report on an experiment showing short range magnetic correlations in 2D frustrated nano-magnet arrangements. A 2D single crystal of NiFe nano cylinders on a triangular lattice was measured using GISANS to observe the magnetic structure factor. We found a short range correlated state that is different between symmetric and distorted lattices and is well described by structure factors modeled by Monte-Carlo simulations.

Nanoscale magnet ensembles show complex ordering behavior due to their long-range dipole-dipole interaction. These systems are of particular interest in frustrated arrangements as degeneracy in the nearest neighbor interactions can be lifted by interactions on longer length scales. Neutron scattering is optimal for investigating the expected short-range correlations (static or dynamic). For 2D lattices on surfaces the limited signal of structures around 50 nm can be increased using Grazing Incidence Small Angle Scattering (GISANS).

We have investigated triangular lattices of Ising spins that were predicted to form anti-ferromagnetic stripe domains at low temperatures and glassy correlations when the temperature is increased. Compressing the lattice leads to an increase in the transition temperature and modifies the structure factor. We used NiFe cylinders that have an out-of-plane shape-anisotropy to generate the Ising spins. The particles were grown on gold coated Silicon substrates using electrodeposition after generating a large triangular pattern using electron beam lithography with a = 55 nm lattice spacing, a cylinder diameter of around $D = 27$ nm and height of 120 - 150 nm. The triangular arrangement was either symmetric or 10% distorted.

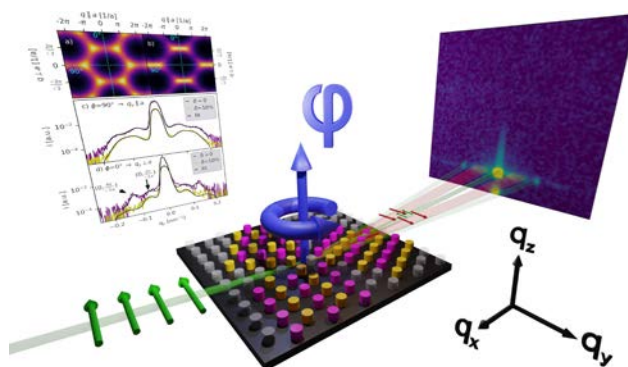
GISANS with polarization analysis was carried out at the MARIA instrument. The samples were rotated around the surface normal (ϕ) to align the lattice with respect to the incident beam.

Record of the magnetic structure factor

Experimentally, structural correlation lengths were above 10 μm . Using fine adjustment of ϕ , we were able, for the most part, to suppress the structural scattering, allowing the measurement of faint and broad magnetic scattering. Polarization analysis confirmed the magnetic nature and out-of-plane moment orientation. Using the higher resolution unpolarized beam with $\phi = 0^\circ$ and $\phi = 90^\circ$, we recorded the magnetic structure factor of both a symmetric and distorted lattice sample. The results were then modeled by the Distorted Wave Born Approximation (DWBA) to extract the magnetic structure factors and compared to the Monte-Carlo models.

[1] P. Pip et al., *Direct observation of spin correlations in an artificial triangular lattice Ising spin system with grazing-incidence small-angle neutron scattering*, *Nanoscale Horizons* 6, 474 (2021)

DOI: 10.1039/D1NH00043H



Sketch of the GISANS experiment with example scattering pattern showing magnetic and nuclear Yoneda lines. Sample rotation ϕ , beam polarization and scattering directions are indicated. In the background, the magnetic structure factor and Yoneda line cuts that were fitted using the model.

Tunable spin-flop transition
in artificial ferrimagnets

N. O. Antropov^{1,2}, E. A. Kravtsov^{1,2}, M. V. Makarova^{1,2}, V. V. Proglyado¹, T. Keller^{3,4}, I. A. Subbotin⁵, E. M. Pashaev⁵, G. V. Prutskov⁵, A. L. Vasiliev^{5,6}, Yu. M. Chesnokov⁵, N. G. Bebenin¹, M. A. Milyaev¹, V. V. Ustinov¹, B. Keimer³, Yu. N. Khaydukov^{3,4,7}

¹Institute of Metal Physics, Ekaterinburg, Russia; ²Ural Federal University, Ekaterinburg, Russia; ³Max-Planck-Institute for Solid State Research, Stuttgart, Germany; ⁴Max Planck Society Outstation at the Heinz Maier-Leibnitz Zentrum (MLZ), Garching, Germany; ⁵National Research Center "Kurchatov Institute", Moscow, Russia; ⁶Moscow Institute of Physics and Technology, Dolgoprudniy, Russia; ⁷Skobeltsyn Institute of Nuclear Physics, Moscow State University, Moscow, Russia

In artificial ferrimagnets (FEMs), the spin-flop transition (SFT) does not require magnetic anisotropies and the transition field can be adjusted by manipulating the exchange coupling in the structure. This was shown using the artificial FEM Fe-Gd, where the usage of Pd spacers allowed us to suppress the transition field by two orders of magnitude.

Spin-flop transition

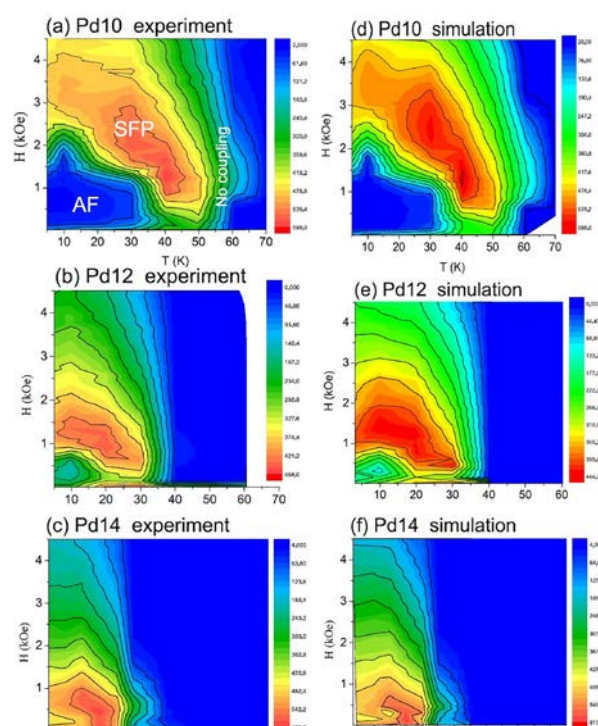
Spin-flop transitions (SFTs) consist of a jump-like reversal of an antiferromagnetic (AF) lattice into a noncollinear state when the magnetic field is increased above a critical value. Potentially, the SFT can be utilized in many applications in the rapidly developing field of AF spintronics. However, the difficulty in using them in conventional antiferromagnets lies in (a) too large switching magnetic fields (b) the need for the presence of a magnetic anisotropy, and (c) the requirement to apply a magnetic field along the correspondent anisotropy axis. Artificial FEMs based on magnetic heterostructures offer the possibility of tuning the SFT field by varying the parameters of ferromagnetic layers and introducing non-magnetic spacers.

Polarized neutron scattering

In the case of artificial FEMs, the magnetic signal from the thin films is heavily polluted by the dia- or paramagnetic signal of the thick substrates. This makes it difficult, if not completely impossible, to use integral magnetometric methods to study the SFTs. Neutron scattering, being a depth-sensitive magnetometric technique, is a widely used method for studying AFs and FEMs. Using PNR at NREX in addition to complementary techniques, we performed a systematic study of the magnetic configuration of [Fe(3.5 nm)/Pd(*t*)/Gd(5.0 nm)/Pd(*t*)]₁₂ heterostructures with *t* = 8 - 28 Å. By

measuring neutron spin-flip scattering, we have detected the presence of a magnetically noncollinear state at temperatures $T < 50$ K in magnetic fields of above $H > 500$ Oe for the samples with $10 \text{ \AA} < t < 14 \text{ \AA}$ (see figure). By using an extended Stoner-Wohlfarth model, we were able to describe the observed transition as a competition of Zeeman energy, bilinear interaction of order of 1 erg/cm^2 , and biquadratic addition of the order of 0.5 erg/cm^2 . The coupling energies can be tuned by varying the thickness of the spacer between 10 and 14 Å leading to the shift of the transition field below the kilo-Oersted range.

[1] N. O. Antropov et al., *Tunable spin-flop transition in artificial ferrimagnets*, *Physical Review B*. V. 104, 54414 (2021)
DOI: 10.1103/PhysRevB.104.054414



(a) - (c) Experimental (H , T) maps of RSF for samples with different Pd spacers. (d) - (f) Simulated maps for these samples.

Spin dynamics study and tunable single-ion anisotropy in multiferroic $\text{Ba}_2\text{CoGe}_2\text{O}_7$ R. Dutta^{1,2}, H. Thoma^{1,2}, I. Radelytskyi², A. Schneidewind², V. Kocsis^{3,4}, Y. Tokunaga^{3,5}, Y. Taguchi³, Y. Tokura^{3,6,7}, V. Hutnanu^{1,2}

¹Institute of Crystallography, RWTH Aachen at MLZ, Garching, Germany; ²Jülich Centre for Neutron Science (JCNS) at MLZ, Forschungszentrum Jülich GmbH, Garching, Germany; ³RIKEN Center for Emergent Matter Science (CEMS), Wako, Saitama, Japan; ⁴Magneto-optical Spectroscopy Research Group, Department of Physics, Budapest University of Technology and Economics, and MTA-BME Lendüle, Budapest, Hungary; ⁵Department of Advanced Materials Science, University of Tokyo, Kashiwa, Japan; ⁶Quantum-Phase Electronics Center, Department of Applied Physics, University of Tokyo, Tokyo, Japan; ⁷Department of Applied Physics, University of Tokyo, Hongo, Tokyo, Japan

The emergence of exotic novel quantum phenomena in strongly correlated electron systems under external stimuli are highly intercorrelated depending on the symmetric exchange, single-ion anisotropy (SIA), and Dzyaloshinskii-Moriya (DM) interactions. Multiferroic $\text{Ba}_2\text{CoGe}_2\text{O}_7$, a square lattice Heisenberg antiferromagnet (SLHAF), ($T_N = 6.7$ K) exhibits a spontaneous induced electric polarization via the spin-dependent d-p hybridization mechanism where the unconventional electromagnon modes appear in the form of strong interplay between SIA, DM and the so called spin-nematic interaction.

Magnetic anisotropy; spin dynamics; multiferroic antiferromagnet

Here, we report a spin-wave study on $\text{Ba}_2\text{CoGe}_2\text{O}_7$ under magnetic fields up to 12 T at 4 K using low-energy inelastic neutron scattering (INS) on the cold-neutron triple-axis spectrometer PANDA at the Heinz Maier-Leibnitz Zentrum (MLZ). Our study presents a detailed picture of the three dimensional nature of the spin dynamics and the two dispersive unconventional electromagnon modes between 2.5 and 4.5 meV. The figure shows the acoustic (T_1) and optical (T_2) modes below 2.5 meV measured at 0 T applied along

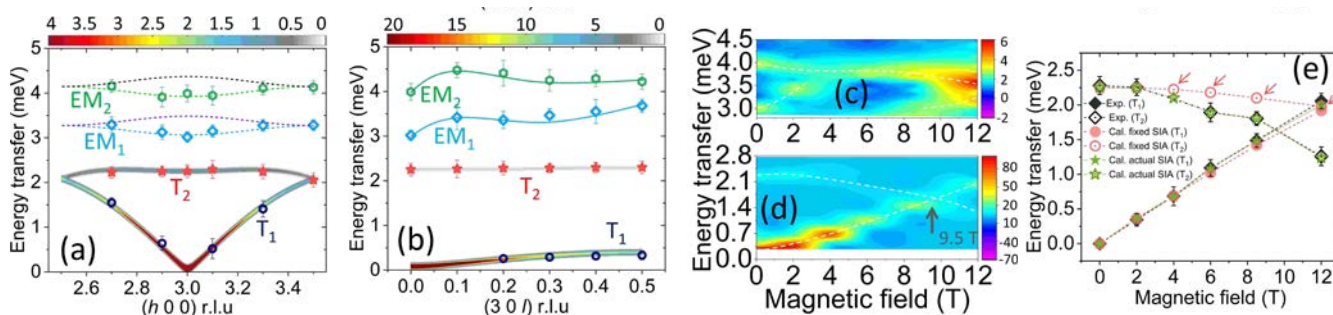
the (a) [010] and (b) [001] directions. Furthermore, the conventional magnons are verified by linear spin wave calculations via the SpinW software presented in figure (a, b).

We have studied the evolution of T_1, T_2 (figure d) and the electromagnon modes (figure c) at the magnetic zone center (300) under high magnetic fields. These measurements reveal the remarkable phenomena of a tunable SIA under magnetic fields in this material [1]. Figure (e) presents a detailed comparison between experimental and theoretical spin wave Eigenvalues of the T_1 and T_2 modes, considering a fixed SIA and the actual variable SIA under magnetic fields.

Our study provides insight into a complex intercorrelation among the easy-plane SIA, the DM interaction, and the external magnetic field in SLHAF materials, leading to interesting key features such as mode crossing near 9.5 T and an anisotropy spin gap of the T_1 and T_2 modes.

[1] R. Dutta et al., Spin dynamics study and experimental realization of tunable single-ion anisotropy in multiferroic $\text{Ba}_2\text{CoGe}_2\text{O}_7$ under external magnetic fields, *Phys. Rev. B* 104, L020403 (2021)

DOI: 10.1103/PhysRevB.104.L020403



(a,b) Calculated magnetic dispersion of $\text{Ba}_2\text{CoGe}_2\text{O}_7$ overplotted with the experimental dispersion points obtained at 4 K and 0 T. (c,d) The evolution of the electromagnon and the T_1, T_2 modes at (300) under magnetic fields. (e) Comparison of energy Eigenvalues of T_1, T_2 modes considering a fixed SIA and the actual SIA under magnetic fields.

Unravelling magnetic field induced quantum spin liquid state in the trillium-lattice $K_2Ni_2(SO_4)_3$

I. Živković¹, V. Favre¹, L. Testa¹, P. Babkevich¹, Y. Su², P. Manuel³, O. Zaharko⁴, H. O. Jeschke⁵, V. Nocolak^{6,7}, J. Reuther^{6,7}, H. M. Rønnow¹

¹Laboratory for Quantum Magnetism, École Polytechnique Fédérale de Lausanne (EPFL), Lausanne, Switzerland; ²Jülich Centre for Neutron Science (JCNS) at MLZ, Forschungszentrum Jülich GmbH, Garching, Germany; ³ISIS Pulsed Neutron and Muon Source, Rutherford Appleton Laboratory, Didcot, United Kingdom; ⁴Laboratory for Neutron Scattering and Imaging, Paul Scherrer Institute (PSI), Villigen, Switzerland; ⁵Research Institute for Interdisciplinary Science, Okayama University, Okayama, Japan; ⁶Dahlem Center for Complex Quantum Systems and Fachbereich Physik, Freie Universität Berlin, Berlin, Germany; ⁷Helmholtz-Zentrum für Materialien und Energie, Berlin, Germany

Quantum spin liquids (QSL) are exotic states of matter that form when strongly frustrated magnetic interactions induce a highly entangled quantum paramagnet far below the energy scale of the magnetic interactions. Three-dimensional cases are rare due to the significant reduction of quantum fluctuations. In this work, we report the experimental realization of the magnetic field induced QSL in the two coupled spin-1 trillium lattices of $K_2Ni_2(SO_4)_3$.

$K_2Ni_2(SO_4)_3$ crystallizes in a cubic unit cell with space group $P213$, in which a three-dimensional network of Ni^{2+} spins form two interconnected trillium lattices, with a Ni-O-S-O-Ni super-superechange mechanism mediating magnetic interactions (see figure a). A substantial geometric frustration can be expected from this novel arrangement of spins. We have carried out comprehensive experimental and computational investigations on the magnetic properties of this compound, including extensive neutron scattering measurements at the DNS instrument at the MLZ. This allows us to obtain compelling evidence for a magnetic field induced QSL behavior.

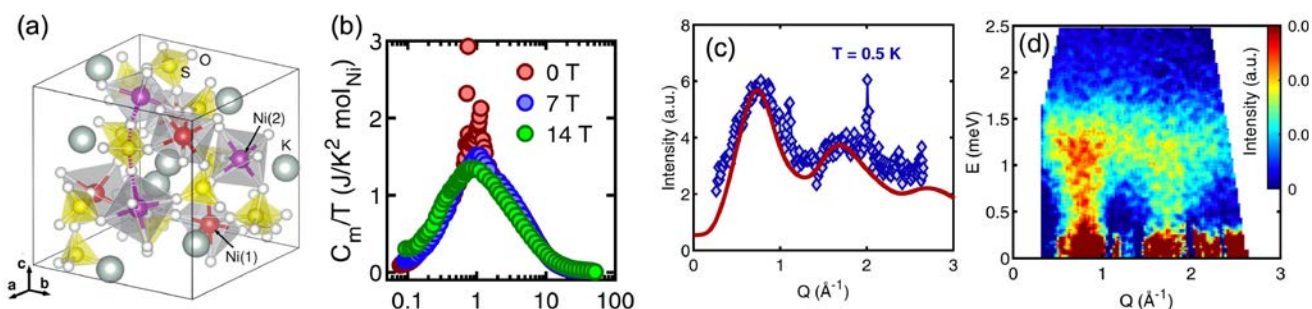
Probing static and dynamic magnetic correlations

In the absence of a magnetic field, magnetization, specific heat, neutron scattering, and muon spin relaxation experiments demonstrate a highly correlated and dynamic state, coexisting with a peculiar, very small static compo-

nent exhibiting a strongly renormalized moment. A magnetic field $B \geq 4$ T diminishes the ordered component and drives the system into a pure QSL state. While the presence of this dominant, dynamic magnetic component can be inferred from the field-insensitive broad hump around 1 K in magnetic specific heat (figure b), its microscopic detection is achieved by both spin-polarized neutron diffraction (figure c) and time-of-flight inelastic neutron scattering (figure d). The upper limit of spin excitations is found to be around 1.8 meV, which agrees well with the estimated strength of magnetic exchange interactions. Furthermore, continuum-like excitations are clearly evident in the spectrum, thus supporting a gapless nature for the QSL state in $K_2Ni_2(SO_4)_3$.

The observed coexistence between fluctuating spins and a small static component that vanishes in a magnetic field could be linked to already developed concepts like field-induced spin liquids in Kitaev-type honeycomb models featuring non-Abelian fractional quasiparticles. The ability to tune its behavior across a quantum critical point (QCP) with a magnetic field into a pristine QSL state is an exciting opportunity that should stimulate further experimental and theoretical studies.

[1] I. Živković et al., *Magnetic Field Induced Quantum Spin Liquid in the Two Coupled Trillium Lattices of $K_2Ni_2(SO_4)_3$* , *Phys. Rev. Lett.* **127**, 157204 (2021)
DOI: 10.1103/PhysRevLett.127.157204



(a) Unit cell of $K_2Ni_2(SO_4)_3$, in which a Ni-O-S-O-Ni super-superechange path contributing to a trillium coupling is marked by dashed lines. (b) T dependence of the magnetic specific heat for several magnetic field values. (c) Pure magnetic scattering pattern derived from the spin-polarized neutron diffraction data taken at 0.5 K at DNS (blue diamonds) and from pseudofermion functional renormalization group simulation (solid line). (d) Time-of-flight inelastic neutron scattering data taken at 0.5 K at DNS.

Magnetic excitations in long-range stripe-ordered $\text{Pr}_2\text{NiO}_{4+\delta}$

A. Maity¹, R. Dutta^{2,3}, A. Marsicano⁴, A. Piovano⁵, J. R. Stewart⁶, W. Paulus⁴

¹Heinz Maier-Leibnitz Zentrum (MLZ), Technical University of Munich, Garching, Germany; ²Institute of Crystallography, RWTH Aachen at MLZ, Garching, Germany; ³Jülich Centre for Neutron Science (JCNS) at MLZ, Forschungszentrum Jülich GmbH, Garching, Germany; ⁴Institut Charles Gerhardt Montpellier, Université de Montpellier, Montpellier, France; ⁵Institut Laue-Langevin, Grenoble, France; ⁶ISIS Neutron and Muon Source, Rutherford Appleton Laboratory, Didcot, United Kingdom.

Magnetic excitations in the stripe-phases of La-based hole-doped 214-nickelates, especially in the Sr-doped ones, have been extensively explored using inelastic neutron scattering studies. In Sr-doped samples, the spin-stripe correlation is relatively short-ranged due to unavoidable disorder introduced by the randomly distributed dopant. However, the results have often been compared with the linear spin wave (LSW) theory based calculations, which assume long-range spin-stripe ordering.

In this work, we have demonstrated the effect of long-range spin-stripe ordering on the magnetic excitations of an O-doped 214-nickelate $\text{Pr}_2\text{NiO}_{4+\delta}$ ($\delta \sim 0.24$), where we find the spin-stripe correlation to be long-range (~ 50 Å) compared to the Sr-doped $\text{Pr}_{2-x}\text{Sr}_x\text{NiO}_4$ (~ 20 Å). For our investigation, we undertook inelastic neutron scattering (INS) measurements using the thermal triple axis spectrometer PUMA at MLZ, IN8 at ILL, and time-of-flight spectrometer MAPS at ISIS.

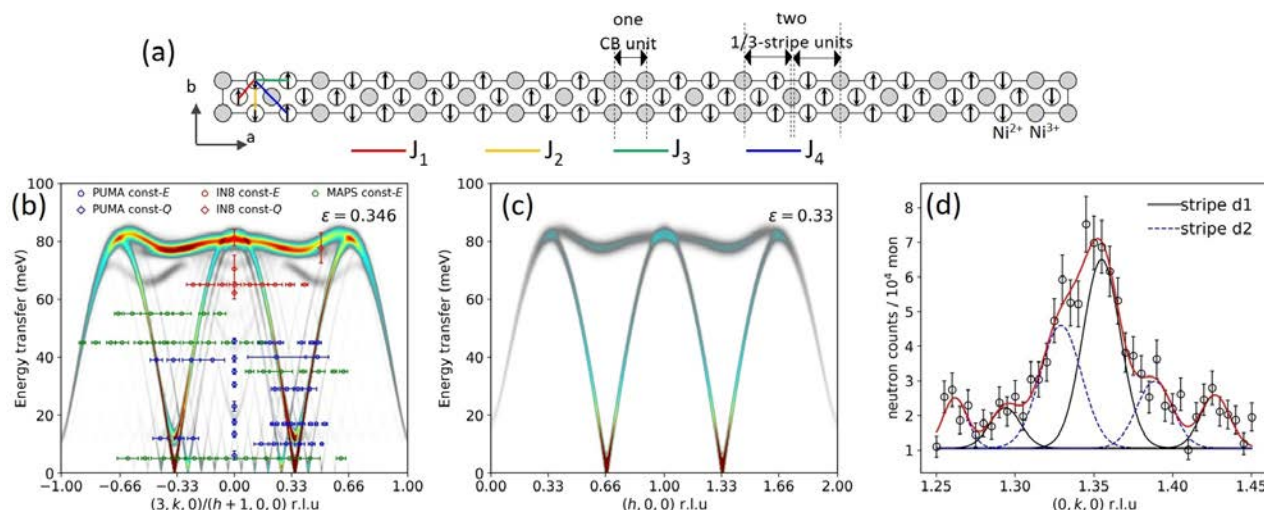
Observation of multiple weak modes

Our investigation presents an intriguing observation of multiple weak modes in the spin wave dispersion of O-doped $\text{Pr}_2\text{NiO}_{4+\delta}$ [1] which, to the best of our knowledge, has never

been reported so far in the 214-type nickelates. We have explained the multiple equidistant ($\Delta\mathbf{q}_m = 0.076$) modes in figure b from the internal periodicity of the discommensurated spin-stripe (DCSS) unit in figure a corresponding to the observed magnetic incommensurability $\mathcal{E} \approx 0.346$ of the long-range spin-stripe ordering. The experimental results show an impressive agreement with the LSW calculation which was performed using SpinW in the DCSS model. The spin wave dispersion is considerably different as compared to the closest commensurate stripe $\mathcal{E} \approx 0.33$ in figure c. Furthermore, magnetic satellites separated by $\Delta\mathbf{q}_m$, which can be inferred from the presence of multiple weak modes, are indeed confirmed in the elastic measurement in figure d.

In summary, our results provide direct experimental evidence of the effect of the long range spin-stripe correlation on the magnetic excitations. Interstitial O plays an important role in establishing such long range spin-stripe ordering. These results will have direct implications in the homologous O-doped 214 cobaltates, and especially in further understanding the effect of interstitial oxygen on T_c and magnetic correlations in O-doped 214 cuprates.

[1] A. Maity *et al.*, *Magnetic excitations in long-range stripe-ordered $\text{Pr}_2\text{NiO}_{4+\delta}$* , *Phys. Rev. B* 103, L100401 (2021)
DOI: 10.1103/PhysRevB.103.L100401



(a) DCSS unit for a single stripe domain along the a -axis corresponding to the spin-stripe incommensurability $\mathcal{E} = 0.346$ obtained from a mixture of $m = 8$ units of $1/3$ stripe and $n = 1$ unit of checkerboard (CB) using the expression $\mathcal{E} = (m + n)/(3m + 2n)$. Exchange interactions are indicated by solid lines in different colors. (b) Spin wave dispersion for $\mathcal{E} = 0.346$ calculated from SpinW using LSW in the above DCSS unit. The measured peak positions from the INS have been overlaid on the calculated dispersion. (c) Calculated spin wave dispersion for the closest commensurate $1/3$ stripe. (d) Elastic scan through the magnetic zone center at $(0, 1.346, 0)$ confirming the multiple magnetic satellites from which the weak modes disperse.

Sign of the Dzyaloshinskii-Moriya interaction in weak ferromagnets disclosed by polarized neutrons

H. Thoma¹, V. Hutanu², H. Deng², V. E. Dmitrienko³, P. J. Brown⁴, A. Gukasov⁵, G. Roth⁶, M. Angst⁷

¹Jülich Centre for Neutron Science (JCNS) at MLZ, Forschungszentrum Jülich GmbH, Garching, Germany; ²Institute of Crystallography, RWTH Aachen University and Jülich Centre for Neutron Science (JCNS) at MLZ, Garching, Germany; ³A. V. Shubnikov Institute of Crystallography, FRSC "Crystallography and Photonics", RAS, Moscow, Russia; ⁴12 Little St Marys Lane, Cambridge, United Kingdom; ⁵Laboratoire Léon Brillouin, CEA-CNRS, CE-Saclay, Gif-sur-Yvette, France; ⁶Institute of Crystallography, RWTH Aachen University, Aachen, Germany; ⁷Jülich Centre for Neutron Science JCNS and Peter Grünberg Institute PGI, JARA-FIT, Forschungszentrum Jülich GmbH, Jülich, Germany

Polarized neutron diffraction (PND) is a powerful technique that can provide detailed insight into magnetic ordering. Here, we report on the application of this technique to the long-standing problem of determining the absolute sign of the Dzyaloshinskii-Moriya interaction (DMI) in relation to the crystal structure. Using the proposed PND method, the DMI sign of different prototypical weak ferromagnets is revealed for the first time.

Identifying, understanding, and predicting fundamental magnetic interactions in magnetic materials is an essential step toward their utilization in novel devices. One of these basic interactions is the Dzyaloshinskii-Moriya interaction (DMI), a type of coupling between neighboring spins that slightly tilts them when they would otherwise tend to align. Although this DMI-induced canting is usually small, it can lead to a tiny net magnetic moment in so-called weak ferromagnetic (WFM) materials. The direction of this WFM moment, which is coupled to the collinear spin direction by the sign of the DMI, has a significant impact on spintronic applications and topological materials. Here, we establish polarized neutron diffraction (PND) as an efficient technique for determining the absolute sign of the DMI in bulk materials.

Application of PND to determine the DMI sign

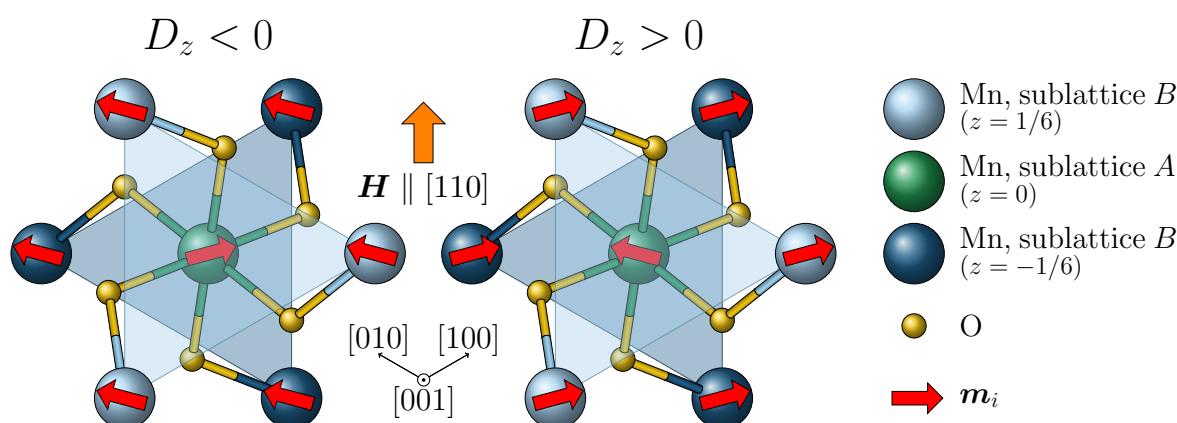
By performing a detailed symmetry analysis, we were able to identify for each compound studied the two possible mag-

netic moment configurations corresponding to a positive and negative DMI sign [1]. This is illustrated for MnCO_3 in the figure. As PND is sensitive to the phase difference between the nuclear and magnetic structure, it can be used to differentiate between the two configurations and thus to determine the absolute sign of the DMI. On performing a PND experiment on MnCO_3 at the single crystal diffractometer POLI, we found a negative DMI sign, which is in agreement with recent resonant magnetic synchrotron scattering results, thereby validating the method.

Applying the PND technique to the prototypical weak ferromagnet $\alpha\text{-Fe}_2\text{O}_3$ (hematite) and further WFM compounds with various crystal symmetries as well, we were able to unambiguously determine their DMI sign for the first time, demonstrating the generality of our method. Additionally, we were in a position to show that the measurement of only a single suitable Bragg reflection can be sufficient to identify the DMI sign, making the PND method particularly efficient to use. Our findings are supported by *ab-initio* calculations, reproducing the experimental results.

[1] H. Thoma et al., *Revealing the Absolute Direction of the Dzyaloshinskii-Moriya Interaction in Prototypical Weak Ferromagnets by Polarized Neutrons*, *Phys. Rev. X* 11, 011060 (2021)

DOI: 10.1103/PhysRevX.11.011060



The two possible magnetic moment configurations of the canted antiferromagnetic sublattices in MnCO_3 for a positive and negative D_z component of the DMI vector and an applied magnetic field in the crystalline $[110]$ direction, aligning the WFM moment. By PND measurements at POLI, the left configuration and thus a negative DMI sign was experimentally determined.

Soliton-mediated magnetic reversal in an all-oxide-based synthetic antiferromagnetic superlattice

K. Zhang^{1,2}, K. Zhernenkov², T. Saerbeck³, A. Glavic⁴, L. Qu¹, C. J. Kinane⁵, A. J. Caruana⁵, E. Hua¹, G. Gao¹, F. Jin¹, B. Ge⁶, F. Cheng⁶, S. Pütter², A. Koutsioubas², S. Mattauch², T. Brückel⁷, Y. Su², L. Wang¹, W. Wu^{1,8}

¹Hefei National Laboratory for Physical Sciences at Microscale, University of Science and Technology of China, Hefei, China; ²Jülich Centre for Neutron Science (JCNS) at MLZ, Forschungszentrum Jülich GmbH, Garching, Germany; ³Institut Laue-Langevin, Grenoble, France; ⁴Laboratory for Neutron and Muon Instrumentation, Paul Scherrer Institute, Villigen, Switzerland; ⁵ISIS Neutron and Muon Source, Science and Technology Facilities Council, Rutherford Appleton Laboratory, Harwell Oxford, Didcot, United Kingdom; ⁶Institutes of Physical Science and Information Technology, Anhui University, Hefei, China; ⁷Jülich Centre for Neutron Science (JCNS-2) and Peter Grünberg Institute (PGI-4), Forschungszentrum Jülich GmbH, Jülich, Germany; ⁸Anhui Key Laboratory of Condensed Matter Physics at Extreme Conditions, High Magnetic Field Laboratory (HFIPS), Anhui, Chinese Academy of Sciences, Hefei, China

In this work, we investigated the layer-resolved magnetic reversal mechanism in the $\text{La}_{2/3}\text{Ca}_{1/3}\text{MnO}_3/\text{CaRu}_{1/2}\text{Ti}_{1/2}\text{O}_3$ superlattice via polarized neutron reflectivity. The magnetization reversal of $\text{La}_{2/3}\text{Ca}_{1/3}\text{MnO}_3$ layers is mediated by the nucleation, expansion, and shrinkage of a magnetic soliton. This magnetic reversal process creates a reversed magnetic configuration after a simple field cycling, which can enable vertical data transfer within the superlattice.

Towards three-dimensional storage elements with high data density

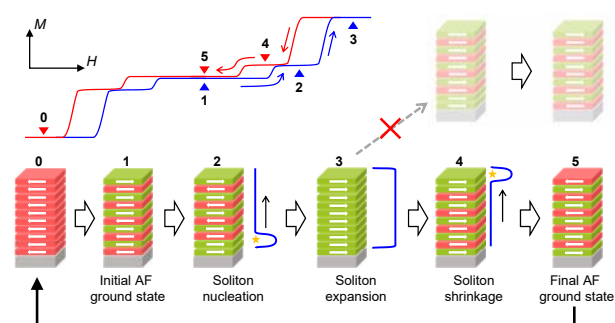
Recently, an all-oxide-based synthetic antiferromagnet (SAF) was realized in an epitaxially-grown manganite/ruthenate superlattice (SL). In this epitaxial system, ferromagnetic $\text{La}_{2/3}\text{Ca}_{1/3}\text{MnO}_3$ (LCMO) layers were separated by non-magnetic $\text{CaRu}_{1/2}\text{Ti}_{1/2}\text{O}_3$ (CRTO) spacers, which provide interlayer exchange coupling (IEC) and induce an anti-parallel alignment of the magnetic moments in the LCMO layers. During the cycling of the external magnetic field (H), the LCMO/CRTO SL gradually changes from the antiferromagnetic ground state, via an intermediate state, to the saturated ferromagnetic state. However, the layer-resolved magnetization reversal mechanism of the all-oxide SAF studied remains elusive.

In this work [1], using polarized neutron reflectivity as a probe, we have determined the layer-resolved magnetic structure of the LCMO/CRTO SL at various states, and therefore revealed the microscopic magnetization reversal mechanism of the LCMO/CRTO SAF during external H cycling. Interestingly, we discovered that the layer-resolved magnetic reversal process is mediated by the nucleation, expansion, and shrinkage of a magnetic soliton. The physical origin of this unique evolution of magnetic configurations could be attributed to a spatial variation of in-plane magnetic anisotropy (IMA) along the out-of-plane direction. As a result, this unique magnetic reversal process creates a

reversed magnetic configuration after a simple field cycling, which can be seen as a vertical data transfer within the SAF. Our work revealed the high sensitivity of reversal sequence to the strength ratio between IMA and IEC in an all-oxide SAF. The IMA and IEC in oxide multilayers can be effectively modulated via strain, layer thickness, chemical doping, interfacial structure, etc. Therefore, it is technically promising to engineer the reversal process of oxide SAFs at microscopic scales and incorporate them in spintronic devices with tailored functionalities. Accordingly, our work provides a new strategy for designing 3-dimensional antiferromagnetic spintronic memory and logic devices via all-oxide-based SAFs.

The PNR measurements were conducted on the polarized neutron reflectometer MARIA at MLZ, Germany, D17 at the ILL, France, and POLREF at ISIS, UK.

[1] K. Zhang et al., *Soliton-Mediated Magnetic Reversal in an All-Oxide-Based Synthetic Antiferromagnetic Superlattice*, *ACS Applied Materials & Interfaces* 13, 20788 (2021)
DIO: 10.1021/acsami.1c02506



Layer-resolved magnetic reversal process of the LCMO/CRTO SAF. Some representative magnetic stages (0 to 5) are labeled by triangles at the schematic M-H loop at the top-left panel, and the layer-resolved magnetic configurations are shown in the bottom panel. The evolution from stage 2 to 4 can be seen as soliton nucleation, expansion, and shrinkage. Therefore, a vertical data transfer is realized from stage 1 to stage 5 after a simple field cycling.

Interaction of nanoparticles with lipid films: the role of symmetry and shape anisotropy

L. Caselli¹, A. Ridolfi^{1,2}, G. Mangiapia³, P. Maltoni¹, J.-F. Moulin³, D. Berti¹, N.-J. Steinke⁴, E. Gustafsson⁵, T. Nylander^{6,7}, C. Montisa¹

¹Department of Chemistry, University of Florence and CSGI, Florence, Italy; ²ISMN-CNR and CSGI, Bologna, Italy; ³German Engineering Materials Science Centre (GEMS) at MLZ, Helmholtz-Zentrum hereon GmbH, Garching, Germany; ⁴ISIS Neutron and Muon Source, Science and Technology Facilities Council, Rutherford Appleton Laboratory, Harwell Oxford, Didcot, United Kingdom; ⁵Department of Chemistry, Uppsala University, Uppsala, Sweden; ⁶Department of Chemistry, Physical Chemistry, Lund University, Lund, Sweden; ⁷NanoLund, Lund University, Institute of Advanced Neutron and X-Ray Science - LINXS, Lund, Sweden

The chemical and biological interactions of nanoparticles with biomolecules and biological interfaces (such as cell membranes) are important to understanding their bioactivity and cytotoxicity. Among other things, the symmetry/shape anisotropy of both nanomaterials and biological interfaces play a role which has not been investigated in great detail. A multitechnical approach has proved fruitful in clarifying many aspects regulating such interaction.

The interaction of nanoparticles (NPs) with biomembranes determines their therapeutic efficacy and harmful effects on human health. In this context, the role of “symmetry” at the nano-bio interface, which must be related both to the shape of NPs and the nanostructure of the membrane, still represents a controversial problem which is far from being fully understood at the present time.

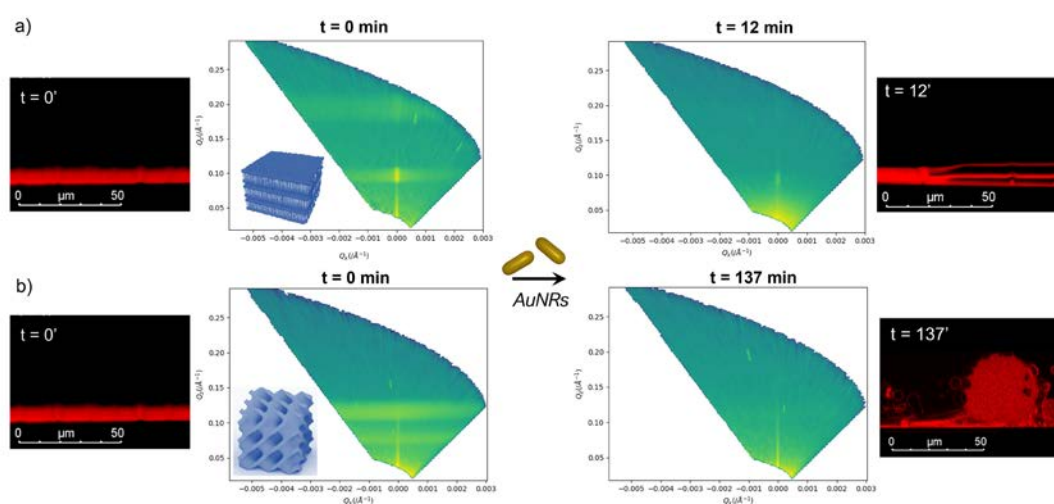
Here, we explore the mutual interplay between the shape of NPs and the nanoscale geometry of the membrane. We compared gold nanospheres and nanorods in their interaction with biomimetic solid-supported lipid films of different nanostructure: From “flat” (2D-symmetrical) membranes, mimicking the most common geometry of biomembranes, to liquid-crystalline “cubic” membranes of 3D symmetry, which develop in cells under pathological conditions.

NP/films interaction: a multiscale characterization

The combination of Neutron Reflectometry (NR) and GISANS, performed at REFSANS (MLZ) and ISIS, with Confocal Laser Scanning Microscopy (CSLM) enabled the characterization of the NPs/membrane interaction at different length scales, from the nano- to the micro-scale. Through NR, we found that the structural stability of the membrane towards NPs depends on the topology of both the lipid film and the NPs, where a higher symmetry gave higher stability (figure). In addition, CSLM showed that NPs interact with model membranes through two distinct mechanisms, triggered by the nanostructure of the lipid films (see figure insets).

The results broaden the current knowledge of nano-bio interactions and provide insights into the biological function of phase transitions as a response strategy to the exposure of NPs.

[1] L. Caselli et al., *Interaction of nanoparticles with lipid films: the role of symmetry and shape anisotropy*, *Phys. Chem. Chem. Phys.*, 24, 2762 (2022), 08 Oct 2021 added to the Royal Society of Chemistry's journals.
DOI: 10.1039/D1CP03201A



(Q_z, Q_x) representations of the off-specular scattering of a lamellar (panel a) and a cubic film (panel b) in absence (left) and at different times from the injection of AuNRs (right) (acquisition in H_2O). As insets, Confocal Laser Scanning Microscopy images (lateral view) are also shown, representing the lamellar and cubic films, labelled with a fluorescent hydrophobic dye, in absence (left) and at different times from the addition of AuNRs.

Employing multiresponsive thin films for ternary nanoswitches

C. Geiger¹, L. P. Kreuzer^{1,2}, J. Reitenbach¹, P. Wang¹, J. E. Heger¹, T. Widmann¹, A. Vagias^{1,2}, C. Henschel³, V. Hildebrand³, G. Mangiapia⁴, M. Haese⁴, J.-F. Moulin⁴, C. M. Papadakis⁵, A. Laschewsky^{3,6}, P. Müller-Buschbaum^{1,2}

¹Physics Department E13, Technical University of Munich, Garching, Germany; ²Heinz Maier-Leibnitz Zentrum (MLZ), Technical University of Munich, Garching, Germany; ³Institute of Chemistry, University of Potsdam, Potsdam-Golm, Germany; ⁴German Engineering Materials Science Center (GEMS) at MLZ, Helmholtz-Zentrum hereon GmbH, Garching, Germany; ⁵Physics Department E59, Technical University of Munich, Garching, Germany; ⁶Fraunhofer Institute for Applied Polymer Research, Potsdam-Golm, Germany

Thin films of multiresponsive polymers are highly sensitive to the surrounding atmosphere. A delicate balance between hydrophilicity and hydrophobicity, and the application of external stimuli make it possible to switch between distinct film states. Neutron reflectometry at REFSANS facilitated the tracking of solvation and exchange processes, which proved essential to understanding the functionality of such nanoswitches.

Multiresponsive polymers have sparked the interest of the soft matter community as a means of creating switchable systems. Most existing research revolves around experiments or computational models featuring a large solvent/polymer ratio. To explore multiresponsive polymers in the presence of a limited amount of solvent, the swelling and contraction of thin films within solvent vapors was investigated. Time-of-flight neutron reflectometry (TOF-NR) at REFSANS served as a tool to study the accessible equilibrium and transitional film states within these nanoscale polymer switches.

A balance of intrinsic properties and external stimuli

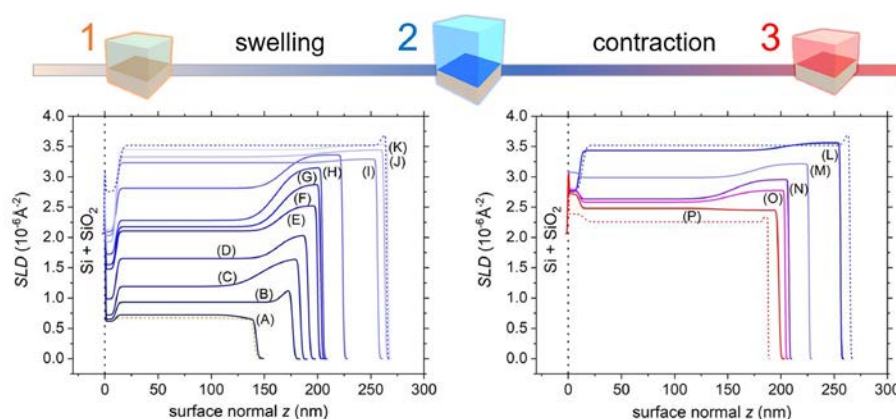
Multiresponsive polymer films feature a large number of distinct film states, due to the strong conformational changes of the polymer that result from individual or combined external stimuli. Hydrophilicity and hydrophobicity of the functional moieties, cononsolvency, temper-

ature, and the effects of salts all influence the solvation. While this provides a chance to extend the functionality of applications, special attention is required when characterizing these systems. Tracking the film thickness and evolving solvent content is essential, and achieved using TOF-NR. A set of SLD profiles obtained during the swelling and solvent exchange of PMMA-*b*-PNIPMAM films is shown in the figure. PNIPMAM, as a lower critical solution temperature (LCST) type block, makes a large contribution to the responsive behavior, while the influence of PMMA, as a hydrophobic block, is small. Three equilibrium states were found using the cononsolvency stimulus [1].

In another study, PSBP-*b*-PNIPMAM, a system with increased complexity, is investigated. This polymer features an orthogonally dual thermoresponsive behavior, with PSBP being a zwitterionic, upper critical solution temperature (UCST) type block attached to a LCST type PNIPMAM block. Four states are found at changing environment conditions. The addition of NaBr (Br⁻ as chaotropic anion), allows tuning of the switching process as well as the solvent content and film thickness in the equilibrium states.

[1] C. Geiger et al., *Ternary Nanoswitches Realized with Multiresponsive PMMA-*b*-PNIPMAM Films in Mixed Water/Acetone Vapor Atmospheres*, *Adv. Eng. Mater.* (23), 2100191 (2021)

DOI: 10.1002/adem.202100191



Schematic experiment (top) and SLD profiles (bottom) obtained from time-resolved TOF-NR data of thin responsive PMMA-*b*-PNIPMAM films during the swelling process in D₂O vapor (lower left, letters A through K) and the contraction process to mixed D₂O/acetone vapor (lower right, letters L through P). In total, three distinct thin film states (1, 2, and 3) are achieved.

Nanoscale aqueous morphologies and hydration in thermoresponsive double hydrophilic block copolymers

A. Vagias¹, A. Papagiannopoulos², L. P. Kreuzer^{1,3}, D. Giaouzi², S. Busch⁴, S. Pispas², P. Müller-Buschbaum^{1,3}

¹Heinz Maier-Leibnitz Zentrum (MLZ), Technical University of Munich, Garching, Germany; ²Theoretical and Physical Chemistry Institute, National Hellenic Research Foundation, Athens, Greece; ³Chair for Functional Materials, Physics Department, Technical University of Munich, Garching, Germany; ⁴German Engineering Materials Science Center (GEMS) at MLZ, Helmholtz-Zentrum hereon GmbH, Garching, Germany

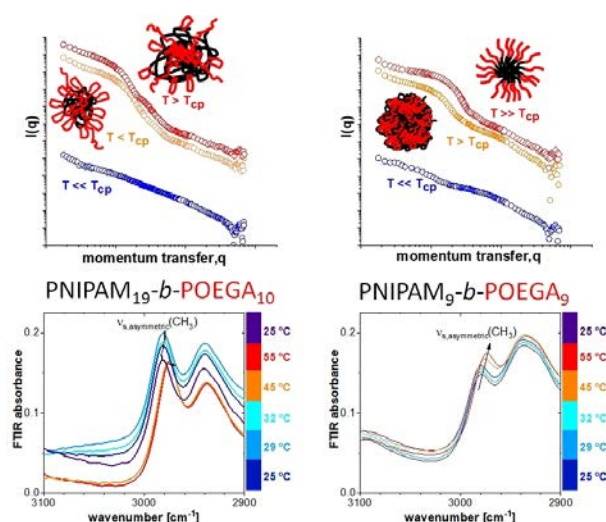
Small angle neutron scattering at SANS-1 and FTIR experiments at the TUM made it possible to characterize the nanoscale aqueous morphologies of double hydrophilic thermoresponsive block copolymers over a broad range of length scales (SANS) as well as the chain hydration (FTIR) at the molecular level as a function of temperature. The proposed strategy is a mandatory control study for tuning the applicability of such templates as smart drug delivery scaffolds.

Double hydrophilic block copolymers represent smart responsive materials successfully utilized in catalysis, biomineralization and drug encapsulation. In thermoresponsive double hydrophilic block copolymers, the temperature-driven alteration in hydrophilicity difference between the two blocks leads to spontaneous self-assembly. PEO-*b*-PNIPAM is a well-known system successful in drug encapsulation whose morphologies have been well-investigated. However, hydrophilic polymers with stealth properties like PEO but more comb-shaped architecture have emerged such as POEGA. PNIPAM-*b*-POEGA has succeeded in encapsulating hydrophobic drugs (indomethacin) in dilute aqueous solutions. By complementing information from scattering and spectroscopic techniques, one can obtain a thorough understanding of the self-assembled characteristics of PNIPAM-*b*-POEGA nanostructures. A detailed overview of the nanostructural organization and molecular hydration as a function of temperature was obtained by small angle neutron scattering (SANS) at SANS-1 and FTIR, respectively, on the aqueous self-assemblies of those thermoresponsive double hydrophilic block copolymers functioning as drug encapsulating scaffolds.

Interplay between end groups, block length asymmetry, hydration and polymer morphologies

The figure presents the set of SANS macroscopic cross-sections together with FTIR spectra at different temperatures. At intermediate length scales, SANS modeling suggests that upon heating the hydrophobic end groups at the end of POEGA blocks in the asymmetric system induce a backfolding of the POEGA blocks towards the micellar PNIPAM-rich core. The symmetric system on the other hand forms spherical structures which transform to crew-cut shaped core-shell micelles upon further temperature increase. From a molecular perspective, the asymmetric stretching vibration of the isopropyl group in the PNIPAM block seen by FTIR is a sensitive probe of hydration alterations upon heating and expresses sharp (asymmetric) and gradual (symmetric) wavenumber shifts.

[1] A. Vagias et al., *Effects of Polymer Block Length Asymmetry and Temperature on the Nanoscale Morphology of Thermoresponsive Double Hydrophilic Block Copolymers in Aqueous Solutions*, *Macromolecules* 54, 15, 7298 (2021)
DOI: 10.1021/acs.macromol.1c01005



Schematic of SANS macroscopic cross-sections (upper row) and FTIR spectra (lower row) for PNIPAM-*b*-POEGA solutions in D₂O at different temperatures (*T*) for asymmetric (left) and symmetric (right) polymer blocks. Block length asymmetry affects the *T*-dependent nanostructures for *T* values slightly below the nominal cloud point (*T*_{cp}), as well as the isopropyl stretching vibration ($\nu_{\text{CH}_3, \text{asymmetric}}$) reflecting dehydration differences at molecular scale.

Structural organization of cardiolipin-containing vesicles mimicking bacterial cytoplasmic membranes

A. Luchini¹, D. Cavasso^{2,3}, A. Radulescu⁴, G. D'Errico^{2,3}, L. Paduano^{2,3}, G. Vitiello^{3,5}

¹Niels Bohr Institute, University of Copenhagen, Copenhagen, Denmark; ²Department of Chemical Sciences, University of Naples Federico II, Naples, Italy; ³Center for Colloid and Surface Science (CSGI), Sesto Fiorentino (FI), Italy; ⁴Jülich Centre for Neutron Science (JCNS) at MLZ, Forschungszentrum Jülich GmbH, Garching, Germany; ⁵Department of Chemical, Materials and Production Engineering, University of Naples Federico II, Naples, Italy

The bacterial cytoplasmic membrane is the innermost bacterial membrane and is mainly composed of three different phospholipid species, i.e., phosphoethanolamine (PE), phosphoglycerol (PG), and cardiolipin (CL). PG and CL are responsible for the negative charge of the membrane and are often the targets of cationic antimicrobial agents, which induce membrane lysis and therefore the death of the bacteria. However, because of the growing resistance toward antibacterial drugs, understanding the structural and dynamic properties of the bacterial cytoplasmic membrane can provide important input for the design of new and more efficient antimicrobial agents. In this context, we have established a detailed structural and dynamic characterization of PE/PG/CL vesicle suspensions with different CL concentrations, i.e., 10 and 20 mol%, thus representing a better mimic of the bacterial cytoplasmic membrane [1].

Cardiolipin tunes membrane fluidity and lipid packing

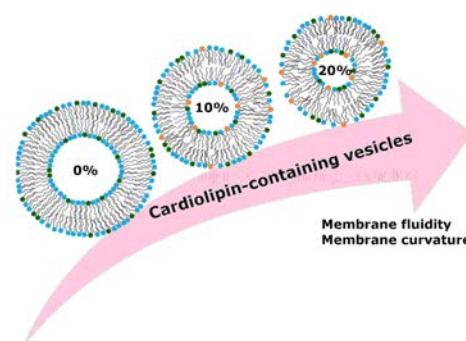
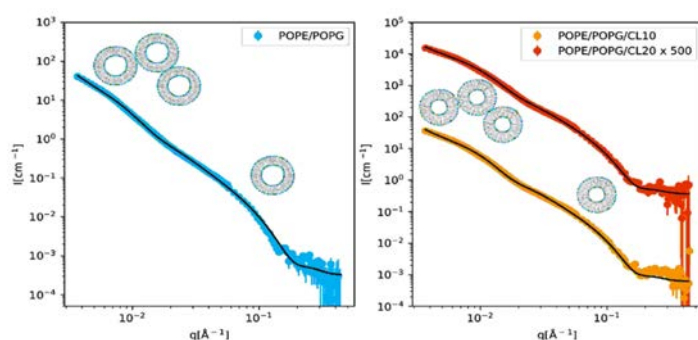
Dynamic Light Scattering (DLS) data and Small-Angle Neutron Scattering (SANS) curves recorded at 25°C on the KWS-2 instrument demonstrated that all the characterized vesicle suspensions turned out to be composed of uni-lamellar vesicles together with larger vesicle aggregates, i.e., of 500 - 580 Å hydrodynamic radii. The presence of CL in the POPE/POPG mixture produced a systematic decrease of

the vesicle core radius and therefore an increment of the membrane curvature. This evidence is consistent with the sorting of CL in high-curvature regions in bacterial membranes previously reported. CL is also responsible for the increment of the bilayer thickness, in the presented cases of ~3 Å. On the other hand, Electron Paramagnetic Resonance (EPR) spectroscopy furnished information on the impact of CL on the membrane fluidity and lipid packing. At 10 mol%, CL mainly perturbs the packing and fluidity of the acyl chain in the inner region of the bilayer, while the effect propagates to the entire acyl chain region when the CL concentration is increased to 20 mol%.

Finally, the study suggested that CL induces the formation of thicker bilayers, which exhibit higher curvature and are overall more fluid (see figure), thus confirming the proposed role of CL in preventing the membrane penetration by drugs and enhancing the membrane stability toward the increased curvature often produced by the drug–membrane interaction. From this point of view, the characterized bacterial membrane models can be used as relevant lipid platforms for testing antimicrobial drug activity.

[1] A. Luchini *et al.*, *Structural organization of cardiolipin-containing vesicles as models of the bacterial cytoplasmic membrane*, *Langmuir* 37, 8508 (2021)

DOI: 10.1021/acs.langmuir.1c00981



SANS curves of POPE/POPG (a) and POPE/POPG/CL at different CL content (b), and schematic description of the CL effect on the fluidity and curvature of phospholipid vesicles.

The charge transport mechanism in Brønsted-acidic protic ionic liquid/water systems – an NMR and QENS study

J. Lin^{1,2}, D. Noferini^{3,4}, E. Veroutis^{5,6}, C. Korte^{1,2}, O. Holderer³

¹Institute of Energy and Climate Research - Fuel Cells (IEK-14), Forschungszentrum Jülich GmbH, Jülich, Germany; ²RWTH Aachen University, Aachen, Germany; ³Jülich Centre for Neutron Science (JCNS) at MLZ, Forschungszentrum Jülich GmbH, Garching, Germany; ⁴European Spallation Source ERIC, Lund, Sweden; ⁵Forschungszentrum Jülich GmbH, Institute of Energy and Climate Research - Fundamental Electrochemistry (IEK-9), Jülich, Germany; ⁶RWTH Aachen University, Institute of Technical and Macromolecular Chemistry, Aachen, Germany

A protic ionic liquid (PIL), 2-Sulfoethylmethylammonium triflate [2-Sema][TfO] is considered as a potential new proton conducting electrolyte for future polymer membrane fuel cells capable of ambient air operation above 100°C. Quasi-elastic neutron scattering (QENS) and PFG-NMR make it possible to study proton mobility with the underlying hopping and vehicular motions.

Protic ionic liquids as electrolytes

Polymer electrolyte fuel cells (PEFCs) operating above 100°C offer some advantages over the typical Nafion type PEFCs with operating temperatures at around 80°C, for example easier water and heat management and fewer CO contamination problems. Protic ionic liquids (PILs) may play an interesting role in the development of high temperature PEFCs due to properties such as their good conductivity and low flammability. Using PILs in PEFCs requires a good understanding of the proton conduction mechanism, e.g. vehicular transport vs. hopping transport, and the role of water in the hygroscopic PILs with its influence on viscosity and conductivity. Quasi-elastic neutron scattering (QENS) at SPHERES provides insight into molecular length scales on the proton motion, while pulse-field gradient (PFG-) NMR measures diffusion on larger length scales. The length

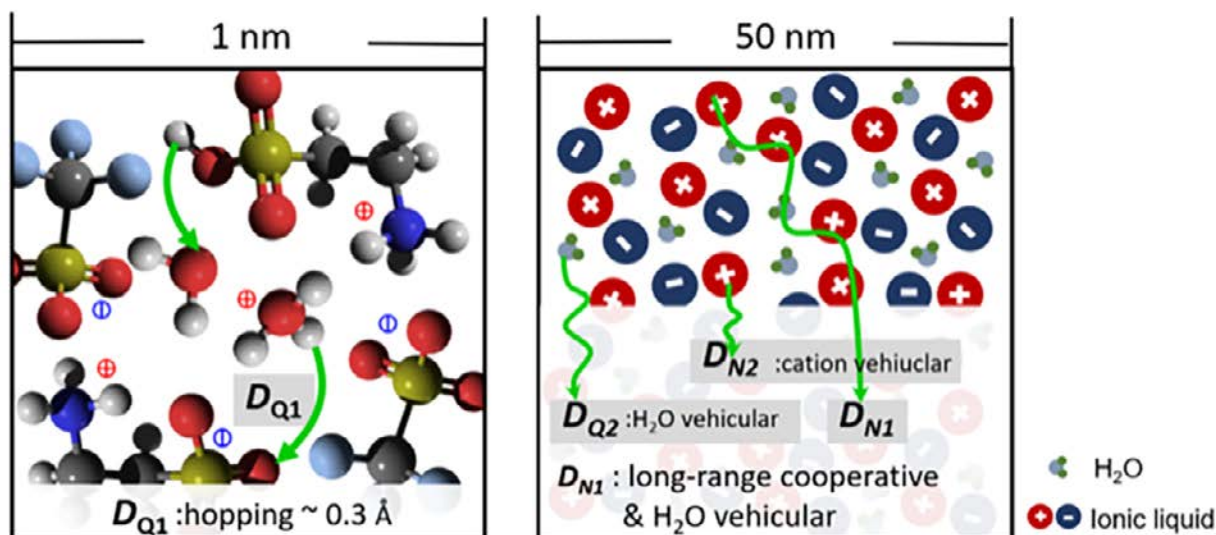
scale dependent analysis helps in understanding the different contributions to the macroscopic conductivity.

Taking a close look into diffusion processes

The figure shows a schematic representation of the equimolar [2-Sema][TfO]-H₂O mixture and the diffusion coefficients on length scales of ~1 nm and 50 nm. D_{Q1} is the diffusion coefficient of the (short range) hopping motion. The jump length of the proton hopping motion deduced from QENS is around 3 Å. D_{N1} corresponds to a population weighted average between the hopping of SO₃H/H₂O protons and a vehicular diffusional motion of H₂O molecules from PFG-NMR. D_{N2} represents the vehicular transport of the [2-Sema]⁺ cation. The slow neutron backscattering components D_{Q2} correspond to the diffusion of the smaller H₂O molecules.

The proton hopping and cooperative transport are expected to have an impact on the conductivity and indicate the potential of the high acidic PILs as candidates for electrolytes in PEFCs operating at elevated temperatures.

[1] J. Lin et al., *The charge transport mechanism in Brønsted-acidic protic ionic liquid/water systems: An NMR and QENS study*, *J. Mol. Liq.* 343, 117712 (2021)
DOI: 10.1016/j.molliq.2021.117712



Schematic representation of the equimolar [2-Sema][TfO]-H₂O mixture and the diffusion coefficients on the relevant nanometric length scales from QENS (D_{Q1} , proton hopping; D_{Q2} , vehicular H₂O motion) and PFG-NMR (D_{N1} , weighted average of long range cooperative of SO₃ H/H₂O and H₂O vehicular; D_{N2} vehicular cation motion).

Co-non-solvency of a responsive polymer – the role of hydration and bulk water dynamics

B.-J. Niebuur¹, W. Lohstroh², C.-H. Ko¹, M.-S. Appavou³, A. Schulte⁴, C. M. Papadakis¹¹Physics-Department, Technical University of Munich, Garching, Germany; ²Heinz Maier-Leibnitz-Zentrum (MLZ), Technical University of Munich, Garching, Germany; ³Jülich Centre for Neutron Science (JCNS) at MLZ, Forschungszentrum Jülich GmbH, Garching, Germany; ⁴Department of Physics and College of Optics and Photonics, University of Central Florida, Orlando, FL, USA

Molecular changes in the water dynamics of poly(*N*-isopropylacrylamide) (PNIPAM) in water-methanol mixtures are revealed across the temperature-pressure phase diagram by quasi-elastic neutron scattering. The amount of hydration water increases with pressure. Release and adsorption of solvents by the polymer chains correlate with a change in the effective solvent composition, as evidenced by the diffusive properties of bulk water.

Neutron scattering experiments

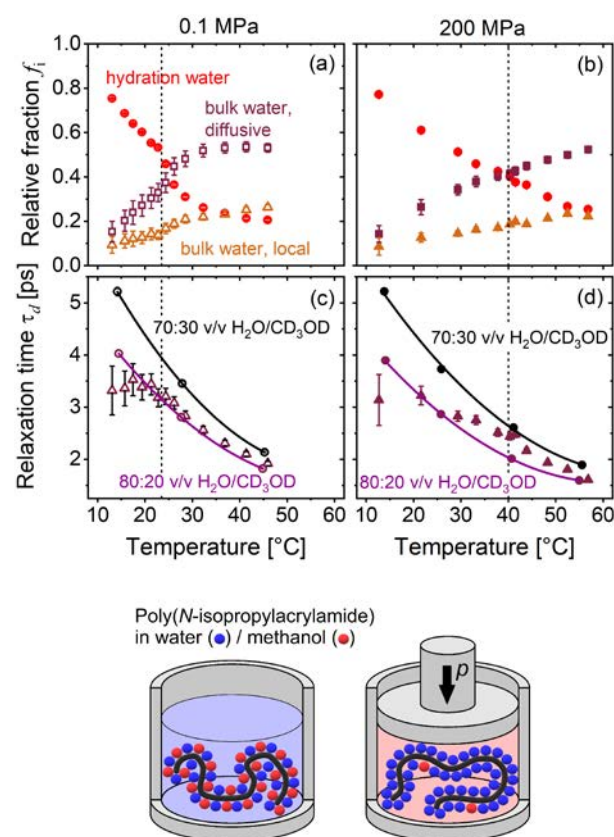
Water-soluble polymers are attracting increasing interest due to a wide range of applications in biotechnology and medicine, including drug delivery. The thermoresponsive poly(*N*-isopropylacrylamide) (PNIPAM) prototype polymer is soluble in both water and methanol at room temperature, however mixtures of these are a poor solvent for PNIPAM. Upon application of pressure, the behavior is reversed.

In the present work, quasi-elastic neutron scattering (QENS) is employed to investigate the dynamics of hydration and bulk water in a concentrated (25 wt%) PNIPAM solution in a water/methanol mixture across the demixing transition. QENS measurements were conducted in the time-of-flight spectrometer TOFTOF at ambient and high pressure. The susceptibility spectra at low temperatures, i.e. in the one-phase region, show strong contributions at low (~ 10 GHz) and high frequencies (~ 1000 GHz), that are present at both pressures. The contribution at low frequencies is due to the relaxation of hydration water, i.e. water molecules that are associated with the polymer chains. The high-frequency contributions are due to dynamic processes in the bulk solvent. At atmospheric pressure, the coil-to-globule transition at the cloud point temperature goes along with an abrupt release of polymer-bound water. In contrast, at high pressure, the fraction f_{H} of bound water decreases gradually with increasing temperature (see figure, top). The relaxation time τ_{d} of the bulk diffusive mode in the polymer solution is compared with that in the neat 80:20 and 70:30 v/v $\text{H}_2\text{O}/\text{CD}_3\text{OD}$ solvent mixtures in the figure (bottom). At a

pressure of 200 MPa, water replaces the majority of the methanol adsorbed on the chains, altering the effective solvent composition. Preferential water adsorption and the hydrophobic interaction thus play a major role in the breakdown of the co-non-solvency effect at high pressures. The results demonstrate that QENS is a powerful approach to gaining molecular insight into the interplay of co-non-solvency and water dynamics.

[1] B.-J. Niebuur et al., *Pressure Dependence of Water Dynamics in Concentrated Aqueous Poly(*N*-isopropylacrylamide) Solutions with a Methanol Cosolvent, *Macromolecules*, 54, 4387 (2021)*

DOI: 10.1021/acs.macromol.1c00111



Relative populations of different water species (top) and relaxation times τ_{d} of the bulk diffusive mode (bottom) as a function of temperature in 25 wt% PNIPAM solutions at ambient (open symbols) and high pressure (full symbols). Full lines indicate τ_{d} in 80:20 and 70:30 v/v $\text{H}_2\text{O}/\text{CD}_3\text{OD}$ mixtures without the polymer. Open and full triangles refer to τ_{d} in 25 wt% PNIPAM solvent mixtures. The vertical dashed lines indicate the cloud points.

Nanosecond structural dynamics of intrinsically disordered β -casein micelles using neutron spectroscopy

H. Nakagawa^{1,2,3}, M.-S. Appavou², J. Wuttke², M. Zamponi², O. Holderer², T. E. Schrader², D. Richter², W. Doster⁴

¹Materials Sciences Research Center, Japan Atomic Energy Agency, Tokai, Ibaraki, Japan; ²Jülich Centre for Neutron Science (JCNS) at MLZ, Forschungszentrum Jülich GmbH, Garching, Germany; ³J-PARC Center, Japan Atomic Energy Agency, Tokai, Ibaraki, Japan; ⁴Physics Department, Technical University of Munich, Garching, Germany

The structural flexibility of β -casein micelles was characterized by small-angle neutron scattering, spin echo spectroscopy and backscattering spectroscopy. Two relaxation processes on a nano-second and a sub-nano-second time scale were observed. The slower process involves density fluctuation of the solvent, and the faster one requires hydration water. The flexibility of a β -casein monomer is preserved in the micelle.

β -casein undergoes a reversible endothermic self-association with increasing temperature, forming micelles of limited size. In its functional state, a single β -casein monomer is unfolded, creating a high structural flexibility, which is supposed to play a major role in preventing the precipitation of calcium phosphate particles. The structural flexibility in terms of nano-second molecular motions was characterized, depending on the temperature, by a combination of small-angle neutron scattering, spin echo spectroscopy and backscattering spectroscopy using KWS-1, J-NSE and SPHERES.

Two relaxation processes can be distinguished

Two relaxation processes on a nano-second and a sub-nano-second time scale were observed for β -casein in solution. Both processes are analyzed via the Brownian Oscillator model, by which the spring constant can be defined in the isotropic parabolic potential. The slower process, which is analyzed by neutron spin echo, seems a characteristic feature of the unfolded structure, and dividing the relaxation time by the solvent viscosity removes most of the temperature dependence (see figure), indicating that the process involves density fluctuations of the solvent. It requires bulk solvent and is therefore not seen in hydrated protein powders.

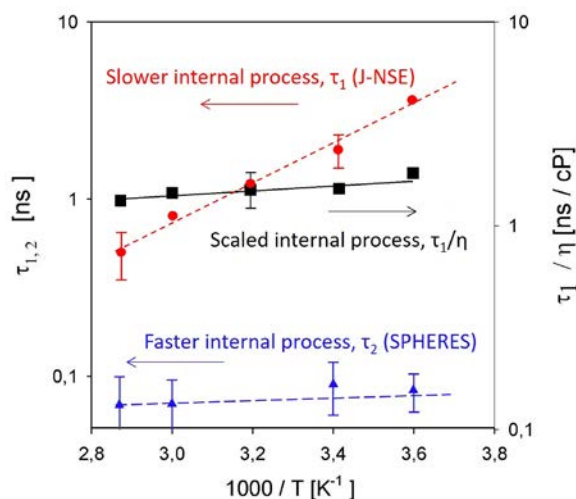
The faster process, which is analyzed by neutron backscattering, has a smaller amplitude and requires hydration water, which is also observed with folded proteins in the

hydrated state. The self-association had no significant influence on internal relaxation, and thus a β -casein protein monomer flexibility is preserved in the micelle.

In contrast, this type of internal structural dynamics is changed upon the folding and unfolding of a globular protein due to the change of the atomic packing. The dynamical change upon the folding or unfolding might also be related to the change of the hydration state since the protein folding is accompanied by dehydration of the polypeptide chain. The small dynamical change of the β -casein monomer upon micellization is compatible with the highly hydrated state inside the casein micelle.

[1] H. Nakagawa *et al.*, *Nanosecond structural dynamics of intrinsically disordered β -casein micelles by neutron spectroscopy*, *Biophys. J.* **120**, 5408 (2021)

DOI: 10.1016/j.bpj.2021.10.032



Arrhenius plots: red circles: internal relaxation time $\tau_1(T)$ by neutron spin echo, dashed line: Fit to Arrhenius law, pre-exponential: $\tau_0 = 0.3 (\pm 0.03)$ ps, activation enthalpy, $H_1 = 21.8 (\pm 0.5)$ kJ/mol. Black squares: relaxation time divided by the solvent viscosity: τ_1/η . The full line is the Arrhenius fit, the activation enthalpy is now reduced to $4 (\pm 1.5)$ kJ/mol, blue triangles: internal relaxation time $\tau_2(T)$ by neutron backscattering spectroscopy.

Formation of nanosized water pockets in an amorphous ionic liquid matrix

J. Kraus¹, F. Pabst¹, S. Kloth¹, M. Kruteva², A. Radulescu³, T. Blochowicz¹, M. Vogel¹

¹TU Darmstadt, Institute for Condensed Matter Physics, Darmstadt, Germany; ²Jülich Centre for Neutron Science (JCNS) at MLZ, Forschungszentrum Jülich GmbH, Garching, Germany; ³Jülich Centre for Neutron Science JCNS (JCNS-1), Forschungszentrum Jülich GmbH, Jülich, Germany

When mixing an ionic liquid (IL) with water, in certain cases nanoscaled water clusters, also known as water pockets, are formed. Combining small angle neutron scattering, molecular dynamics simulations and Raman spectroscopy, we found evidence for the existence of such water pockets in a mixture of [BMIM][DCA] with 72 mol% water. Moreover, no crystallization occurs on cooling, opening the way to studying supercooled nanoscale water clusters in an amorphous IL matrix.

Nanosized water domains in ionic liquids

When studying ionic liquids (ILs), water has long been considered as a possible additive, but only more recently has the existence of so-called water pockets, which form as nanoscale water clusters when adding certain amounts of water to some ILs, been reported. This was observed in a recent study by combining small angle neutron scattering (SANS), performed at the KWS-2 small angle refractometer at the MLZ, Raman spectroscopy (RS) and molecular dynamics simulations (MDS) for mixtures of [BMIM][DCA] and water [1].

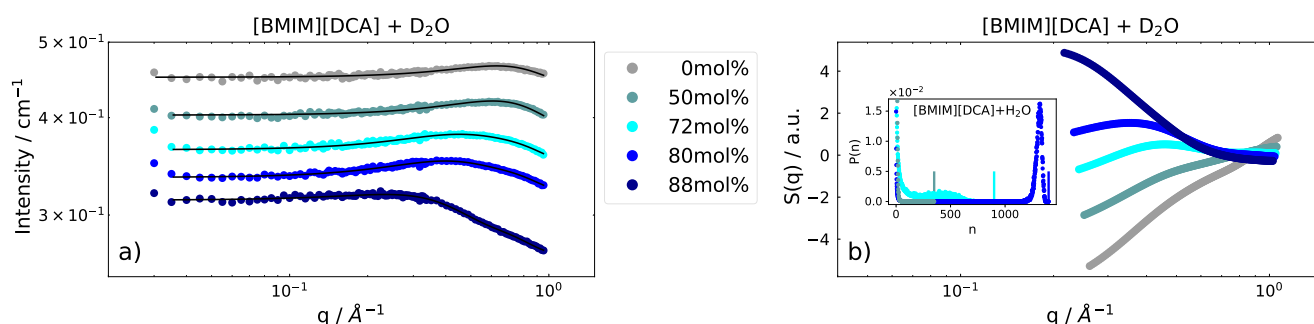
As can be seen in figure a, a structure peak shows up in the SANS spectra of all samples. To fit the spectra, a core shell model was used. Interestingly, at 50%, the SANS spectrum is almost identical to that of the neat IL while at higher concentrations, the average size of the CS structures increases

and the peak shifts to lower q values. At the same concentration region, the description changes from a spherical to an elliptical CS-model and in RS a specific, so-called DDAA peak appears that indicates fully bonded H_2O molecules, which implies a clustering of water in larger structures. At 72%, the size of the structure is ~ 2 nm across on the long axis of the ellipsoid.

The neutron scattering structure factors $S(q)$ from the atomic positions in the MDS were calculated (figure b) and show a shoulder for lower concentrations that develops into a peak that shifts to lower q with increasing water content, very similar to the SANS results. The inset of figure b shows the probability of a H_2O molecule being in a cluster of size n . For the case of 50%, all water molecules are located in very small clusters, while for 80% almost all molecules are located in a very large cluster so the size is nearly equal to the total number of water molecules. However, for 72% H_2O , a broad distribution of cluster sizes is found. Combining those results points to the existence of water pockets at that concentration. As no crystallization occurs upon cooling, this paves the way to studying supercooled nanoscale water clusters in an amorphous IL matrix.

[1] F. Pabst, et al., *Evidence of supercoolable nanoscale water clusters in an amorphous ionic liquid matrix*, *Chem. Phys.*, 155 (17), 174501 (2021)

DOI: 10.1063/5.0066180



(a) SANS spectra at 5°C for different D₂O concentrations. The solid lines represent fits with a core-shell model. (b) Full structure factor from MDS, highlighting the qualitative similarity with the SANS data. Inset: Probability of a H_2O molecule being located in a water cluster of size n calculated from MDS for the water concentrations 50, 72 and 80%. The vertical lines indicate the total amount of water molecules in the respective mixture.

The impact of glycerol on an affibody conformation and its correlation to chemical degradation

I. Ramm¹, A. Sanchez-Fernandez¹, J. Choi¹, C. Lang², J. Fransson³, H. Schagerlöf⁴, M. Wahlgren¹, L. Nilsson¹

¹Department of Food Technology, Engineering and Nutrition, Lund University, Lund, Sweden; ²Jülich Centre for Neutron Science (JCNS) at MLZ, Forschungszentrum Jülich GmbH, Garching, Germany; ³Swedish Orphan Biovitrum International AB (SOBI), Stockholm, Sweden; ⁴Department of Chemical Engineering, Lund University, Lund, Sweden.

Glycerol is often added to protein solutions to hinder the denaturation and aggregation of proteins. However, it is not a practice generally used to combat chemical degradation. The chemical degradation of proteins is a deteriorative mechanism that causes a loss of functionality in proteins. In this study, the impact of glycerol on the conformation of a model protein has been examined using SANS and connected to the chemical degradation propensity of the protein.

GA-Z is a therapeutic affibody consisting of two domains connected by a flexible linker. The chemical degradation of GA-Z in the presence and absence of glycerol was investigated in a time-dependent accelerated stability study performed at 37°C in solution. The chemical degradation of GA-Z was determined using liquid chromatography-mass spectrometry and -UV spectroscopy, and the result showed that the protein was degraded by deamidation, isomerisation, and hydrolysis. Interestingly, the addition of glycerol significantly reduced the chemical degradation of GA-Z (see figure).

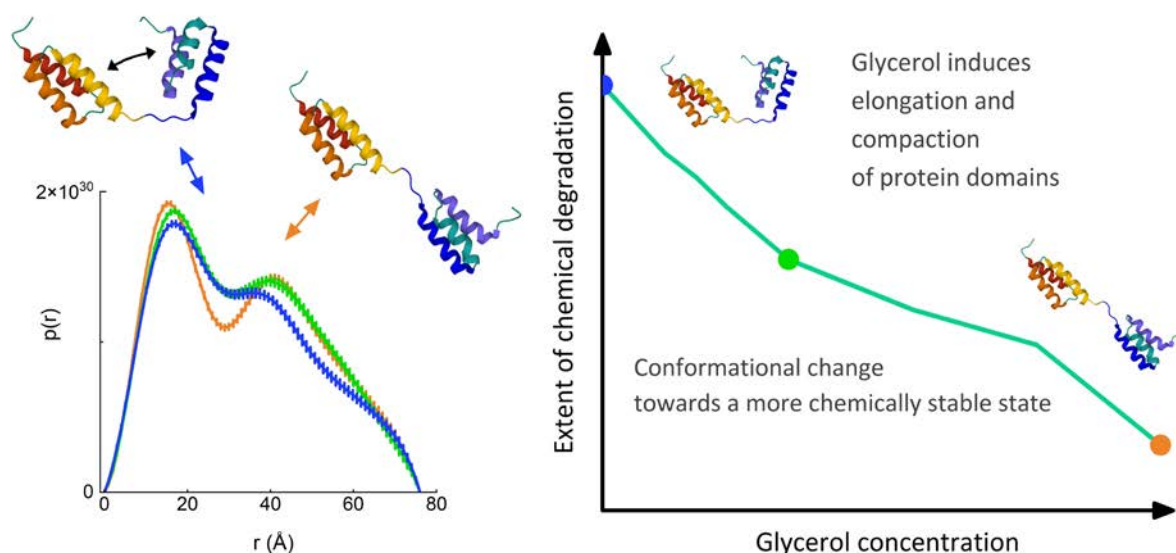
Glycerol-induced conformational changes

The conformational changes of GA-Z induced by the addition of different amounts of glycerol to the solution (0 - 90% v/v glycerol) were examined with asymmetric field-flow

fractionation and SANS. The SANS experiments were performed on the KWS-2 instrument at the Heinz Maier-Leibnitz Zentrum. Two detector distances were used (2 and 8 m) and a neutron wavelength of 5 Å. The combined data from these two configurations provided a combined q-range of 0.008 - 0.45 Å⁻¹. The SANS data were analyzed using Indirect Fourier Transform and by using a model-based approach. The shape of GA-Z can be appropriately described using a mathematical model that accounts for the scattering of a barbell structure. Upon the addition of glycerol, the tertiary structure of the protein changes and two effects are observed: (1) the compaction of the globular domains and (2) the elongation of the flexible linker (see figure). The results aligned with the glycerol-induced conformational changes observed with the asymmetric field-flow fractionation.

In summary, the addition of glycerol favors a more compact and less mobile state, leading to lower rates of deamidation and isomerization. The results presented, for this model protein, will help to develop improved methods for the formulation and preservation of proteins of pharmaceutical and technological interest.

[1] I. Ramm et al., *The Impact of Glycerol on an Affibody Conformation and Its Correlation to Chemical Degradation*, *Pharmaceutics* 13, 1853 (2021)
DIO: 10.3390/pharmaceutics13111853



The addition of glycerol decreases the chemical degradation of GA-Z. SANS was used to study glycerol-induced conformational changes. The study reveals that glycerol favors a more compact and chemically stable state. $p(r)$ functions from the Indirect Fourier Transform analysis of SANS data in 0% (●), 30% (●), and 70% (●) v/v glycerol-d8.

Neutron reflectometry unveils the structural asymmetry of plant membranes

V. Rondelli¹, A. Koutsioubas², J. Pršič³, E. Deboever^{4,5,6}, J. M. Crowet⁷, L. Lins⁴, M. Deleu⁴

¹Department of Medical Biotechnology and Translational Medicine, Università degli Studi di Milano, Milano, Italy; ²Jülich Centre for Neutron Science (JCNS) at Heinz Maier-Leibnitz Zentrum, Forschungszentrum Jülich GmbH, Garching, Germany; ³Microbial Processes and Interactions Laboratory (MiPI), TERRA Research Center, Gembloux Agro-Bio Tech, Université de Liège, Gembloux, Belgium; ⁴Laboratoire de Biophysique Moléculaire aux Interfaces, Structure Fédérative de Recherche Condorcet, TERRA Research Center, Gembloux Agro-Bio Tech, Université de Liège, Gembloux, Belgium; ⁵Laboratory of Natural Molecules Chemistry, Gembloux Agro-Bio Tech, University of Liège, Gembloux, Belgium; ⁶FytoFend S.A., Isnes, Belgium; ⁷Université de Reims Champagne-Ardenne, UFR Sciences Exactes et Naturelles, Reims, France

Biomimics of plant plasma membranes have been experimentally and theoretically investigated by Langmuir films, *in silico* simulations and neutron reflectometry. The aim was the study of the spontaneous distribution of components upon which membrane structure and functionality depend. Our results showed that a strong direct interaction between glucosylceramide and sitosterol exists in the PLPC phospholipid matrix, driving their distribution within leaflets.

Plant biomembranes

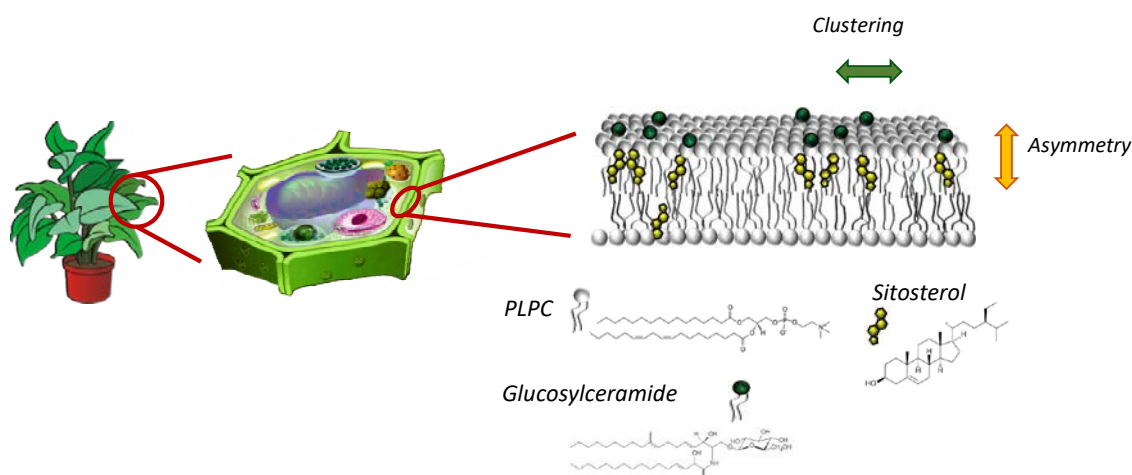
Biomembranes are assemblies of macromolecules of vital importance for animal and plant cells. They combine structural and functional roles, which depend not only on cell specificity, but also on the membrane domain considered. Indeed, thousands of molecules belonging to the diverse membranes distribute unevenly in the lateral and transversal directions, conferring different local properties on the assemblies. Membrane rafts are domains with lower fluidity with respect to the rest of the membrane, with the peculiarity of being enriched in sterols and glycosphingolipids. Increased amounts of sterols, sitosterol in plants, induce in raft components a lower lateral mobility and increase membrane rigidity. Glucosylceramide, among the most abundant plant glycosphingolipids is, instead, involved in signalling and is essential for the viability of cells and of the whole plant.

Plant membrane mimics are not homogeneous

In our study, a multitechnique approach involving different plant plasma membrane models was applied to investigate the glucosylceramide-sitosterol structural coupling within a matrix of palmitoylphosphatidylcholine (PLPC), the typical phospholipid of plant membranes. Langmuir films, *in silico* simulations and neutron reflectometry, revealed that a strong direct interaction exists between the two molecules and governs their lateral and transversal distribution within membrane leaflets. In particular, neutron reflectometry experiments performed on the MARIA reflectometer at the MLZ, made it possible to investigate the distribution of sitosterol in the leaflets, which was found to depend on the presence of glucosylceramide. Indeed, when the two molecules are present in the phospholipid bilayer, they laterally clusterize and co-localize in the same leaflet, making the membrane fully asymmetric. Besides opening up the possibility of building up complex models for plant plasma membranes for future studies, an understanding of the driving forces that govern molecule clustering and segregation in subdomains is of interest for the understanding of the whole membrane structure and functionality.

[1] V. Rondelli et al., *Sitosterol and glucosylceramide cooperative transversal and lateral uneven distribution in plant membranes*, *Sci. Rep.* 11, 21618 (2021)

DOI: 10.1038/s41598-021-00696-7



Complementary experiments and MD simulations make it possible to unveil lateral clustering and full asymmetry of molecules in complex plant membrane mimics.

Structural characterization of CO₂/EO surfactant micelles and their temperature dependence

V. J. Spiering¹, A. Prause¹, L. Noirez², M.-S. Appavou³, M. Gradzielski¹

¹Stranski-Laboratory for Physical and Theoretical Chemistry, Institute of Chemistry, Technical University of Berlin, Berlin, Germany; ²Laboratoire Léon Brillouin (CEA-CNRS), Université Paris-Saclay, Gif sur Yvette Cedex, France; ³Jülich Centre for Neutron Science (JCNS) at MLZ, Forschungszentrum Jülich GmbH, Garching, Germany

The properties of nonionic surfactants can be tuned by incorporating carbonate groups (using CO₂ as a resource) into the hydrophilic head group. SANS experiments show reduced hydration of the head group, larger micelle size, and a much increased temperature-induced growth with increasing CO₂ content. The outcome is that one can tailor the properties of nonionic surfactant in a systematic way, and at the same time reduce the use of petrol-based resources.

Structural Characterization

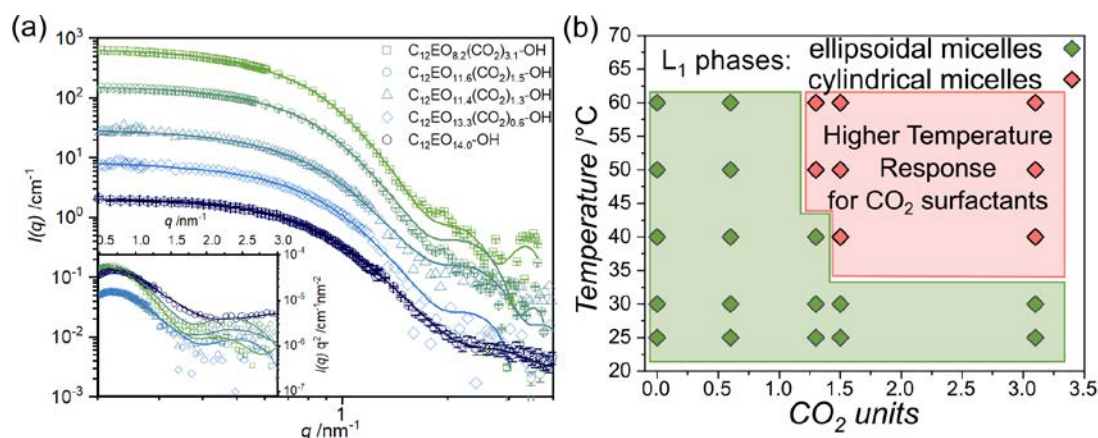
In this study, we investigated the effect of incorporating CO₂ moieties, in the form of carbonate groups, into the EO head group of nonionic surfactants on their micellar structures as a function of concentration and temperature. Structural information obtained from light and neutron scattering measurements at KWS-1 showed that globular micelles are formed at room temperature with a core radius in the size range of 1.2-1.8 nm, a shell thickness (head groups) of approximately 2.0 nm, and an overall increase in size with increasing CO₂ content. The analysis of the SANS data via the form factor of the head group corona and the Porod regime shows that the head groups are more compact for the CO₂ surfactants and more swollen Gaussian chains for the pure EO and the PO surfactant. These results are in good agreement with previous studies that also showed more interpenetration for the CO₂ head group (see figure).

The study of the temperature dependence demonstrates that the structure of pure EO surfactants is little affected by a temperature increase up to 60°C. In contrast, the CO₂ surfactants with higher CO₂ content (> 1.5 units/molecule) show an increase in size with increasing temperature, i.e., the classical sphere-rod transition that occurs upon approaching the cloud point. The incorporation of CO₂ moieties lowers the cloud point and facilitates the temperature response, which correspondingly can be tuned by modifying the content of CO₂ in the head group.

As a result, we can state that incorporating CO₂ into nonionic surfactant head groups is a way to tailor their temperature-dependent properties. This study is an example where a fundamental investigation of the structural properties of a surfactant system allows for a systematic understanding based on the molecular architecture of the surfactants. In addition, surfactants containing CO₂ contribute to the goal of more sustainable chemistry as the petrol-based EO is replaced by CO₂ (by up to 20%).

[1] V. J. Spiering et al., *Structural Characterization of Nonionic Surfactant Micelles with CO₂/Ethylene Oxide Head Groups and Their Temperature Dependence*, *Langmuir* 2021, 37, 13235 (2021)

DOI: 10.1021/acs.langmuir.1c01737



(a) SANS curves at low concentration (1 wt%) for the CO₂ surfactants and the reference surfactant at 25°C (KWS-1). Continuous lines represent the model fit. The curves are scaled on the y-axis. Inset shows $I(q)q^2$ of the scattering curves. (b) Temperature vs. CO₂ content phase diagram of the CO₂ surfactants.

A look inside PNIPAM microgels: nanomechanics and dynamics at solid–liquid interfaces

J. Witte¹, T. Kyrey², J. Lutzki¹, A. M. Dahl¹, M. Kühnhammer³, R. von Klitzing³, O. Holderer², S. Wellert¹

¹Department of Chemistry, Technische Universität Berlin, Berlin, Germany; ²Jülich Centre for Neutron Science (JCNS) at MLZ, Forschungszentrum Jülich GmbH, Garching, Germany; ³Department of Physics, Technische Universität Darmstadt, Darmstadt, Germany

New synthesis routes lead to a variety in the structure and functionality of colloidal hydrogels. A fundamental understanding of the influence of these substrates on the physical properties is essential. Grazing incidence scattering is suited to probing samples at planar solid substrates and allows a z-resolution. NSE under grazing incidence and AFM nanoindentation characterized adsorbed microgels prepared by batch and continuous monomer feeding methods.

Adsorbed microgels eyeballed from all sides

The influence of the internal structure of highly cross-linked PNIPAM microgel particles (10 mol% BIS) with different internal structures on their nanomechanics in the adsorbed state is investigated using a combination of AFM imaging, AFM force mapping, and GINSES. AFM nanoindentation probes the nanomechanical properties of the top region of an individual particle, GINSES has access to the near-surface layers and offers z-resolution. The microgels were prepared using a conventional batch method and a continuous feeding method as representatives for “hard” and “soft” microgels.

AFM carves out a microgels Young’s modulus

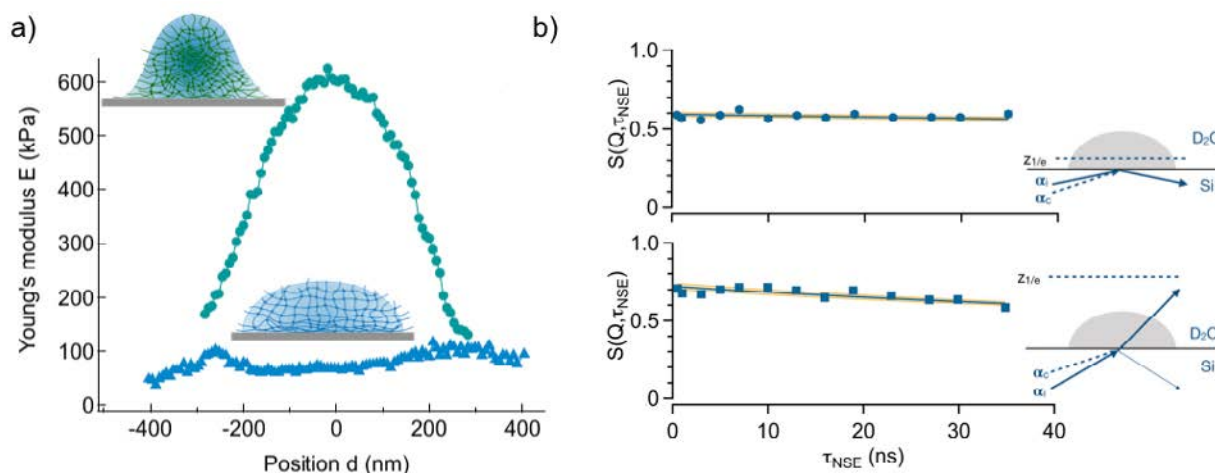
The batch microgel has a maximum Young’s modulus in the center which decreases to 1/3 of the maximum value toward the edge of the particle. This supports the hypothesis that the particle core acts as a stabilizing scaffold in the ad-

sorbed state. In comparison, the feeding microgel displays no such stiffness gradient. Instead, Young’s moduli vary between approximately 50 and 100 kPa without a maximum in the center. We conclude that the feeding microgel lacks a dense core, and is much softer overall.

NSE shows the polymer network’s elasticity

Neutron spin echo spectroscopy under grazing incidence at J-NSE “PHOENIX” allows us to draw conclusions about the internal nanomechanics over the entire particle height. The results indicate that the deformation upon adsorption to a solid surface of soft microgel particles with a homogeneous cross-link distribution leads to a dense polymer layer with suppressed dynamics in close proximity to the surface. At infinite penetration depth, the dynamics approach bulk dynamics. In contrast, harder microgels with a highly cross-linked core and a fluffy shell display similar dynamics in the bulk and in the adsorbed state, independent of the penetration depth. This suggests a scaffold-like nature of the core region. The internal dynamics in the vicinity of a solid substrate differ strongly for soft, homogeneous, and harder, inhomogeneous microgels. Therefore, the higher loading capacity of the homogeneous microgels prepared by the continuous feeding method in the bulk does not necessarily translate to surface applications.

[1] J. Witte et al., *Looking inside Poly(N-isopropylacrylamide) Microgels: Nanomechanics and Dynamics at Solid–Liquid Interfaces*, *ACS Appl. Polym. Mater.* 3, 2, 976 (2021) DOI: 10.1021/acsapm.0c01265



(a) Cross sections of the Young’s modulus of individual feeding (blue) and batch (green) microgels in water at 20°C. The insets sketch the different inner architectures. (b) Intermediate scattering functions of adsorbed feeding microgels measured in reflection geometry with GINSES at infinite penetration (bottom) and about 10 nm penetration (top) into the sample. Also shown are the fits to the data (solid lines) and the confidence intervals of the fits.

Multiple field-induced phases in the frustrated triangular magnet $\text{Cs}_3\text{Fe}_2\text{Br}_9$

D. Brüning¹, T. Fröhlich¹, D. Gorkov^{1,2}, I. Císařová³, Y. Skourski⁴, L. Rossi⁵, B. Bryant⁵, S. Wiedmann⁵, M. Meven^{6,7}, A. Ushakov⁸, S. V. Streltsov^{8,9}, D. Khomskii¹, P. Becker¹⁰, L. Bohatý¹⁰, M. Braden¹, T. Lorenz¹

¹II. Physikalisches Institut, Universität zu Köln, Köln, Germany; ²Heinz Maier-Leibnitz Zentrum (MLZ), Technical University of Munich, Garching, Germany; ³Department of Inorganic Chemistry, Charles University in Prague, Prague, Czech Republic; ⁴Hochfeld-Magnetlabor Dresden (HLD-EMFL), Helmholtz-Zentrum Dresden-Rossendorf, Dresden, Germany; ⁵High Field Magnet Laboratory (HFML-EMFL) and Institute for Molecules and Materials, Radboud University, Nijmegen, The Netherlands; ⁶Institute of Crystallography, RWTH Aachen at MLZ, Garching, Germany; ⁷Jülich Centre for Neutron Science (JCNS) at MLZ, Forschungszentrum Jülich GmbH, Garching, Germany; ⁸M.N. Mikheev Institute of Metal Physics, Ural Branch, Russian Academy of Sciences, Ekaterinburg, Russia; ⁹Ural Federal University, Ekaterinburg, Russia; ¹⁰Work group Materials Crystallography, Institute of Geology and Mineralogy, University of Cologne, Cologne, Germany

We report the phase diagram and magnetic structure of the recently discovered material $\text{Cs}_3\text{Fe}_2\text{Br}_9$ that consists of triangular layers formed by Fe_2Br_9 bi-octahedra. The large degree of frustration results in an extraordinarily rich phase diagram with at least 10 different phases occurring under magnetic field. Comprehensive neutron scattering studies reveal a ground state at zero field with ferromagnetic intradimer arrangement and various propagation vectors at finite fields and higher temperature.

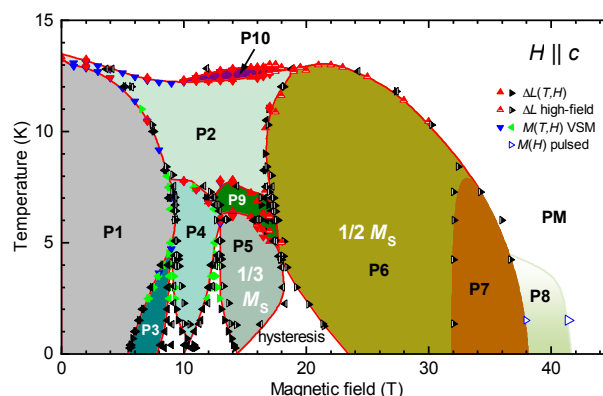
Competing interaction in a triangular lattice implies a rich variety of magnetic phases and magnetization plateaus

The hexagonal compound $\text{Cs}_3\text{Fe}_2\text{Br}_9$ consists of separated Fe_2Br_9 bi-octahedra that form triangular lattices stacked along the c direction. Fe is three-valent in this material and hosts $S = 5/2$ spin moments that exhibit a strong easy-axis anisotropy along c . Upon cooling, the compound shows magnetic order passing two magnetic phase transitions, at $T_{N1} = 13.29$ K and at $T_{N2} = 13.12$ K. The magnetic structure of the low-temperature phase was determined on the HEIDI diffractometer and the temperature dependence of the magnetic response was studied on the KOMPASS spectrometer. In the low-temperature phase at zero magnetic field, $\text{Cs}_3\text{Fe}_2\text{Br}_9$ exhibits a simple commensurate order with propagation vector $(1/2\ 0\ 0)$ while the tiny intermediate phase is incommensurate. Most interestingly, the two spins in the bi-octahedra are aligned parallel, yielding a ferromagnetic dimer [1].

$\text{Cs}_3\text{Fe}_2\text{Br}_9$ exhibits strong magneto-elastic coupling at zero as well as at finite magnetic fields. Combining magnetization, specific heat and thermal expansion measurements at high fields with neutron diffraction experiments, we studied the phase diagrams for fields vertical and parallel to the magnetic easy axis. While the phase diagram for vertical fields is relatively simple, the large degree of frustration due to (various) competing intradimer and interdimer couplings results in 10 different phases occurring for magnetic fields along the easy axis c (see figure). Most interestingly, there are phases with magnetization plateaus that amount to $1/2$ and $1/3$ of the saturation magnetization in the fully polarized state [1]. The remarkably rich variety of magnetic ordered phases in a simple system renders $\text{Cs}_3\text{Fe}_2\text{Br}_9$ most promising for studying different phenomena such as frustration, quantum phase transitions or Bose condensation.

[1] D. Brüning et al., *Multiple field-induced phases in the frustrated triangular magnet $\text{Cs}_3\text{Fe}_2\text{Br}_9$* , *Phys. Rev. B* **104**, 064418 (2021)

DOI: 10.1103/PhysRevB.104.064418



The phase diagram of $\text{Cs}_3\text{Fe}_2\text{Br}_9$ is shown for magnetic fields applied along the magnetic easy axis (parallel c). The critical fields and temperatures were determined by high-field measurements of thermal expansion, magnetization and specific heat.

Single-crystal diffraction studies
on multiferroic $\text{LiFe}(\text{WO}_4)_2$ S. Biesenkamp¹, D. Gorkov^{1,2}, D. Brüning¹, A. Bertin¹, T. Fröhlich¹, X. Fabrèges³, A. Gukasov³, M. Meven^{4,5}, P. Becker⁶, L. Bohatý⁶, T. Lorenz¹, M. Braden¹¹II. Physikalisches Institut, University of Cologne, Cologne, Germany; ²Heinz Maier-Leibnitz Zentrum (MLZ), Technical University of Munich, Garching, Germany; ³Laboratoire Léon Brillouin, CEA/CNRS, Cedex, France; ⁴Institute for Crystallography, RWTH Aachen at MLZ, Garching, Germany; ⁵Jülich Centre for Neutron Science (JCNS) at MLZ, Forschungszentrum Jülich GmbH, Garching, Germany; ⁶Workgroup Crystallography, Institute of Geology and Mineralogy, University of Cologne, Cologne, Germany

Multiferroic materials offer the possibility of controlling magnetic order through an electric field and can be used in new data-storage technologies that consume less energy. However, the known compounds are not viable in a technical device. Therefore, the search for new multiferroic materials with improved properties is most important. $\text{LiFe}(\text{WO}_4)_2$ has recently been reported to exhibit a multiferroic phase [1] but so far only polycrystalline samples have been available, thereby limiting all experimental studies.

The recently discovered multiferroic material $\text{LiFe}(\text{WO}_4)_2$ differs from related tungstates such as MnWO_4 and $\text{NaFe}(\text{WO}_4)_2$ by the alternating occupation of zigzag chains with magnetic Fe and non-magnetic Li. Like multiferroic MnWO_4 , the double tungstate was proposed to develop first a spin-density wave (SDW) until below the second transition, the magnetic arrangement transforms into a chiral spin structure, which is accompanied by the emergence of ferroelectric polarization. The full determination of such complex magnetic structures requires single-crystal diffraction experiments.

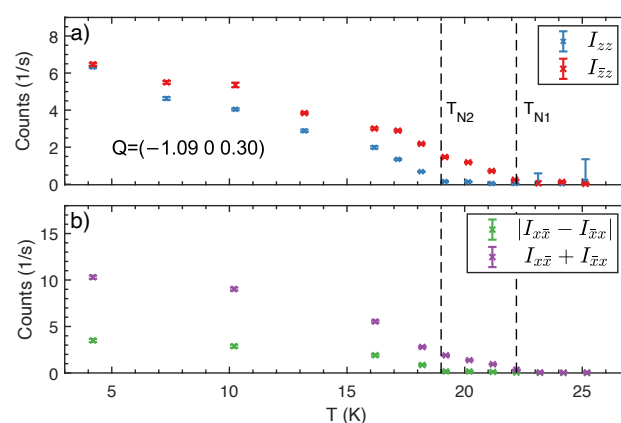
Diffraction studies characterized the simple sequence of magnetic phases in multiferroic $\text{LiFe}(\text{WO}_4)_2$

Thus, large single-crystals of $\text{LiFe}(\text{WO}_4)_2$ were grown at Cologne University and facilitated studies by specific heat, susceptibility, and X-ray and various neutron diffraction techniques. Surprisingly, crystals differed with regard to their magnetic transitions, depending on growth conditions. Experiments at the four-circle diffractometer HEiDi revealed that a minor occupation of the Li-site by Fe is capable of shifting the transition temperatures at $T_{N1} = 22.2$ K and $T_{N2} = 19$ K. Utilizing longitudinal polarization analysis

at the cold triple-axis spectrometer KOMPASS confirmed the confinement of the SDW in the ac-plane, whereas an additional b-component arises only in the multiferroic phase (see figure a). The polarization analysis further revealed the chiral character of the magnetic structure in the lower phase arising from an unbalanced multiferroic domain distribution (see figure b). Our results, including the output of neutron diffraction experiments at the FRM II, are published in reference [1]. Compared to most known type-II multiferroic materials, $\text{LiFe}(\text{WO}_4)_2$ is better suited for further studies as there is only a single magnetic constituent and because there is no other phase competing with the multiferroic phase at low-temperature.

[1] S. Biesenkamp et al., *Single-crystal investigations on the multiferroic material $\text{LiFe}(\text{WO}_4)_2$* , *Phys. Rev. B* 103, 134412 (2021)

DOI: 10.1103/PhysRevB.103.134412



By using the conventional coordinate system for polarization analysis with $Q \parallel x$ and scattering geometry (100)/(001), the spin-flip (SF) channel I_{zz} along z-direction senses the magnetic ac-component, whereas the non-spin-flip (NSF) channel I_{zx} describes the magnetic b component. The vector chirality can be measured by the difference of SF-channels I_{xx} and I_{xx} , which are proportional to $M_x M_x^* \pm i(M_x \times M_x^*)_x$.

Structural investigation into magnetic spin orders of a manganese phosphatic oxyhydroxide, $\text{Mn}_5[(\text{PO}_4)_2(\text{PO}_3(\text{OH}))_2](\text{HOH})_4$

S.-H. Park¹, A. Hartl^{1,2}, D. Sheptyakov², M. Hölzel³, A. Arauzo^{4,5}

¹Department of Geo- and Environmental Sciences, Section of Crystallography, Ludwig-Maximilians-Universität München (LMU), Munich, Germany; ²Paul Scherrer Institute (PSI), Villigen, Switzerland; ³Heinz Maier-Leibnitz Zentrum (MLZ), Technical University of Munich, Garching, Germany; ⁴Instituto de Nanociencia y Materiales de Aragón (INMA), Departamento de Física de la Materia Condensada, CSIC-Universidad de Zaragoza, Zaragoza, Spain; ⁵Physical Measurements Service, University of Zaragoza, Zaragoza, Spain

The ferri- and antiferromagnetic structures of a hureaulite-type synthetic compound, $\text{Mn}^{2+}_5(\text{PO}_4)_2(\text{PO}_3(\text{OH}))_2(\text{HOH})_4$, were elucidated by neutron powder diffraction in combination with magnetic susceptibility and heat capacity measurements. It has been found that the paramagnetic phase ($\text{C}2/c$) transforms at 6.17 K into a ferrimagnetic order ($\text{C}2'/c'$), followed at 1.86 K by an incommensurately modulated antiferromagnetic order ($\text{P}2_1/c.10(a0g)00s$) [1].

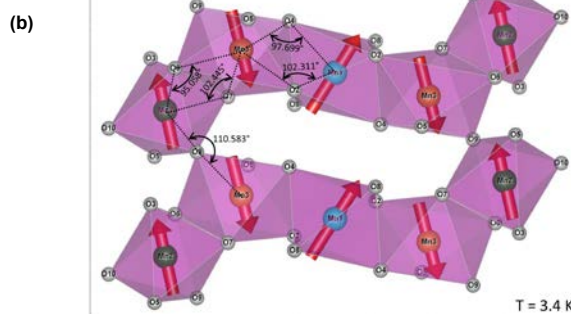
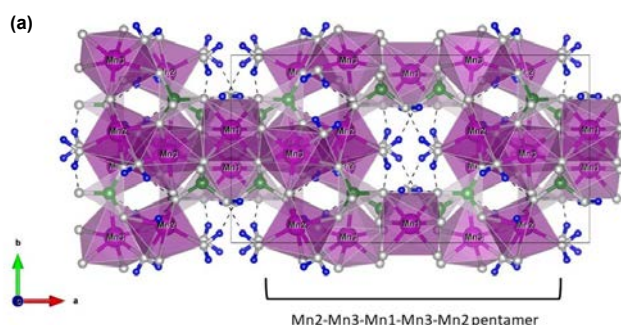
Crystal structure

Structure-related properties in phosphatic oxyhydroxides like charge transport and proton tunnelling over hydrogen bond networks are attractive application-relevant research topics. Moreover, it is conceivable that new (multi)ferroic and magnetic structures, depending on the type and arrangement of 3d transition metal atoms in these materials, can be found. The current study aimed to determine the magnetic structures of the pure manganese hureaulite-type solid solution $\text{Mn}^{2+}_5(\text{PO}_4)_2(\text{PO}_3(\text{OH}))_2(\text{HOH})_4$ (denoted as Mn-hureaulite). Characteristically, this structure contains pentamers of three edge-sharing unique $\text{Mn}1\text{O}_6$, $\text{Mn}2\text{O}_4(\text{HOH})_2$ and $\text{Mn}3\text{O}_5(\text{HOH})$ octahedra at Mn2-Mn3-Mn1-Mn3-Mn2 atomic sites. These pentamers are connected to each other via corner-sharing $\text{Mn}2\text{O}_4(\text{HOH})_2$ and $\text{Mn}3\text{O}_5(\text{HOH})$ octahedra along with PO_4 and $\text{PO}_3(\text{OH})$ tetrahedra to form zigzag-like interconnected pentamer slabs parallel to the a axis (figure a).

Magnetic structure

To determine the magnetic order as a function of temperature, high-resolution neutron powder diffraction was carried out on SPODI (MLZ, $\lambda = 2.5360 \text{ \AA}$, 6.5 and 3.4 K) and HRPT (PSI, $\lambda = 2.4500 \text{ \AA}$, 6.5, 6.1, 4.5, 1.7, and 1.5 K), in combination with previous magnetic susceptibility and heat capacity measurements. Based on these data $\text{C}2'/c'$ was identified as a correct magnetic space group for the ferrimagnetic phase at 3.4 K. In the ferrimagnetic state ($6.2 \text{ K} > T > 1.9 \text{ K}$), antiferromagnetic interactions are dominant for both intra and inter pentamers of $\text{Mn}^{2+}(\text{O}, \text{HOH})_6$ octahedra. Differently aligned spin-canting sublattices seen in the ferrimagnetic models at 3.4, 4.5 and 6.1 K explain a weak ferromagnetism (figure b). Below 1.86 K, an antiferromagnetic order occurs in the magnetic superspace group $\text{P}2_1/c.10(a0g)00s$ with the incommensurate modulation vector $\mathbf{k} = (0.523(2), 0, 0.055(1))$. The observation of magnetic moments vigorously changing in a small temperature range of 6.1 - 1.5 K indicates a highly complex interplay of structural and magnetic orders as well as their dynamics in this manganese phosphatic oxyhydroxide.

[1] S.-H. Park et al., *Structural Investigation into Magnetic Spin Orders of a Manganese Phosphatic Oxyhydroxide, $\text{Mn}_5[(\text{PO}_4)_2(\text{PO}_3(\text{OH}))_2](\text{HOH})_4$* , *Symmetry* 13, 1688 (2021) DOI: 10.3390/sym13091688



(a) The framework of Mn-hureaulite is built with pentamers of $\text{Mn}(\text{O}, \text{HOH})_6$ octahedra which are connected to each other via PO_4 and $\text{PO}_3(\text{OH})$ tetrahedra. Mn, P, O, and H atoms are illustrated in pink, green, gray, and blue, respectively. (b) Spin-canting configurations indicate dominant antiferromagnetic couplings for inter and intra pentamers in the ferrimagnetic phase.

Mechanism of magnetization reduction in iron oxide nanoparticles

T. Köhler^{1,2,3}, A. Feoktystov¹, O. Petravic², E. Kentzinger², T. Bhatnagar-Schöffmann^{2,3,4}, M. Feygenson⁵, N. Nandakumar^{2,3}, J. Landers⁶, W. Heiko⁶, A. Cervellino⁷, U. Rucker², A. Kovács⁴, R. Dunin-Borkowski⁴, T. Brückel^{2,3}

¹Jülich Centre for Neutron Science (JCNS) at MLZ, Forschungszentrum Jülich GmbH, Garching, Germany; ²Jülich Centre for Neutron Science JCNS-2, and Peter Grünberg Institute PGI-4, JARA-FIT, Forschungszentrum Jülich GmbH Jülich, Germany; ³Lehrstuhl für Experimentalphysik IV C, RWTH Aachen University, Aachen, Germany; ⁴Ernst Ruska-Centre for Microscopy and Spectroscopy with Electron and Peter Grünberg Institute, Forschungszentrum Jülich GmbH, Jülich, Germany; ⁵Jülich Centre for Neutron Science (JCNS-1) and Institute for Complex Systems (ICS-1), Forschungszentrum Jülich GmbH, Jülich, Germany; ⁶Faculty of Physics and Center for Nanointegration Duisburg-Essen (CENIDE), University of Duisburg-Essen, Duisburg, Germany; ⁷Paul Scherrer Institute, Swiss Light Source, Villigen PSI, Switzerland.

Iron oxide nanoparticles are promising for medical applications in targeted drug delivery and magnetic hyperthermia. In this work, the origin of their reduced magnetization compared to bulk samples is investigated using a number of complementary techniques. We conclude that the presence of a non-magnetic surface alone cannot explain the reduced magnetization and therefore propose antiphase boundaries as the main mechanism.

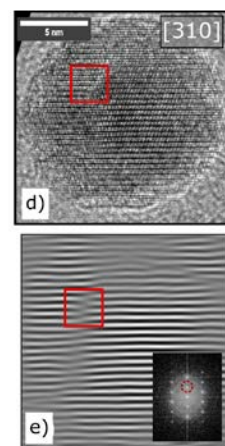
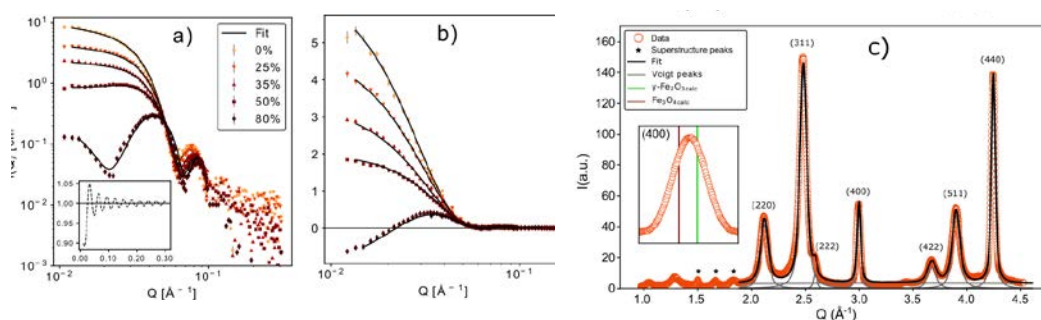
Different models for the magnetization distribution in iron oxide nanoparticles have been proposed in the past. These include a magnetic core-shell structure with a magnetically dead or depleted surface layer, spin disorder around defects, reduced magnetization due to reversed moments and spin frustration or the presence of antiphase boundaries (APBs), i.e. lattice defects that modify the bond angle between iron ions, leading to spin disorder. In our study [1], we investigated commercially available iron oxide nanoparticle samples from Ocean NanoTech ($\varnothing = 15$ nm) by combining SANS at KWS-1 (FRM II), SAXS at GALAXI (JCNS), SQUID-magnetometry (JCNS) with elemental analysis, synchrotron powder diffraction and PDF-analysis at the beamline X04SA (PSI), Mößbauer spectroscopy (University of Duisburg-Essen) and HR-TEM (ER-C).

Reduced magnetization mainly due to APBs

SAXS gives the parameters of a lognormal size distribu-

tion $R_0 = 7.8$ nm and $\sigma = 0.095(1)$. From X-ray powder diffraction and Mößbauer spectroscopy, a composition of 15% Fe_3O_4 and 85% $\gamma\text{-Fe}_2\text{O}_3$ is determined. Room temperature magnetometry gives a saturation magnetization of 60(1) Am^2/kg , which is significantly lower than the bulk reference value of 77 Am^2/kg for the assumed composition. The aforementioned APBs are clearly visible with HR-TEM. Additionally, the selective peak broadening observed in the X-ray powder diffraction pattern supports this finding. PDF-analysis shows a slightly disordered crystal structure with an increase in iron vacancies. Polarized SANS shows a non-magnetic surface layer of 0.3(1) nm thickness and a magnetic core scattering length density (SLD) of $9.4(2) \times 10^{-7} \text{ \AA}^{-2}$, which relates to a saturation magnetization of 58(4) Am^2/kg , in good agreement with the magnetometry results. In conclusion, our results suggest that the reduced magnetization may be explained by the combination of vacancies, structural disorder, a non-magnetic surface and, to a large extent, by the presence of antiphase boundaries.

[1] T. Köhler et al., *Mechanism of magnetization reduction in iron oxide nanoparticles*, *Nanoscale* 13, 14, 6965 (2021)
DOI: 10.1039/D0NR08615K



(a) SANS fits to the sectors parallel to the applied field. (b) Fits to the perpendicular sector to determine the non-magnetic surface layer thickness and the magnetic SLD. (c) XRD profile showing hkl-dependent peak broadening, associated with APBs. (d) HR-TEM micrograph of a particle containing an APB as indicated with the red square. (e) Inverse FFT of (d) after masking the 220 reflection, making the APB shift more apparent.

Interdependent scaling of long-range oxygen and magnetic ordering in nonstoichiometric $\text{Nd}_2\text{NiO}_{4.10}$

S. R. Maity^{1,2}, M. Ceretti³, L. Keller¹, J. Schefer¹, M. Meven⁴, E. Pomjakushina⁵, W. Paulus³

¹Laboratory for Neutron Scattering and Imaging, Paul Scherrer Institute, Villigen, Switzerland; ²University of Geneva, Department of Quantum Matter Physics (DQMP), Geneva, Switzerland; ³ICGM, Université de Montpellier, CNRS, ENSCM, Montpellier, France; ⁴Institute of Crystallography, RWTH Aachen at MLZ, Garching, Germany; ⁵Laboratory for Multiscale Materials Experiments, Paul Scherrer Institute, Villigen, Switzerland

The interplay of structural, orbital, charge and spin degrees of freedom often leads to novel physical properties in magnetic oxides. Employing neutron diffraction, a unique coupling between structural and spin order was found in low oxygen doped layered rare-earth $\text{Nd}_2\text{NiO}_{4.10}$. Here, the spin ordering below 48 K adopts the same modulation vectors as the oxygen order, suggesting O-doping/order to be a promising concept to chemically induce long-range spin ordering.

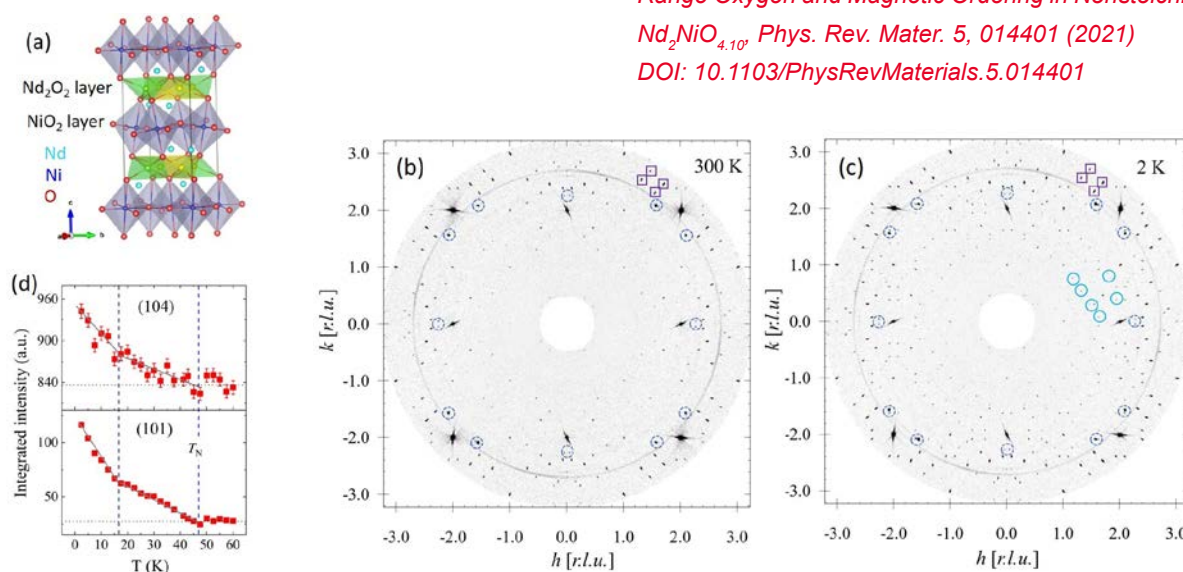
Exploring oxygen and magnetic order correlation

Hole-doped layered rare-earth Ruddlesden-Popper nickelates Ln_2NiO_4 are strongly correlated electronic systems with exciting physical and electronic properties originating from the subtle interplay of structural, orbital, charge, and spin degrees of freedom. Hole doping can be achieved either by substituting the trivalent Ln atoms with bivalent alkaline earth metals or by oxygen doping, yielding $\text{Ln}_2\text{NiO}_{4+\delta}$. The extra oxygen atoms, occupying the interstitial sites, remain mobile close to room temperature (figure a), leading to complex ordering scenarios depending on δ and T. Here, we study the interplay between oxygen and spin order for a low oxygen doping concentration i.e. $\text{Nd}_2\text{NiO}_{4.10}$ [1].

Reciprocal plane mappings were performed on a $\text{Nd}_2\text{NiO}_{4.10}$ single crystal at variable temperatures on the neutron powder diffractometer DMC at SINQ (PSI). Integrated intensities of selected Bragg reflections were recorded on the four-circle diffractometer HEiDi at the FRM II.

Detailed analysis of diffraction data revealed a low-temperature tetragonal (LTT) crystal structure with space group $P4_2/nm$ in the temperature range of 2-300 K. The extra satellite reflections observed at 300 K are due to a complex 3D oxygen ordering, the modulation vectors being $\pm 2/13\mathbf{a}^* \pm 3/13\mathbf{b}^*$, $\pm 3/13\mathbf{a}^* \pm 2/13\mathbf{b}^*$ and $\pm 1/5\mathbf{a}^* \pm 1/2\mathbf{c}^*$ (figure b-c). T-dependent measurements suggest two magnetic phase transitions at $T_N = 48$ K and 20 K, related to the magnetic ordering of the Ni and Nd sublattice (figure d). The modulation vectors of the magnetic ordering were found to adopt exactly those of the oxygen order. This is atypical so far and not previously encountered for the homologous nickelates. Thus, the mediation achieved between magnetic and oxygen ordering in $\text{Nd}_2\text{NiO}_{4.10}$ yields a promising concept to establish long-range magnetic ordering, essentially based on long-range oxygen ordering.

[1] S. R. Maity et al, *Interdependent Scaling of Long-Range Oxygen and Magnetic Ordering in Nonstoichiometric $\text{Nd}_2\text{NiO}_{4.10}$* *Phys. Rev. Mater.* 5, 014401 (2021)
DOI: 10.1103/PhysRevMaterials.5.014401



(a) The LTT unit cell of $\text{Nd}_2\text{NiO}_{4.10}$, consisting of an alternate stacking of NiO_2 and Nd_2O_2 layers along the c -axis. The $4b$ sites (green) are only occupied by the excess oxygen atoms while $4e$ sites (yellow) are empty. $(hk0)$ neutron diffraction planes (DMC at PSI) at (b) 300 K and (c) 2 K. Bragg peaks resulting from oxygen (squares) and spin order (full circles), as well as from epitaxial grown NiO impurity intergrowth phase (dashed circles), are shown. (d) Intensity evolution with T for selected magnetic peaks (HEiDi at FRM II).

Breaking the magnetic symmetry in the HoFeO_3 in an external magnetic field

A. Ovsianikov^{1,2}, H. Thoma^{1,3}, O. Usmanov², P. J. Brown⁴, T. Chatterji⁵, A. Sazonov^{1,2}, S. Barilo⁶, L. Peters¹, V. Hutanu^{1,3}

¹Institute of Crystallography, RWTH Aachen University, Aachen, Germany; ²Petersburg Nuclear Physics Institute named by B.P. Konstantinov of NRC «Kurchatov Institute», Gatchina, Russian Federation; ³Jülich Centre for Neutron Science JCNS at Heinz Maier-Leibnitz Zentrum (MLZ), Forschungszentrum Jülich GmbH, Germany; ⁴12 Little St. Marys Lane, Cambridge, UK; ⁵Institut Laue-Langevin, Grenoble, France; ⁶GO National Science and Practice Center Academy of Sciences of Belarus in Materials Science, Minsk, Belarus.

Polarized neutron diffraction (PND) is a powerful method for studying magnetic ordering on the microscopic level. Recently, a new PND setup was implemented on the diffractometer POLI at the Heinz Maier-Leibnitz Zentrum (MLZ) in Garching Germany. The goals of the present research are to both investigate the detailed temperature-field evolution of the magnetic reorientation phase transition from phase Γ_4 to phase Γ_1 near 50 K in HoFeO_3 , and check the reliability of the new PND option at different wavelengths [1].

A cryogen-free 2.2 T, compact high- T_c superconducting magnet was employed. Two series of measurements were also made to test the feasibility of the setup used at different wavelengths: The first using a neutron wavelength of 1.15 Å and the second of 0.71 Å. The crystal of HoFeO_3 studied was aligned with its [001] axis nearly parallel to the ω diffractometer axis (sample rotation axis), which is also the magnetic field axis and neutron polarization direction. Using a lifting detector, a set of in-plane and out-of-plane (hkl) Bragg reflections, with $l = 0, -1$ and -2 , was measured at four field values: 0.15, 0.5, 1.0 and 2.2 T respectively.

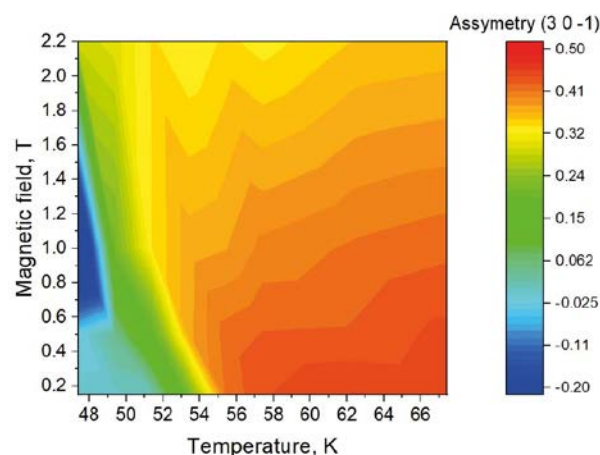
Asymmetry of Bragg reflection and phase transition

The experimentally measured asymmetry map for the exemplary G-type reflection (3 0 - 1) is shown in the figure. Below 53 K in the lowest field (0.15 T), the magnitude of the x-component of the Fe moment decreases abruptly whilst that of the y-component increases. This behavior is

consistent with the reorientation transition to the Γ_1 structure observed in zero field. Further increasing the applied field lowers the temperature of the transition, until it does not occur within the scanned temperature range for 2.2 T. However, an attempt to fit the intermediate phase as a linear combination of different volume fractions of Γ_1 and Γ_4 phases did not lead to a converging solution. The fact that this intermediate phase breaks the magnetic symmetry could not be explained as a linear combination of the Γ_4 and Γ_1 phases and should be considered as a new low-symmetry magnetic phase.

[1] A. Ovsianikov et al., *Breaking the Magnetic Symmetry by Reorientation Transition Near 50 K in Multiferroic Magneto-caloric HoFeO_3* , *IEEE Transactions on Magnetics*, 58, 2, 1 (2022), 21 May 2021 added to IEEE Xplore.

DOI: 10.1109/TMAG.2021.3082324



Temperature/field map for the measured asymmetry of G-type peak (3 0 - 1). The reddish area corresponds to the magnetic phase Γ_4 , blue to Γ_1 , celestial-greenish to the intermediate monoclinic magnetic phase.

Structural influences on the ionic conductivity of Li⁺ conductors in the polymorphs α - and β -Li₈SnP₄

S. Strangmüller¹, H. Eickhoff¹, W. Klein¹, G. Raudaschl-Sieber², H. Kirchhain³, T. Kutsch^{4,5}, V. Baran⁶, A. Senyshyn⁶, L. van Wüllen³, H. A. Gasteiger⁴, T. F. Fässler¹

¹Chair of Inorganic Chemistry, Department of Chemistry, Technical University of Munich, Garching, Germany; ²Chair of Inorganic and Metal-Organic Chemistry, Department of Chemistry, Technical University of Munich, Garching, Germany; ³Department of Physics, University of Augsburg, Augsburg, Germany; ⁴Chair of Technical Electrochemistry, Department of Chemistry, Technical University of Munich, Garching, Germany; ⁵TUMint Energy Research GmbH, Garching, Germany; ⁶Heinz Maier-Leibnitz Zentrum (MLZ), Technical University of Munich, Garching, Germany

Understanding the structure-property relationships of solid electrolytes is crucial for the further development of materials that are suitable for application in all-solid-state batteries. In this context, the class of lithium phosphidotetrelates represents a family of promising solid ion conductors whose structure-property relationships require more detailed investigations as its members combine a rich structural variety and diverse properties within a close structural relationship.

Applying the concept of isovalent substitution to the compound (α -)Li₈SiP₄ not only gave access to the lithium phosphidotetrelates α -Li₈GeP₄ and α -Li₈SnP₄ but also revealed the existence of a second polymorph of the heavier homologues. Since the materials β -Li₈GeP₄ and β -Li₈SnP₄ feature distinctly increased ionic conductivities as compared to the corresponding α -modifications, the two polymorphs α - and β -Li₈SnP₄ have been thoroughly investigated by applying X-ray and neutron diffraction experiments as well as nuclear magnetic resonance and electrochemical impedance spectroscopy, revealing the small structural differences that are responsible for the varying conductivities.[1]

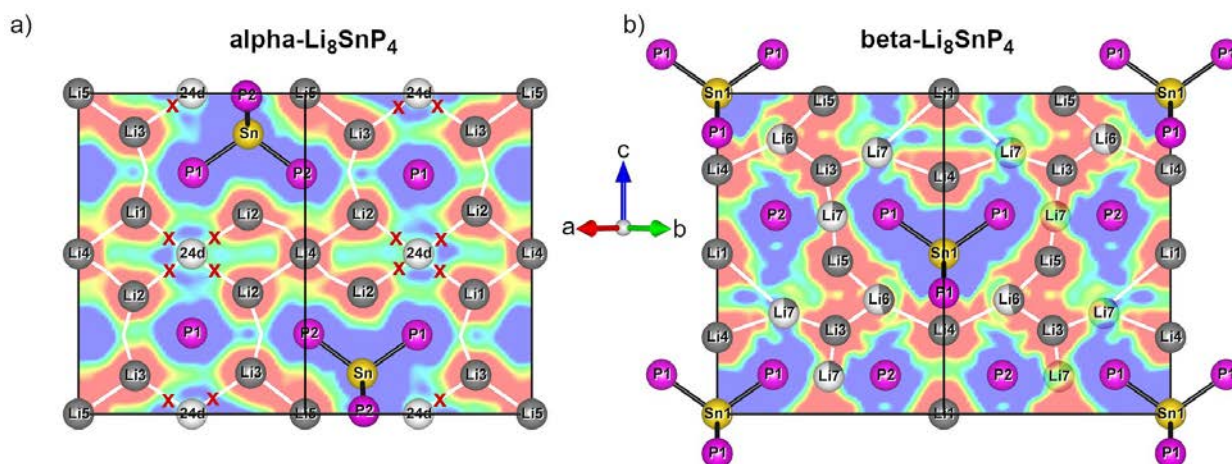
For the powder neutron diffraction experiments the samples were sealed in a niobium tube container under argon atmosphere. Powder diffraction patterns were collected over

a wide temperature range of 4 - 1023 K at the instrument SPODI at a wavelength of 1.5482 Å.

Li pathway revealed

Of the materials investigated, only lithium (in its natural isotope composition) possesses a negative scattering length. The analysis could therefore be limited to the negative component of scattering density distribution to obtain accurate information on lithium diffusion pathways. The data evaluation was carried out by applying the maximum entropy method as well as the one-particle potential from negative nuclear densities. The results reveal lower activation barriers, and thus, a preferred Li-ion diffusion via well-resolved necks connecting face-sharing tetrahedral and octahedral sites. However, due to the unoccupied octahedral site (24d) in α -Li₈SnP₄ which hint for a higher potential of this site, the Li-ions alternatively migrate *via* the less favored common edge of the adjacent tetrahedral sites (figure a). This bypass is found to be the reason for the reduced ionic conductivity of the α -phase when compared to β -Li₈SnP₄ as in the latter all occurring voids are at least partially occupied, which allows for alternating ion migration through adjacent tetrahedral and octahedral sites (figure b).

[1] S. Strangmüller et al., *Synthesis, structure and diffusion pathways of fast lithium-ion conductors in the polymorphs α - and β -Li₈SnP₄*, *J. Mater. Chem. A* 9, 15254 (2021)
DOI: 10.1039/D1TA03021C



Selected 2D section cuts of the one-particle-potential (red $\hat{=}$ low, blue $\hat{=}$ high) of α - and β -Li₈SnP₄ revealing differences of Li-ion diffusion within the two modifications. Possible diffusion pathways are depicted as white lines and red crosses mark blocked pathways due to unoccupied octahedral voids. Sn, P and Li atoms as well as vacant sites are drawn as gold, pink, gray and white spheres, respectively.

The new positron diffractometer at NEPOMUC – instrumentation and beam characterization

M. Dodenhöft², S. Vohburger¹, C. Hugenschmidt¹

¹Heinz Maier-Leibnitz Zentrum (MLZ), Technical University of Munich, Garching, Germany; ²Physics-Department, Technical University of Munich, Garching, Germany

The topmost layer sensitivity of total-reflection high-energy positron diffraction (TRHEPD) allows the accurate determination of surface structures.

To make TRHEPD measurements possible, the availability of a bright monoenergetic positron beam is mandatory. We designed and installed a new TRHEPD instrument at the high-intensity positron source NEPOMUC. Results from first experiments for beam characterization were shown to be in good agreement with our simulations.

The crystalline structure of surfaces plays a crucial role for a variety of physical phenomena and for many technical processes, such as the epitaxial growth of ultra-thin films or heterogeneous catalysis. Moreover, accurate models of the surface structure are necessary to calculate the electronic structure at the surface. The surface and bulk crystal structure can differ since the atoms at the surface experience a different crystal potential that becomes evident, e.g., by surface reconstructions.

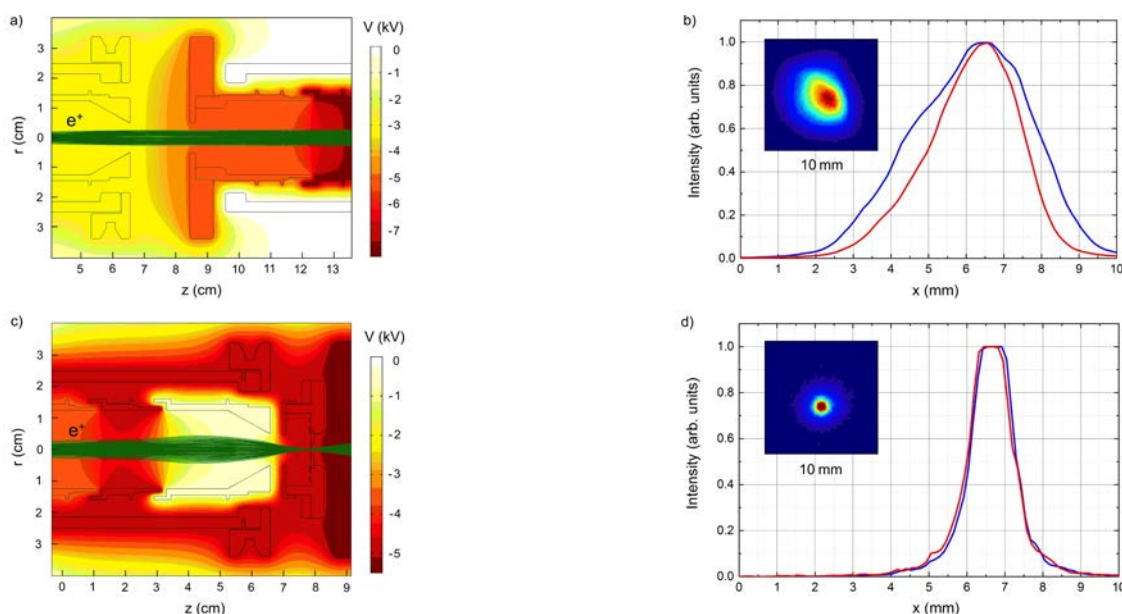
TRHEPD, i.e. positron diffraction in grazing incidence, is a powerful technique for the determination of the crystal structure of topmost and subsurface atomic layers. In contrast to electrons, positrons experience a repulsive crystal potential

and thus exhibit total reflection for small glancing angles, which allows structure analysis with outstanding surface sensitivity.

In order to enable positron diffraction experiments at NEPOMUC, we tested crucial elements of our new TRHEPD setup, e.g., the magnetic field termination, the optional brightness enhancement device and the electrostatic beam optics. The positron trajectories of the remoderated NEPOMUC beam and the twofold remoderated beam have been simulated to optimize the system. During a first beamtime, we characterized the direct beam with and without an additional remoderator (see figure). After twofold remoderation and acceleration up to 10 keV, we obtained a parallel positron beam with a diameter of less than 1.3 mm. The results are in agreement with simulations of the positron trajectories and the beam properties are demonstrated to be well suited for diffraction experiments. Within the next beamtime, a first diffraction pattern will be recorded to benchmark the setup.

[1] M. Dodenhöft et al., Total-reflection high-energy positron diffractometer at NEPOMUC — Instrumentation, simulation, and first measurements, *Rev. Sci. Instrum.* 92, 11, 115103 (2021)

DOI: 10.1063/5.0062412



Simulation and experimental characterization of the positron beam for TRHEPD. Computed positron trajectories in the section of the optional remoderator for brightness enhancement (a) without and (c) with applied remoderator. Experimentally determined beam profile of (b) the 15 keV remoderated NEPOMUC beam and (d) the 10 keV twofold remoderated positron beam.

How ultracold neutrons interact with surfaces and bulk material

S. Döge^{1,2,3}, J. Hingerl^{1,2}, E. V. Lychagin⁴, C.-Y. Liu⁵, A. R. Young⁶, C. Morkel²

¹Institut Laue-Langevin, Grenoble, France; ²Physics Department, Technical University of Munich, Garching, Germany; ³Heinz Maier-Leibnitz Zentrum (MLZ), Technical University of Munich, Garching, Germany; ⁴Frank Laboratory of Neutron Physics, JINR, Dubna, Russia; ⁵Department of Physics, Indiana University, Bloomington, Indiana, USA; ⁶Department of Physics, North Carolina State University, Raleigh, North Carolina, USA

Understanding the interaction of ultracold neutrons (UCN) with surfaces and bulk material is key to improving UCN sources. We measured UCN losses on rough metal surfaces and provide a way to calculate the 1-phonon up-scattering cross section of solid deuterium for UCNs.

Efforts have been made for many years to improve the output of sources of ultracold neutrons (UCN) and to develop new source designs. For both purposes, it is important to understand the interaction of UCNs with the walls of transport guides and vacuum windows on the one hand, and inside the moderator medium on the other. The moderator is the volume, in which cold neutrons are decelerated by inelastic collisions to ultracold-neutron velocities. In some cases, solid ortho-deuterium is used for this purpose.

We have revisited the theory of 1-phonon up-scattering in bulk materials. We found that the commonly used incoherent approximation (IA) yields UCN up-scattering cross sections that are a factor of 2 - 5 too high for solid deuterium, which is a predominantly coherent neutron scatterer. Applying the Placzek-Van Hove correction, we showed a way of calculating the true 1-phonon up-scattering cross-sections for materials at cryogenic temperatures.

To extract a maximum UCN flux from a source, it is important not only to have a large UCN production cross section but also a low loss cross section. Previous interpretations of transmission experiments with UCNs on solid deuterium, which relied on the IA, attributed all UCN losses to up-scattering to higher neutron energies. This cannot be upheld any more.

Theoretical model versus experimental results

To understand the interactions of UCNs with rough surfaces, we measured the transmission of UCNs through metal foils. We applied a theoretical scattering model by Steyerl to

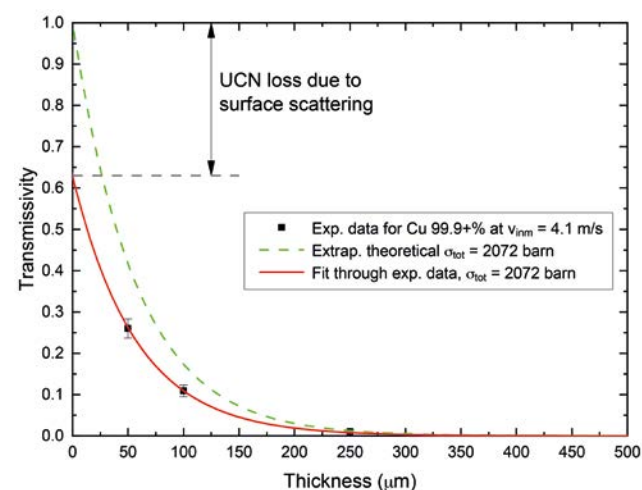
these data and were able to extract the surface roughness of these foils as seen by the neutrons. Next, we compared these roughness values with those obtained by mechanical means of measurement. Both showed only qualitative agreement. We concluded that it is thus very important to actually measure the UCN losses due to rough surfaces and not only to calculate or simulate them based on other measurements. We also found, in the case of thin copper foils, that the rough surface alone scatters as many UCNs out of the direct beam as several tens of micrometers of bulk material (see figure).

[1] S. Döge et al., *Scattering of ultracold neutrons from rough surfaces of metal foils*, *Physical Review C* 102, 064607 (2020)

DOI: 10.1103/PhysRevC.102.064607

[2] S. Döge et al., *Incoherent approximation for neutron up-scattering cross sections and its corrections for slow neutrons and low crystal temperatures*, *Physical Review C* 103, 054606 (2021)

DOI: 10.1103/PhysRevC.103.054606



The measured transmissivity of Cu foils of three different thicknesses is plotted for UCNs of an in-medium velocity of 4.1 m/s. The red line represents a fit to the measured data using the transmission equation including a surface scattering term. The dashed green line represents the transmissivity as expected if the sample caused no surface scattering.

Implementing cryogenic temperatures at the high-pressure instrument SAPHiR

C. M. Howard¹, N. P. Walte²

¹Bayerisches Geoinstitut (BGI), University of Bayreuth, Bayreuth, Germany; ²Heinz Maier-Leibnitz Zentrum (MLZ), Technical University of Munich, Garching, Germany

A new cooling system for the SAPHiR 6-6 multi-anvil instrument in the Neutron Guide Hall East of the FRM II extends the available temperature range of the instrument to 80 - 2300 K at pressures up to 15 GPa. Consisting of liquid nitrogen cooled rings, the secondary anvils and the sample are cooled to < 90 K in 10 minutes. This new system allows for static experiments, controlled deformation studies, and cryogenic recovery of high-pressure phases.

The new cooling system at SAPHiR

The ability to perform high-pressure experiments at low temperature is of great interest in Earth and material science, but has previously been limited by the pressures available for large sample volumes, which are required for neutron scattering studies.

Therefore, we developed a cooling system for the SAPHiR instrument at the FRM II neutron source, a multi-anvil device with six independently-controlled 8 MN rams that allow both hydrostatic and non-hydrostatic experiments to be performed at pressures < 15 GPa and controlled strain rates between ca. 10^{-3} and 10^{-7} s⁻¹, whilst maintaining large sample volumes.

The system [1] consists of liquid nitrogen cooled aluminium rings that enclose the base of each of the secondary anvils, cooling the sample to < 90 K in 10 minutes. By varying the flow-rate of liquid nitrogen to the cooling rings, temperatures can be controlled to ± 5 K of a selected temperature. The relative simplicity of the system means it can be used with existing assemblies, with the internal geometry kept simple, thereby allowing for large sample volumes.

This new system allows for static experiments, controlled deformation studies, and cryogenic recovery of high-pressure phases to be performed, in principle, over the whole pressure range of the press at cryogenic temperatures, in

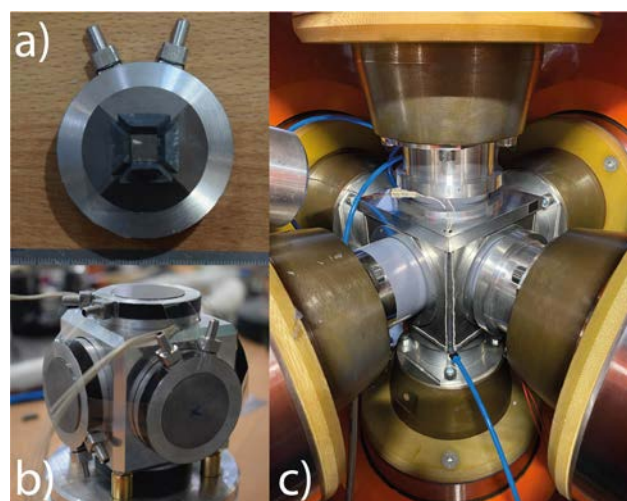
addition to conventional heated experiments. Some examples of novel applications include deformation of high-pressure ices to understand icy moons of the outer solar system, studies of high temperature superconductivity, and testing of super-hard alloys under cryo-conditions.

Further developments of the system are planned, such as increasing the temperature control. Investigations of gasket materials will be performed to reduce blow-out risk at low temperature, with the added goal of reducing unwanted scattering from the sample environment.

This system extends the available conditions to future users. Until neutrons are available, the SAPHiR instrument is operated offline, with conditions of 83 - 2300 K and < 15 GPa available.

[1] C. M. Howard, et al., *New cooling system for a three-axis multi-anvil press with 6-6 geometry*, *High Press. Res.* 41, 2, 119 (2021)

DOI: [10.1080/08957959.2021.1910254](https://doi.org/10.1080/08957959.2021.1910254)



Cooling system assembly used in SAPHiR. (a) Tungsten carbide secondary anvils with pyrophyllite gaskets are (b) mounted using an aluminium guide frame, with the sample inside. (c) The assembly is moved into SAPHiR and placed between the six independently controlled rams inside an air-tight box to prevent icing in the instrument.

Oscillatory magnetic fields for neutron resonance spin-echo spectroscopy

J. K. Jochum¹, A. Hecht², O. Soltwedel^{2,3}, C. Fuchs¹, J. Frank¹, E. Faulhaber¹, J. C. Leiner², C. Pfeleiderer², C. Franz^{1,2,4}

¹Heinz Maier-Leibnitz Zentrum (MLZ), Technical University of Munich, Garching, Germany; ²Physics Department, Technical University of Munich, Garching, Germany; ³Institut für Festkörperphysik, Technische Universität Darmstadt, Darmstadt, Germany; ⁴Jülich Centre for Neutron Science (JCNS) at MLZ, Forschungszentrum Jülich GmbH, Garching, Germany

The generation of high frequency oscillatory magnetic fields is essential for the successful implementation of neutron resonant spin-echo spectrometers, a class of instrumentation critical for high-resolution measurements of dynamic processes in materials. Here, we demonstrate that the new resonant circuits at the spectrometer RESEDA are capable of functioning at frequencies up to 3.6 MHz, pushing the energy resolution of RESEDA below 10 neV.

In neutron spin-echo, the achievable resolution is proportional to the size and magnetic field strength of the solenoids used to create the spin precession zones. The polarization of the neutron beam is limited by the field inhomogeneity, which becomes increasingly difficult to maintain as the solenoid size increases. Golub and Gähler showed that replacing the solenoids with pairs of compact resonant spin-flippers negates the need for correction coils while achieving comparable resolutions. These radio-frequency (RF) spin flippers, together with the resonating circuits driving them, make up the heart of neutron resonant spin-echo spectrometers, including the MIEZE (modulation of intensity with zero effort) variant of the technique.

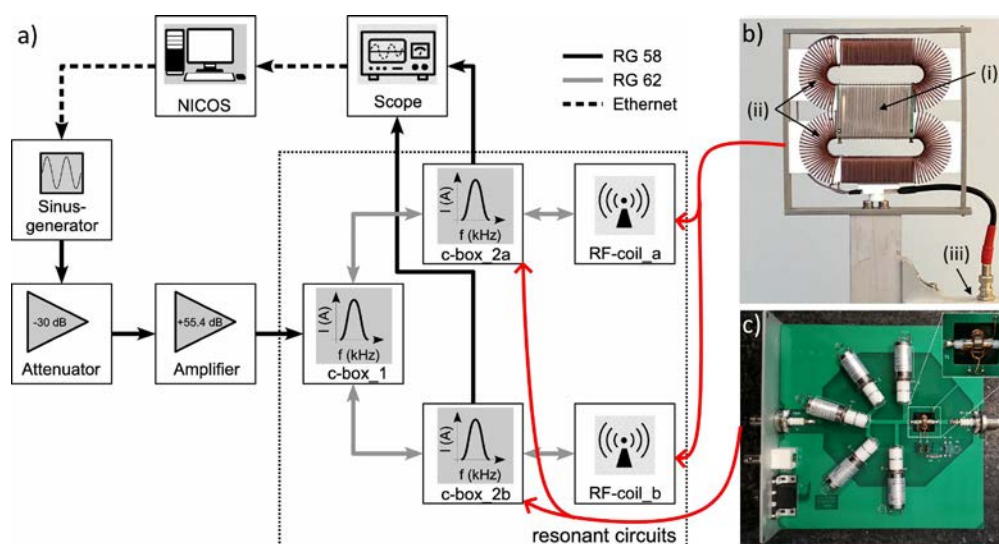
The development of the newest resonant circuits used at the spectrometer RESEDA was necessary to increase its resolution to 100 ns (with 10 Å neutrons) and beyond.

The resonant circuit is depicted schematically in figure a. It consists of a signal generator which feeds into an amplifier, via an attenuator. The signal then connects to a matching circuit which is split into two parts: one part for frequencies below 1 MHz (C-box1), and a second part for higher frequencies (C-box2, figure c). The latter is fixed directly to the coils to reduce the length of the cables between it and the RF coil (figure b), minimizing parasitic capacitances from the cables. The matching circuit is connected to the RF coils as well as to an oscilloscope providing feedback to the operating software NICOS to allow for fast regulation.

The RF coil itself consists of a main coil and two compensation coils (see figure b). The compensation coils (ii) are connected in parallel to each other and in series to the main coil (i). They compensate for the stray fields produced outside the main coils in the path of the polarized neutron beam, thereby preventing perturbations of the static field and reducing power losses from induced currents in the adjacent metallic structures.

[1] J. K. Jochum et al., *Oscillatory magnetic fields for neutron resonance spin-echo spectroscopy*, *Meas. Sci. Technol.* 32, 045902 (2021)

DOI: 10.1088/1361-6501/abce3b



(a) Schematic representation of the resonating circuits; (b) RF-coil with (i) main coil (ii) compensation coils and (iii) C-box2 indicated; (c) C-box2; inset shows the pick-up coil

Fast neutron induced
gamma-ray spectrometry (FaNGaS)E. Mauerhofer¹, Z. Ilic^{1,2}, C. Stieghorst³, Z. Révay³, M. Rossbach⁴, J. Li¹, T. H. Randriamalala¹, T. Brückel^{1,2}

¹Jülich Centre for Neutron Science (JCNS-2), Forschungszentrum Jülich GmbH, Jülich, Germany; ²Lehrstuhl für Experimentalphysik IVc, RWTH Aachen University, Aachen, Germany; ³Heinz Maier-Leibnitz Zentrum (MLZ), Technical University of Munich, Garching, Germany; ⁴Im Heidehof, Kreuzau Untermaubach, Germany

FaNGaS is a worldwide unique facility which uses the intense fission neutron beam delivered by the SR10 channel of the FRM II to investigate fast-neutron induced prompt gamma-ray emission to create a modern and comprehensive catalogue of (n,n'γ)-reactions. It offers new possibilities for the chemical analysis of large or small samples and is a complementary method to conventional cold-neutron based PGAA. Results obtained from the measurement of indium are presented by way of an example.

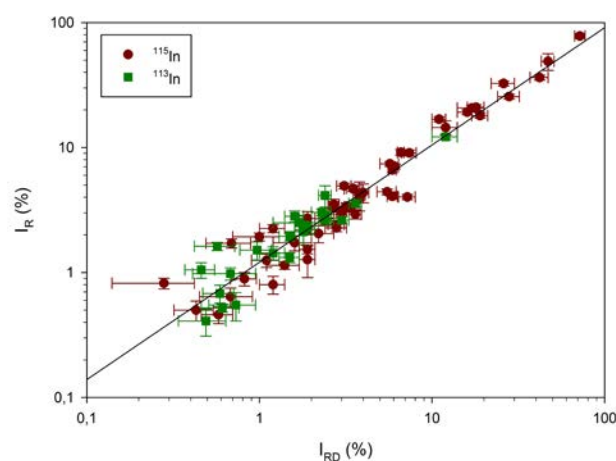
Prompt and delayed gamma emission induced by the capture of epithermal and fast neutrons and by the inelastic scattering of fast neutrons on indium was investigated using FaNGaS [1]. The gamma-ray spectrum was recorded via a well-shielded electromechanically cooled HPGe-detector (relative efficiency of 50% and a resolution of 2.1 keV at 1.33 MeV). The measurement was performed at an angle of 90° between the neutron beam direction and detector with an integral neutron flux of $1.42 \times 10^8 \text{ cm}^{-2}\text{s}^{-1}$ and an epithermal flux of $1.85 \times 10^6 \text{ cm}^{-2}\text{s}^{-1}$ at the sample position. The sample-to-detector distance was 67 cm.

A total of 42 neutron capture gamma lines issued from the $^{115}\text{In}(n,\gamma)^{116}\text{In}$ reaction were detected. Their absolute intensities were calculated with a spectrum-averaged reaction cross section of 0.55 b and found to be comparable to the absolute intensities of the corresponding thermal neutron capture lines. From the delayed gamma rays of $^{116\text{m}}\text{In}$ and $^{116\text{m}2}\text{In}$, spectrum-averaged cross sections of $508 \pm 24 \text{ mb}$ and $201 \pm 10 \text{ mb}$ were determined for the $^{115}\text{In}(n,\gamma)^{116\text{m}}\text{In}$ and $^{115}\text{In}(n,\gamma)^{116\text{m}2}\text{In}$ reactions, respectively.

Fast and epithermal neutron reactions on indium

Additionally, we show the necessity to reevaluate the thermal neutron cross section of the $^{115}\text{In}(n,\gamma)^{116\text{m}2}\text{In}$ reaction. A total of 94 prompt gamma lines arising from $^{115}\text{In}(n,n')^{115}\text{In}$ and $^{113}\text{In}(n,n')^{113}\text{In}$ reactions were observed and their relative intensities (using the 933 keV gamma ray of ^{115}In as reference) and spectrum-averaged production cross sections were determined. In a comparison with the work of Demidov, 13 additional gamma lines were detected. Several lines mentioned in the Demidov Atlas were identified as neutron capture gamma lines or decay gamma lines of $^{113\text{m}}\text{In}$, $^{114\text{m}2}\text{In}$ and $^{115\text{m}}\text{In}$. For the reactions $^{113}\text{In}(n,n')^{113\text{m}}\text{In}$, $^{113}\text{In}(n,\gamma)^{114\text{m}2}\text{In}$ and $^{115}\text{In}(n,n')^{115\text{m}}\text{In}$ we determine spectrum-averaged cross sections of 143 ± 22 , 288 ± 13 and $194 \pm 18 \text{ mb}$, respectively. The relative intensities of the prompt gamma lines measured in our work agree reasonably well (1.6σ level) with the values given in the Demidov Atlas (see figure).

[1] E. Mauerhofer et al., *Prompt and delayed gamma rays induced by epithermal and fast neutrons with indium*, *J. Radioanal. Nucl. Chem.* 331, 535 (2022), 02 December 2021 added to Hybrid (Transformative Journal) of JRNC DOI: 10.1007/s10967-021-08102-2



Relationship between the relative intensities I_R of the prompt gamma rays induced by fast neutron inelastic scattering on indium measured in this work and the relative intensities I_{RD} tabulated in Demidov Atlas (Demidov et al, Atlas of Gamma-ray Spectra from the Inelastic Scattering of Reactor Fast Neutrons, Moscow, Atomizdat, 1978). The solid line represents the fit of the data with $I_R = a \times (I_{RD})^b$, $a = 1.21 \pm 0.06$ and $b = 0.94 \pm 0.03$.

Lead halide ionic liquids for
high-spatial-resolution fast neutron imagingK. Sakhatskyi^{1,2}, M. V. Kovalenko^{1,2}¹Department of Chemistry and Applied Biosciences, ETH Zürich, Zurich, Switzerland; ²Empa-Swiss Federal Laboratories for Materials Science and Technology, Dübendorf, Switzerland

The fast neutron imaging technique with recoil proton detection harbors significant potential for imaging, however there is the challenge of finding efficient fast neutron scintillators with high spatial resolution. This work [1], conducted at the NECTAR beamline for fast neutron imaging, investigates the scintillation properties of ionic liquids, showing both higher spatial resolution and lower γ -ray sensitivity compared to commercial ZnS:Cu screens.

The list of requirements for high-spatial-resolution scintillators is long and demanding: A proton-rich, scattering-free material combining high light yield with the absence of light reabsorption. To meet these challenges, we looked for a suitable material in a rising class of OD organic-inorganic Pb(II) halide hybrids. The use of large organic cations results in room-temperature ionic liquids that combine highly Stokes-shifted reabsorption-free, and efficient emission from molecularly small and dense emitting centers.

Spatial resolution evaluation

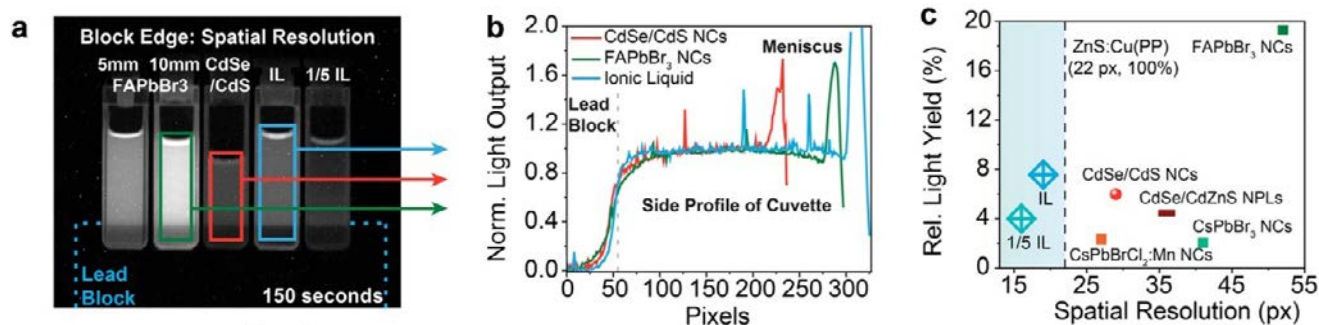
To test the IL-based scintillator spatial resolution, a lead block (2.5 cm thick) is placed in the path of the fast neutron beam to provide a sharp edge to the transmitted beam, leading to light (unblocked) and dark (attenuated) regions in the

image (figure a). The spatial resolution is then estimated by comparing the sharpness of the edge in the change in light yield across this region, as shown in the side profile of the cuvette (figure b). We utilize the 10–90% rise as a conservative numeric measure of the edge sharpness, normalizing the light and dark regions to 1 and 0 light output, respectively, and measuring the number of pixels needed to go from 0.1 to 0.9 (each pixel represents ~ 0.1 mm). The edge measured with the IL is sharper than that of the ZnS:Cu(PP) reference. This result also demonstrates that the lack of a scattering phosphor-plastic interface can yield improvements even over the commercial standard ZnS:Cu(PP).

This work demonstrates the proof-of-concept for IL-based fast neutron scintillators and provides guidelines to identify promising IL-metal halide compositions. Pb(II) halide ILs display a compelling set of characteristics required for fast neutron imaging: They are scattering-free, include proton-rich cations, and permit a high density of the emitting centers. These qualities, together with high PLQY (60%) and large Stokes shift (up to 1.7 eV), result in a spatial resolution superior to the established ZnS:Cu scintillators.

[1] V. Morad et al., *Luminescent Lead Halide Ionic Liquids for High-Spatial Resolution Fast Neutron Imaging*, *ACS Photonics* 8 (11), 3357 (2021)

DOI: 10.1021/acsp Photonics.1c01348



(a) Radiograph of IL and colloidal NCs with a lead block in the beam for a sharp edge to measure spatial resolution, 150 s fast neutron beam exposure. (b) Side profile of the light output from the ionic liquid cuvette, with the unattenuated fast neutron beam normalized to 1, while the 0 is set to the dark value of the lead-blocked beam. (c) Summary of fast neutron imaging characteristics of these ionic liquids and colloidal NCs.

Progress towards a confined pair plasma in a dipole trap: combining positrons with an electron cloud

M. Singer¹, M. R. Stoneking^{2,3}, E. V. Stenson³, S. Nißl^{1,3}, A. Deller³, A. Card³, J. Horn-Stanja³, T. Sunn Pedersen^{3,4}, H. Saitoh⁵,
C. Hugenschmidt¹

¹Heinz Maier-Leibnitz Zentrum (MLZ), Technical University of Munich, Garching, Germany; ²Department of Physics, Lawrence University, Appleton, Wisconsin, USA; ³Stellarator Edge and Divertor Physics Division, Max Planck Institute for Plasma Physics, Greifswald, Germany; ⁴Department of Physics, University of Greifswald, Greifswald, Germany; ⁵Department of Physics, The University of Tokyo, Kashiwa, Japan

The APEX collaboration aims to confine and study electron-positron pair plasmas in magnetic traps.

For the first time, we report a combined system of these particles. To do this, an e^- source was placed inside the confinement region of a dipole magnetic field and used to establish a space potential (-42 V). We demonstrate that the presence of this e^- cloud does not interfere with e^+ injection and, in fact, extends the parameter range.

Due to its compelling simplicity, a confined, magnetized low-energy electron-positron pair plasma is a system that has fascinated theorists for decades. Experimentally, however, one of the main challenges to establishing such a plasma is the limited availability of positrons. The APEX (A Positron Electron eXperiment) collaboration is nevertheless making progress toward generating pair plasmas by combining positrons and electrons in tabletop-sized toroidal traps whose closed field lines allow the simultaneous trapping of both species.

As an intermediate step, a prototype trap based on a permanent magnet was used to develop the required techniques. Positrons from the NEPOMUC source are losslessly injected on one side of the confining dipole magnetic field using an ExB drift. To combine both species, and to force their orbits to overlap despite their opposite toroidal drift directions around the magnet, an e^- source was placed inside the confining volume, 180° away from the e^+ injection site. The electrons emitted generated a space potential as low as -42 V, corresponding to a density in the range of 10^{12} m^{-3} and a Debye length between 1 and 3 cm, which qualifies as a non-neutral plasma.

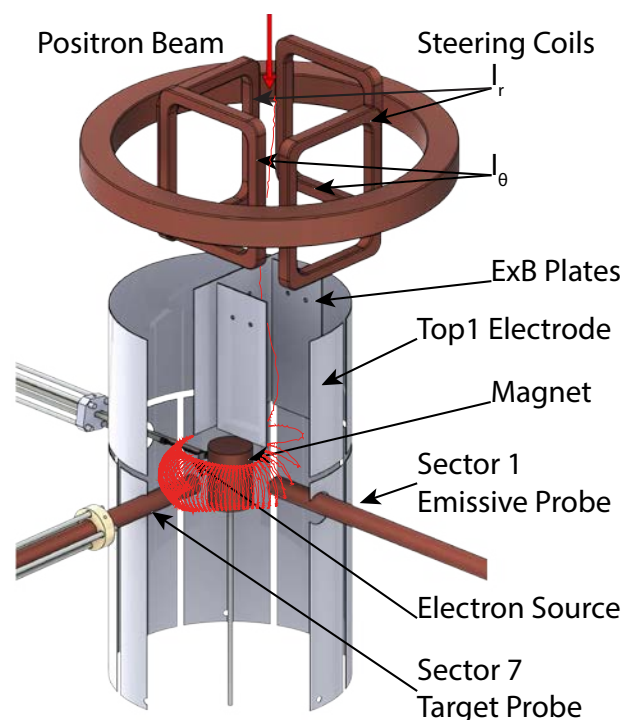
How does the e^- cloud affect the e^+ ?

Both the bias potential of the e^- source (-78 V) and the established space charge significantly alter the electrostatic landscape that is optimized for injecting the 5 eV e^+ beam. We therefore needed to test whether our drift injection technique was still viable in such a scenario.

It was found that, even though the effects of the potentials are clearly visible, the capability to inject positrons without losses was preserved and even modestly extended in parameter space. This represents a major milestone, since plasma densities were obtained in the APEX prototype trap for the first time and a combined system of electrons and positrons was established. This validates our strategy for achieving a pair plasma. The next steps will be to create a space charge using e^- edge injection and to confine both species for long periods of time.

[1] M. Singer et al., *Injection of positrons into a dense electron cloud in a magnetic dipole trap*, *Phys. Plasmas* **28**, 062506 (2021)

DOI: 10.1063/5.0050881



Positron injection into the dipole trap: The e^+ beam enters the setup from above and passes steering coils that adjust the beam position before its injection. The drift induced by the ExB plates allows the particles to transition from the beam line-guiding field to the confining field of the magnet, centered inside a segmented cylindrical wall. This technique also works when an e^- cloud is emitted from a location opposite to the e^+ injection site.





Reactor & Development



No neutrons delivered, but challenging tasks completed

A. Pichlmaier

Forschungs-Neutronenquelle Heinz Maier-Leibnitz (FRM II), Technical University of Munich, Garching, Germany

In 2021, no neutrons were able to be delivered for the scientific community and other users of the FRM II. The reason for this was the unexpected failure of the cold neutron source, the detailed investigation of the case that followed and the process of its removal. With this task completed, we look forward to the resumption of reactor operation without the cold neutron source.

At any production facility, the unexpected is part of the routine operation. The FRM II is a production facility, and the unexpected dominated in 2021. The year was remarkably busy from the very outset with in-service and other inspections, mainly in the heavy water (D₂O) systems. The reason for this was that in such work the emission of even tiny amounts of the radionuclide C-14 can never be completely excluded; therefore, as a precautionary measure in the wake of the C-14 incident of 2020 (ME-01/2020, cf. last year's report) all such work had been suspended until the end of 2020. However, such inspections still need to be carried out; they were performed safely and calmly in the new calendar year. These inspections included pressure tests of the D₂O/H₂O heat exchanger and of the redundant vessel containing the D₂O cleaning resins. These are demanding tests; they were carried out under the close supervision of the regulator and external experts in a novel way so as to minimize any risk of contamination or even further C-14 emission. Conformity with the specified conditions was confirmed.

With all technical and administrative measures required for the restart of the reactor completed and the pandemic on the retreat, the authorities responsible gave permission to resume reactor operation. The restart was undertaken on March 31, 2021. During the start-up, at about 10% of nominal power, a pressure increase in the deuterium system of the cold neutron source (CNS) above 170 kPa triggered an automatic reactor shut-down ("scram"), as foreseen in such a situation.

The FRM II cold neutron source

The CNS is one of the so-called experimental installations. It consists of the inpile section and the machinery to generate the required cold. The inpile section is located in the heavy water tank, a mere 25 cm from the fuel assembly. It consists of a double walled vessel containing the cold moderator (approximately 12 l of D₂), at a temperature of about 21 K (-252°C), a heat exchanger and the necessary an-

cillary systems. It takes a refrigerator of significant size to keep the liquid deuterium at a working temperature of 21 K given that it is located only a few centimeters from the fuel assembly, a 20 MW heat source. At the FRM II, the required Helium-compressor is driven by a 600 kW motor situated in the UTA-building. The compressed Helium is transported at room temperature over more than 100 m to a room adjacent to the reactor hall where it is decompressed in two turbines turning at about 150'000 rpm, thereby producing the cold necessary (about 7 kW at 21 K) to keep the D₂ liquid.

A very sensitive measure for the state of the whole system is the pressure of the gaseous D₂. It is under constant surveillance and any deviation in pressure from the specified limits automatically trips the reactor. When the reactor is in operation, the cold source needs to be cold to protect itself from possible damage due to gamma and neutron induced heating.

Investigation of the cold source phenomena

The investigation focused initially on the production of the cold. The whole system was thoroughly examined by the FRM II staff with the help of local, national and even world-renowned experts in Helium refrigeration and cryosystems. Since no malfunctioning was detected, the focus of the investigation shifted to the inpile section. At very low reactor power, the neutrons counted at the scientific instruments comprised only about 20% of the anticipated numbers and, even more surprising, the imaging instrument ANTARES was able to observe an unexpected shadow when looking at the cold source; additionally, prompt gamma activation analysis (PGAA) revealed a clear sign of cadmium in the cold neutron source's moderator vessel. These results led to the conclusion of a damaged inpile section, very likely a displaced piece of cadmium shielding. With no repair possible, the decision was taken to remove the inpile section from the moderator vessel (Fig. 1).

The way to recovery

While having understood a phenomenon is good news in principle, its consequences can still be dire. The removal of the cold source, an operation similar to open heart surgery, had always been foreseen at the FRM II but never before seriously considered as a "real" option, let alone carried out. After detailed preparation, on the December 6, 2021 the removal of the cold source from the moderator vessel was successfully completed. Nonetheless, at the time of writing, one



Fig. 1: The inpile section of the cold neutron source is being pulled from the moderator vessel (left) and placed for intermediate storage in the spent fuel pool (right).

more obstacle prevents the start-up of the FRM II: a slight leak in the central channel housing the fuel element, from the cooling water H_2O into the leak detection system, was automatically discovered by the system designed and installed for such an occurrence. While the rate of leakage (not more than one drop per several minutes) is almost negligible and no radioactivity was released, this finding was reported to the nuclear safety authorities as a reportable incident because the central channel is classed as equipment with relevance to nuclear safety. In order to remedy this situation, it will be necessary to replace the central channel: A challenging task both for procurement/fabrication and installation. This will cause another significant delay to the restart of the FRM II.

Transport of fresh and spent fuel remains a daunting task

For the transport of fresh fuel, the FRM II is working in close cooperation with the French fuel manufacturer and the transport company to obtain the license for transport from the relevant authorities. However, there has been only limited success to date in getting final approval for the transport. The main difficulty stems from the fundamentally different, sometimes even contradictory, security requirements in France and in Germany.

For spent fuel, the transport still awaits the license. While the preparations have been completed on the FRM II side, the receiving party has so far not been able to meet all the technical and administrative requirements. In particular, complying with the more stringent measures for IT-security poses formidable challenges. Reading a crystal ball is not one of the FRM II's core competencies, hence a date cannot be given at this time. Therefore, alternative methods to mitigate this situation are being explored. This transport requires both a license to transport and to store the spent fuel. These licenses are intricately connected and will most likely be granted at more or less the same time. Transport of the spent fuel in 2022 would be highly desirable: The spent fuel pool is close to 100% full; soon this situation may pose another obstacle to reactor operation. At the FRM II, we do all we can to make the transport of spent fuel happen – but not everything lies within our power.

Outlook

What will be on the agenda for 2022? Bringing the FRM II back into operation for the scientific and other users! Everybody in the "Betrieb" (the reactor division of FRM II) will do his and her very best to meet this goal.

Update from reactor physics: progress towards conversion

C. Reiter¹, J. P. Acuna¹, D. Bonete-Wiese¹, J. Brotz¹, C. Ehrich¹, M. Kirst¹, J. Mercz¹, T. Schlitt¹, R. Schönecker¹, K. Shehu¹, P. Weimer¹, R. Macian-Juan², W. Petry¹

¹Forschungs-Neutronenquelle Heinz Maier-Leibnitz (FRM II), Technical University of Munich, Garching, Germany; ²Chair of Nuclear Technology, School of Engineering and Design, Technical University of Munich, Garching, Germany

Using a high level of automation and modern computational techniques, a huge parameter space in plate length, fuel thickness etc. – all of which has to be explored for core designs that are suitable for conversion of the FRM II to lower enrichment. Their development was also continued in 2021. At the end of 2022, the working group will present possible core designs for all three fuel candidates that are currently under development. In 2021, two important projects were launched: Using Neural Networks for reactor calculations and the validation of Computational Fluid Dynamic Codes (CFD). Neural networks were successfully implemented to study boiling phenomena and for the automated evaluation of pictures. As a next step, Neural Networks will help to optimize core designs. In the following article, the endeavor to validate the CFD codes and how this is rooted in international efforts are explained.

Joining forces for conversion

The international community aims to eliminate the use of Highly Enriched Uranium in civilian facilities, which includes a large number of research and test reactors. In this context, the European operators of High Performance Research Reactors (HPRR), together with the fuel element manufacturer Framatome CERCA, have formed the HERACLES consortium to develop future compact cores operating with lower enriched fuel, but still keeping their respective scientific appeal. Furthermore, the HERACLES partners engage in extensive scientific exchanges on the topic with US laboratories like ANL, ORNL, INL and LANL.

The conversion of these HPRR necessitates designing new fuel elements. Developing such designs requires extensive neutronic and thermal-hydraulic calculations both in steady and unsteady conditions. In both cases, preliminary studies have shown the use of advanced Computational Fluid Dynamics (CFD) calculations to be of significant benefit.

Hence, it is important to create a solid validation and verification basis for CFD codes in both steady and transient conditions as these analyses are the basis for ensuring the safety and performance of reactors under normal and abnormal conditions. As this is a requirement that goes far beyond the conversion of the FRM II, the Reactor Physics Group at the FRM II, HFIR at ORNL and RHF at ILL, together with the

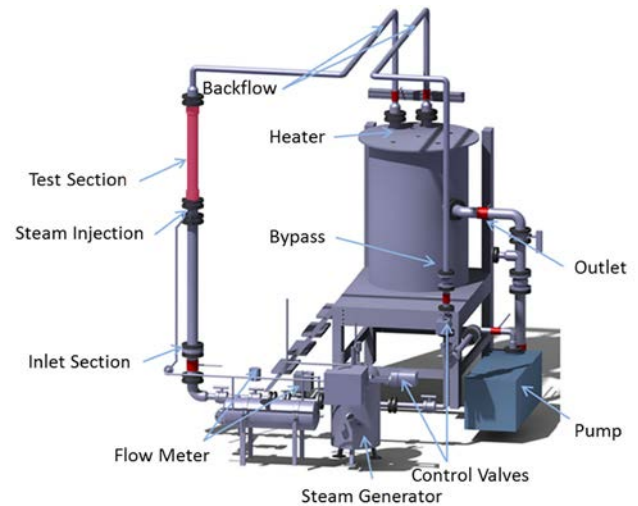


Fig. 1: Current setup of the loop. The test section (red) will be exchangeable so that various geometries can be tested under different conditions.

Argonne National Laboratory (ANL), have joined forces to form the Involute Working Group (IWG) and help each other in this endeavor.

Recently, the IWG has been able to gather experimental data covering the operating conditions of high-performance research reactors and build high-fidelity CFD simulations of these experiments. While being useful, these experiments are often narrow in scope (e.g. geometry, operating conditions) and lack critical input data (e.g. measurement uncertainty). These shortcomings are compounded by the fact that, often, conversion analysis leads to changes from current design (channel dimensions) which further narrows the range of applicability of these experiments. It is therefore critical for the high-performance research reactors to gather additional experimental data, which should be acquired using state of the art technology and suited for CFD validation. For transient analyses, the need is particularly acute as there is currently no experimental facility available that satisfies the needs of high-performance research reactors.

God of Thunder: The new experiment for validation TUM.THOR

Hence, TUM, together with input from the IWG, is upgrading its existing test loop at the Chair of Nuclear Technology to suit high-performance research reactor conditions and designs. This new experiment is called “TUM Thermal Hy-

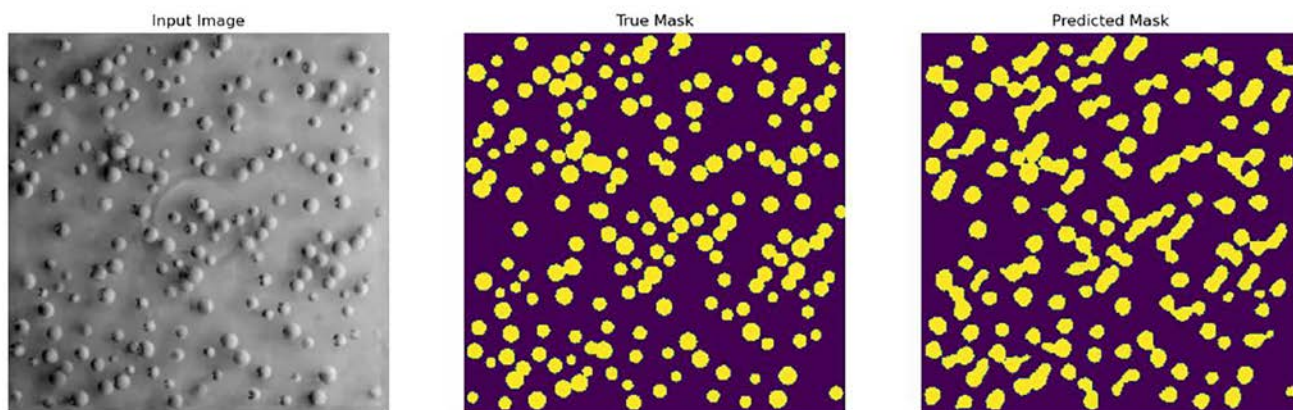


Fig. 2: Workflow of the self-developed neural network

draulic Loop for Research Reactors” (TUM.THOR). Figure 1 depicts the status of the loop, whereas the test section is highlighted in red. Without losing the actual capabilities of steam injection, the loop will be up-graded for pressures up to 20 bar and mass flows between 4 and 5 kg/s. The test section will be designed such that it can be easily exchanged and replaced by other geometries. In total, a max. heating power of 300 kW for the test section will be installed in order to reach heat fluxes covering the challenging conditions of high-power research reactors. A novel “heat pixel” technology will be installed that provides the necessary heating as well as the capability to model different heating profiles. These pixels are planned to have an area of ca. 4 cm² and a heating power of 2 kW each. With a new and state of the art control system, the heat pixels will also be capable of modelling a time dependent heat source to simulate e.g. the decay heat of a reactor. A newly installed heat exchanger will allow for different inlet temperatures.

Several bypass tubes and discharge valves will allow the study of various accident scenarios such as Loss of Coolant Accident (LOCA) or Loss of Flow Accident (LOFA). State of the art metrology and data acquisition methods will be installed, in close cooperation with the TUM engineering department and the IWG partners, to monitor the coolant mass flows in the test section as well as in the bypasses.

In parallel to the experiments conducted with TUM.THOR, high-fidelity numerical models of the loop will be created. In addition to CAD models needed for the construction of the experiment, it is also planned to generate CFD as well as a RELAP5 model of the experimental setup.

With TUM.THOR will come the unique possibility to simulate the challenging conditions of high-power research reactors. With several flow bypasses, transient scenarios like LOCA and LOFA can be studied in combination with the heat pixels for simulating decay heat scenarios. With modern measure-

ment techniques, TUM.THOR will be the perfect tool to generate urgently needed experimental data to validate modern CFD codes for either steady-state or transient cases.

Neural Networks in Reactor Physics

Today, CFD programs used for the calculation of transients do not sufficiently capture boiling at low pressures. For this purpose, TUM has already set up and commissioned a small experiment, TUM Loop for Obtaining Knowledge In nucleate boiling (TUM.LOKI), which can be used to study the vapor bubble content and its detachment from the wall. In contrast to TUM.THOR, TUM.LOKI is specifically designed for the investigation of boiling processes at low pressures and allows optical data evaluation, e.g. by means of a high-speed camera and self-developed neural networks.

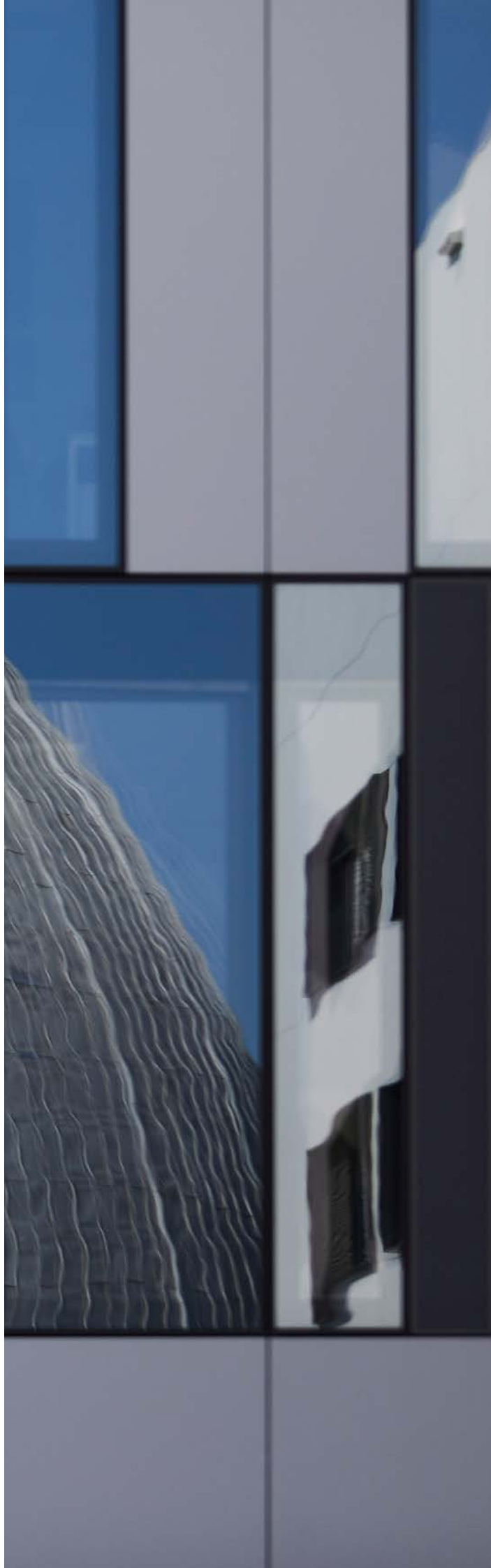
To simplify the analysis of high-speed images from TUM LOKI, a neural network was built that can segment these images and distinguish between bubbles and background. Since the images vary little or not at all between frames, a method was developed to train the neural network using computer simulated data. This method can be refined by e.g. adjusting the lighting conditions as well as the shading by an evolutionary genetic algorithm of the computer itself, thus achieving greater similarity to the original images.

Acknowledgement

This work was supported by a combined grant (FRM2023) from the Federal Ministry of Education and Research (BMBF) and the Bavarian State Ministry of Science and the Arts (StMWK).



Facts & Figures



The year in pictures



January 1st

Prof. Dr. Martin Müller is installed as the new director at the Heinz Maier-Leibnitz Zentrum (MLZ), succeeding Prof. Dr. Stephan Förster in the role. A materials physicist, he now represents the Helmholtz partners Forschungszentrum Jülich and Helmholtz-Zentrum hereon on the Scientific Directorate of the MLZ. By rotation, Martin Müller will also be the spokesman of the Directorate for a period of two years.

January 1st

Dr. Thomas Keller from the Max Planck Institute for Solid State Research in Stuttgart and instrument scientist at the spin echo spectrometer TRISP is newly elected as a member of the German Committee for Research using neutrons (KFN). His leading objectives are developing new instruments and inspiring young scientists to work with neutrons.



March 3rd

Can electrons waltz? On the occasion of the public talk “Wissenschaft für Jedermann” streamed via Deutsches Museum on YouTube, Dr. Johanna Jochum says: “As an Austrian, there is no doubt in my mind: Cooper pairs dance Viennese waltzes.”



March 8th

Inaugural visit of Prof. Dr. Mirijam Zobel, Director of the Institute of Crystallography at the RWTH Aachen university, with MLZ and FRM II scientific director Prof. Dr. Peter Müller-Buschbaum.

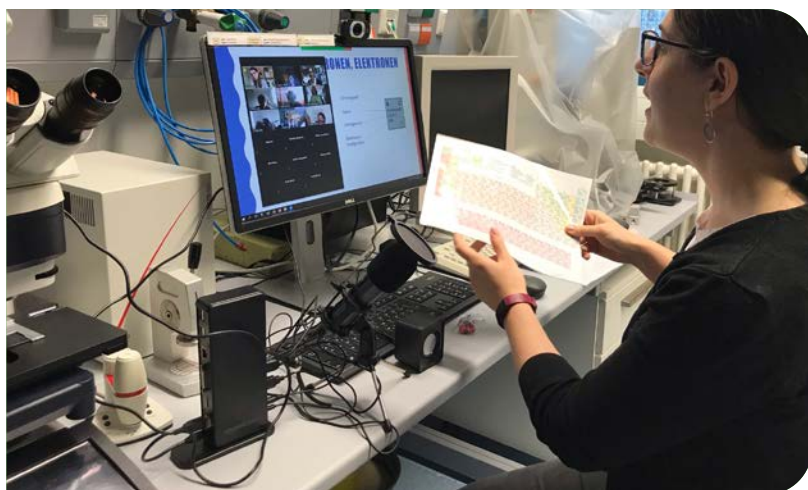
**March 10th**

The president of the Technical University of Munich (TUM), Prof. Dr. Thomas F. Hofmann (3rd from right) visits the directors of the FRM II, Prof. Dr. Peter Müller-Buschbaum (2nd from right), Dr. Axel Pichlmaier (3rd from left) and Robert Rieck (2nd from left) with TUM-chancellor Albert Berger (m.), science manager Dr. Maralena Weil and spokesperson for the president Ulrich Meyer (r.).

March 19th

He knew the Atomic Egg when it was still in its early stages and showed great commitment to the FRM II research neutron source: Dr. Hans Boysen (r.) died at the age of 76. The picture shows him in 2018 at a celebratory colloquium in conversation with colleagues of his Chair of Crystallography at Ludwig-Maximilians-University of Munich, Prof. Dr. Sohyun Park (l.) and Prof. Dr. Friedrich Frey.





April 22nd

Liquid nitrogen, escape game and a surprise via mail: The virtual girls' day at the MLZ enables 15 girls scattered all over Germany to participate and have fun despite only a virtual presence due to the Corona pandemic.

July 28th

Welcome to new assistant, post-Doc and engineer: The three directors (middle in front row from left) Dr. Axel Pichlmaier, Prof. Dr. Peter Müller-Buschbaum and Robert Rieck take 14 new employees aboard on a dedicated day for the newbies.

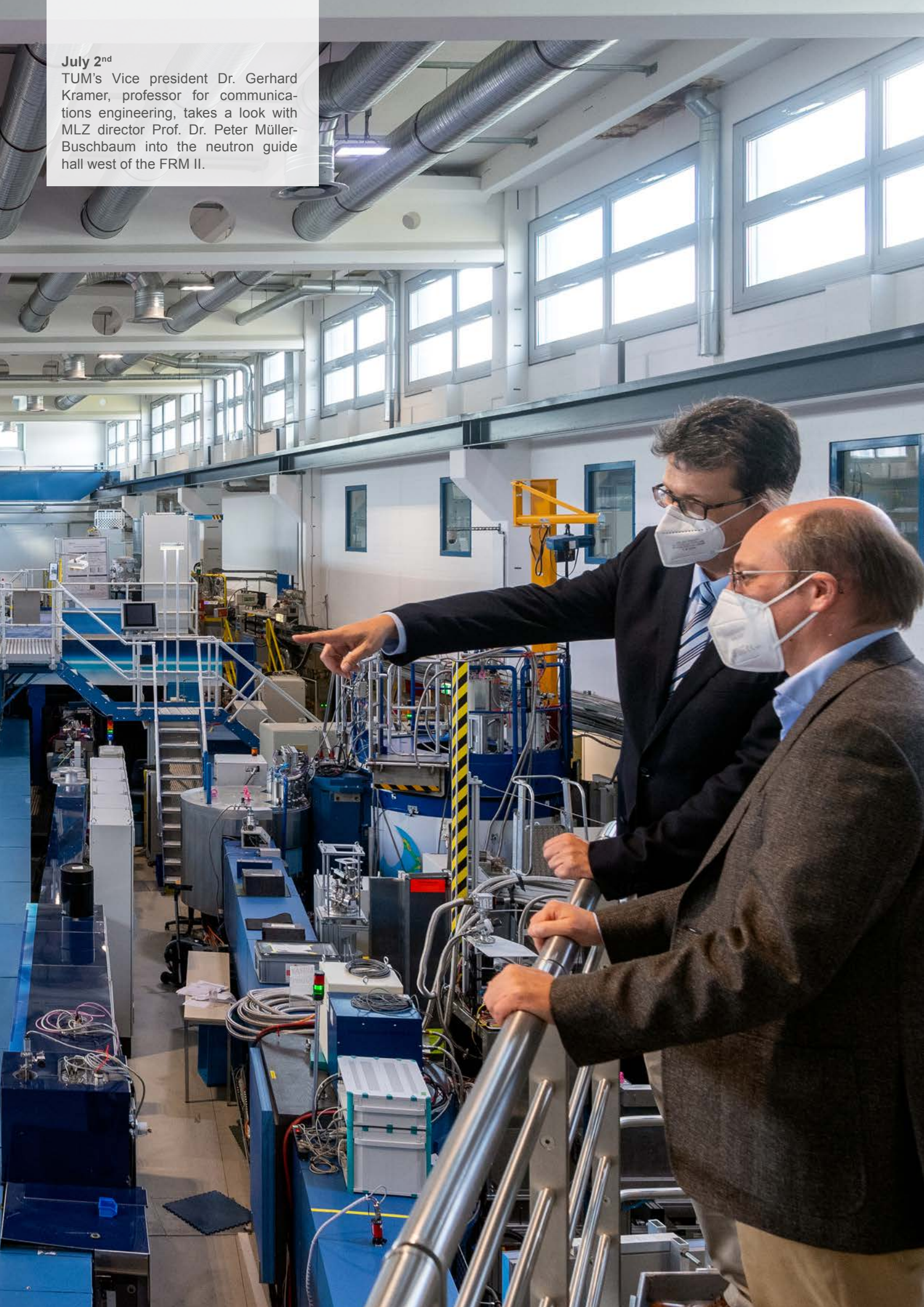


August 3rd

Exploring the neutron source in reality. Thanks to an easing in the corona restrictions, this becomes a possibility for eight female explorers from all over Bavaria. As one of 17 projects at the Technical University of Munich, the course "Flight, Materials, Radiation" brought the girls to the FRM II.

July 2nd

TUM's Vice president Dr. Gerhard Kramer, professor for communications engineering, takes a look with MLZ director Prof. Dr. Peter Müller-Buschbaum into the neutron guide hall west of the FRM II.





September 24th

Five scientific instruments designed, built and commissioned at the neutron source in Garching: Prof. Dr. Peter Böni, Technical University of Munich, receives the MLZ's prize for instrumentation and scientific use from Prof. Dr. Peter Müller-Buschbaum.

September 6th

The new Ministerialrat Dr. Albert Schmid (2nd from left), in charge of the Technical University of Munich at the Bavarian Ministry for Science and the Arts, tours the neutron source with FRM II scientific director Prof. Peter Müller-Buschbaum (2nd from right), administrative director Robert Rieck (l.) and technical director Dr. Axel Pichlmaier.



September 27th

A visit from the neighbors: The investors of the new adjacent Galileo building housing a hotel and lecture halls as well as gastronomy, Doris and Jürgen (3rd from left) Hesz, get a tour of the FRM II with the president of the Technical University of Munich, Prof. Dr. Thomas F. Hofmann (r.), and the three directors of the FRM II (from the left) Prof. Dr. Peter Müller-Buschbaum, Robert Rieck and Dr. Axel Pichlmaier.

October 3rd

Ice cream crowns the end of each children's tour of the neutron source. The day of the mouse from the popular German TV show for children is now almost a tradition at the FRM II and was of course fully booked well in advance. 70 children and 139 adults enjoy the guided tours, talks and stands at the open day with the mouse.





November 24th

He has an IQ of 145, holds a degree in physics and is only twelve years old. During his internship at the adjacent Laser Lab, Laurent Simons from Belgium tours the Heinz Maier-Leibnitz neutron source and is fascinated.

November 25th

Job fair going digital: The traditional booth at the Munich University of Applied Sciences for recruiting staff members and students for these and projects is held in a digital format with online interviews and films about the MLZ.



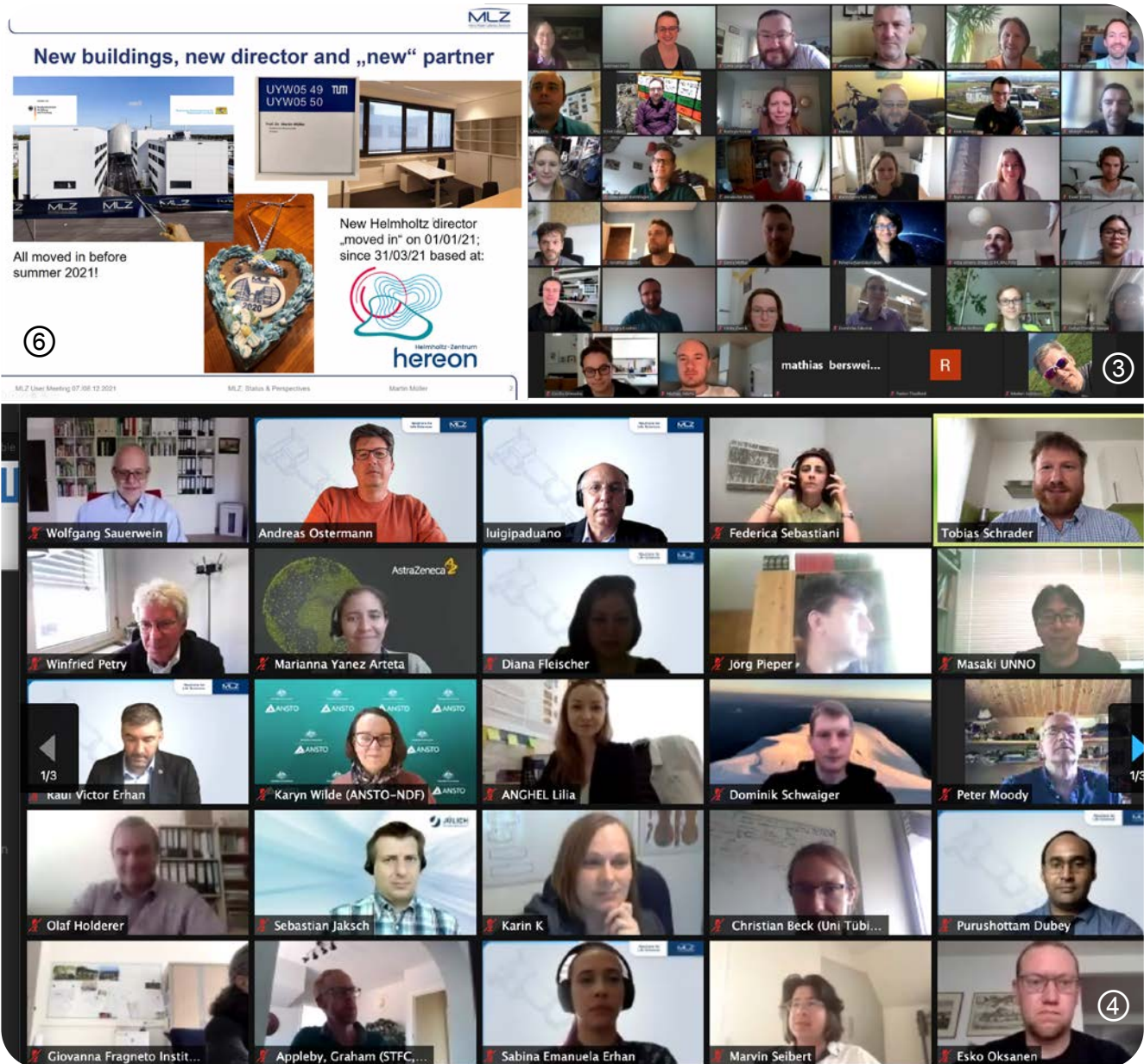
December 15th

For more than 19 years, Wenzel Schürmann (l.) photographed the eventful history of the FRM II and the MLZ in many thousands of pictures. An exhibition shows a best-of in the new building of the research neutron source. Here, he celebrates the inauguration with the three directors of the FRM II (from left): Prof. Dr. Peter Müller-Buschbaum, Dr. Axel Pichlmaier and Robert Rieck.



Workshops, Conferences and Schools

①	18 January - 20 December	Seminar: Neutrons in Research and Industry, Garching: online	TUM / MLZ
②	27 January - 3 February	F-Praktikum, Hands-on training for TUM physics students, Garching	TUM / MLZ
③	30 May - 3 June	Workshop "725 th WE-Heraeus-Seminar: Magnetic Small Angle Neutron Scattering – from Nanoscale Magnetism to Long-Range Magnetic Structures", Evangelische Akademie Tutzing as well as online/hybrid	TUM / MLZ Wilhelm und Else Heraeus Stiftung
④	6 - 11 June	MLZ Conference 2021: Neutrons for Life Sciences, Garching: online	TUM / MLZ
⑤	7 - 11 June	F-Praktikum, Hands-on training for TUM physics students, Garching: online	TUM / MLZ
⑥	7 - 8 December	MLZ User Meeting 2021, Garching: online	MLZ



Science in place of crisis

A. Voit, A. Görg, T. Kiechle

Heinz Maier-Leibnitz Zentrum (MLZ), Technical University of Munich, Garching, Germany

The press team increased its output once more in 2021, managing to generate more science-based media contributions than ever thanks to 21 press releases. Several virtual and real events for the public were held despite the pandemic. We enhanced our activities on social media platforms and opened new accounts on Instagram, YouTube and LinkedIn and offer a service of graphic design for scientists.

479 media articles appeared on the Research Neutron Source (FRM II) and the Heinz Maier-Leibnitz Zentrum (MLZ) in 2021 in print and online media, as well as on TV and radio. This is a continuous increase compared to previous years. We attained a new record of 426 contributions in 2019, with the outlier being the previous record year 2020 (882 contributions), which had 400 contributions on the C-14 incident alone. This confirms the sustained media interest we have been observing for many years. This time, the number of 208 scientific media contributions is gratifying, being the highest in the past ten years of communication at the FRM II and the MLZ (see Fig. 1).

Record number of press releases

This year, we succeeded in reaching almost as high a number of media articles on science topics, events and people as on reactor-related topics. This is mainly due to the highest output ever of press releases. We have increased the number to date to 21 press releases.

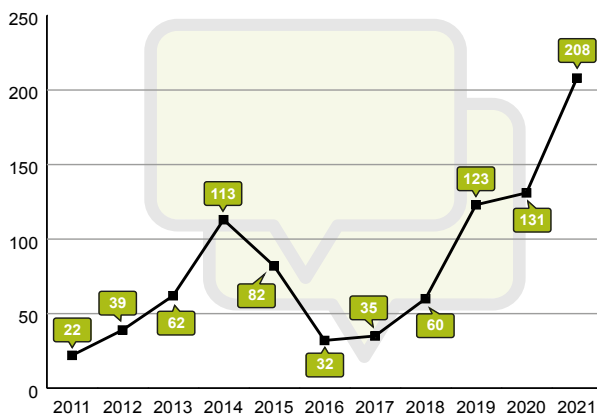


Fig. 1: The number of media articles on scientific topics has increased continuously over the past ten years. In 2021, it reached a record high.

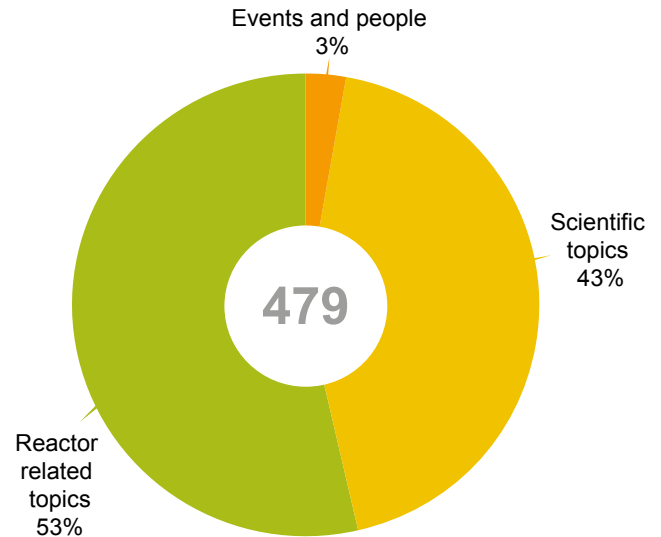


Fig. 2: Science topics accounted for 43 percent of all articles about the MLZ and FRM II in 2021. Neutron source topics include the C-14 incident upgraded to an INES 1 event and FRM II fuel conversion.

Social media booming

In 2021, we significantly developed the social media presence of the FRM II and the MLZ. In addition to Facebook and Twitter, we now have an Instagram account, a YouTube channel and a LinkedIn company page. On our Facebook page www.facebook.com/frmII we had 210 subscribers (in 2020: 178) and 159 posts (in 2020: 110).

The MLZ's English-language Twitter account @mlz_garching performed very successfully in 2021. With 379 followers, we were once again able to greatly increase our Twitter community in 2021 – in comparison: There were 236 followers in 2020. With 246 tweets, including 213 of our own and 33 retweets, we more than tripled the content on Twitter compared to last year (2020: 68 tweets).

New on Instagram, YouTube and LinkedIn

We have now also been present on our channel [instagram.com/frm_ii/](https://www.instagram.com/frm_ii/) since the end of the year. Overall, the platform is characterized by a higher user growth than Facebook and has many followers, especially among the younger generation. In 2021, we were able to gain 131 subscribers on Instagram from a standing start, with 53 post contributions. We also posted 112 story posts.

FRM II's own YouTube channel opens up many new possibilities. With 35 subscribers and two uploaded videos at about 200 views each the channel, which launched in 2021, is still in its infancy. However, more science and explanatory videos



Fig. 3: Film students shoot videos of scientists for YouTube.

as well as an image film are in the pipeline and we are looking forward to an increase in the number of subscribers as well as video clicks.

Another new platform on which the Research Neutron Source has been presenting itself since the end of 2021 is LinkedIn (www.linkedin.com/company/frm-ii/). There, current, but also potential future employees will be addressed – with news

from operations, science and research, as well as relevant job postings. After a good two months, 84 people were already following us on LinkedIn.

Since 2020, we have also been offering graphic design for scientific papers (see a selection of covers on page 102) and greatly encourage our researchers to take advantage of this service. For many news and press releases as well as for our websites and printed products, the graphics boost the visibility of our texts.

807 visitors

Numerous events took place in virtual form, such as the lecture on the “Dance of Electrons” in the series “Wissenschaft für Jedermann” at the Deutsches Museum, the Girls’Day at the MLZ and the “Café und Kosmos” lecture on pallasites.

In summer and early autumn, the Corona restrictions became less stringent and so the visit of the TUM discoverers as well as the MLZ’s own open day in particular and the parallel mouse door opener day in October were able to take place in person. In total, there were as many as 807 visitors at the neutron source, mainly professional people and students.



facebook.com/FRMII



instagram.com/frm_ii



twitter.com/mlz_garching



linkedin.com/company/frm-ii



FRM II -
Forschungs-Neutronenquelle

Another virtual year at the User Office

F. Erdem¹, I. Lommatzsch², R. Schurek²

¹Heinz Maier-Leibnitz Zentrum (MLZ), Technical University of Munich, Garching, Germany; ²Jülich Centre for Neutron Science (JCNS-4) at MLZ, Forschungszentrum Jülich GmbH, Garching, Germany

The second year of the pandemic became a year devoid of any users for the User Office. Thus, no hotel bookings, no travel cost reimbursement processes, no desperate calls from the middle of nowhere (if a user had confused “Garching bei München” with “Garching an der Alz”...), no invitation letters for those who need a visa – and worst of all, no users just dropping in for a quick chat!

Instead, we stayed virtual. In order to keep in touch with users and those who would like to join their ranks, we featured the MLZ at a virtual booth at the 84th Annual Meeting of the DPG and the DPG Meeting of the Condensed Matter Section (SKM). This was a really nice experience: It was possible to create a cool booth where GhOST welcomed the visitors and where links to movies, brochures and web pages could be provided anywhere. For the visitors, it was not only possible to chat with us via a kind of messenger, but also to connect via video. It was also great to see many familiar faces there and get some news from them! We were happy to deliver updates from Garching in this convenient format.



Fig. 1: The MLZ booth at the IUCr – located next to the famous Hradshchin at Prague.

We had another virtual booth at the 25th Conference of the International Union of Crystallographers – but because this was held in a hybrid format, we only backed up the colleagues who went to Prague and represented the MLZ at a booth on-site at the conference center. Several MLZ scientists (mainly from our Science Group “Structure Research”) took turns at the booth and met real (!) people.

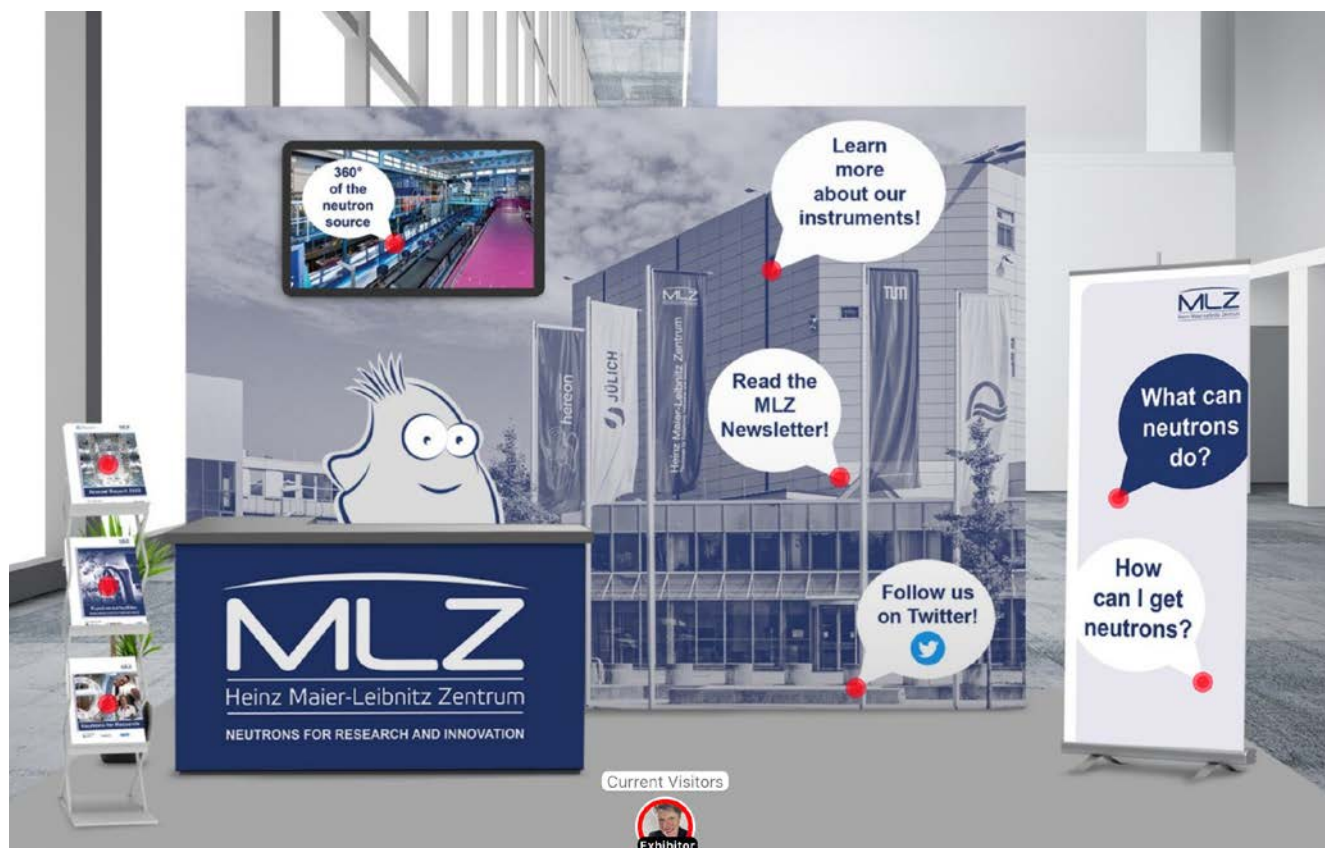


Fig. 2: The virtual MLZ booth at the DPG meeting. The red dots mark the clickable links. Most popular: Our interactive plan of the halls with links to all instruments. During the five days, 156 visitors participated in the chat and we had a video call with an additional 36.

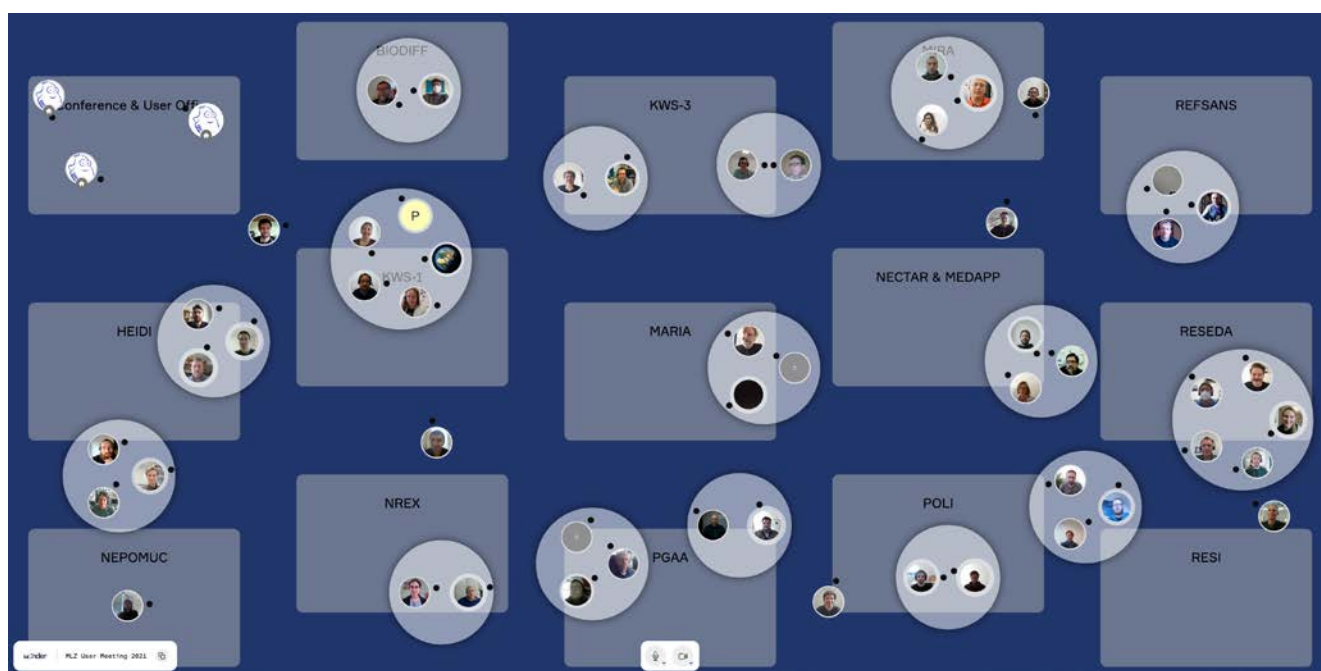
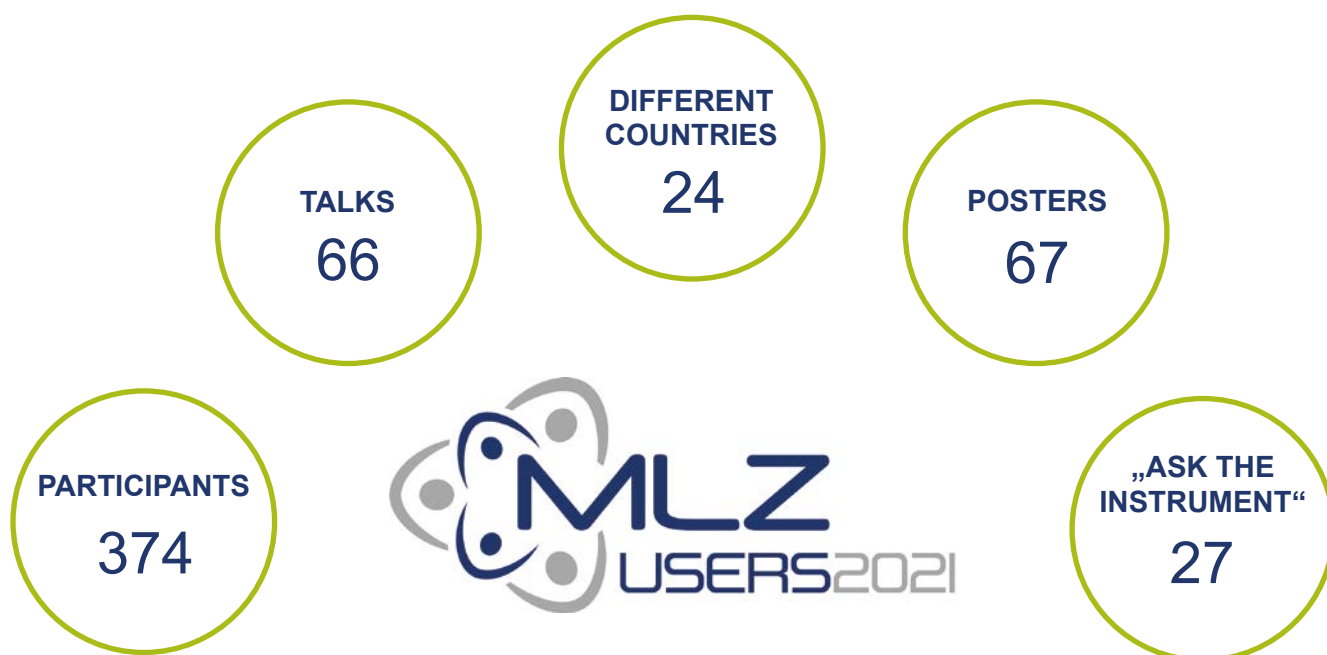


Fig. 3: For this year's User Meeting, we created the new format "Ask the instrument". In dedicated areas of a Wonder-space, the instrument teams were available for questions and discussions regarding future experiments. It was fun to see people mingle!

The year ended with another online User Meeting. The decision to cancel the usual in-person-meeting and opt for a virtual meeting had already been made in the early stages of planning. This turned out to be a good decision: The rules became far more stringent just before the User Meeting!

374 participants from 24 different countries registered for this event and enjoyed two packed days. On the first day, seven parallel workshops of the MLZ Science Groups made it hard to decide which session to visit. Day 2, dedicated to plenary talks, started with detailed information on status and

perspectives at the MLZ by its director and spokesman, Martin Müller. Stimulating plenary talks were delivered by Walter Richtering (on microgels) and Joao Cabral (on PA membranes) before new services at the MLZ were introduced.

In order to offer a measure of variety between more passive (like listening to talks) and active participation, talks alternated with poster sessions and the new format "Ask the instrument" on both days. This was well received and the interaction was great. But nevertheless, all participants hope for a real meeting next year!

Organization

FRM II and MLZ

The Forschungs-Neutronenquelle Heinz Maier-Leibnitz (FRM II) provides neutrons for research, industry and medicine and is operated as a Corporate Research Center by the Technical University of Munich (TUM). Scientific use of the FRM II, with around 1000 user visits per year, is organized within the Heinz Maier-Leibnitz Zentrum (MLZ).

The chart below shows the overall network comprising the Neutron Source FRM II and the MLZ, as well as the funding bodies and the scientific users that perform experiments at the MLZ, addressing the major challenges facing present-day society.

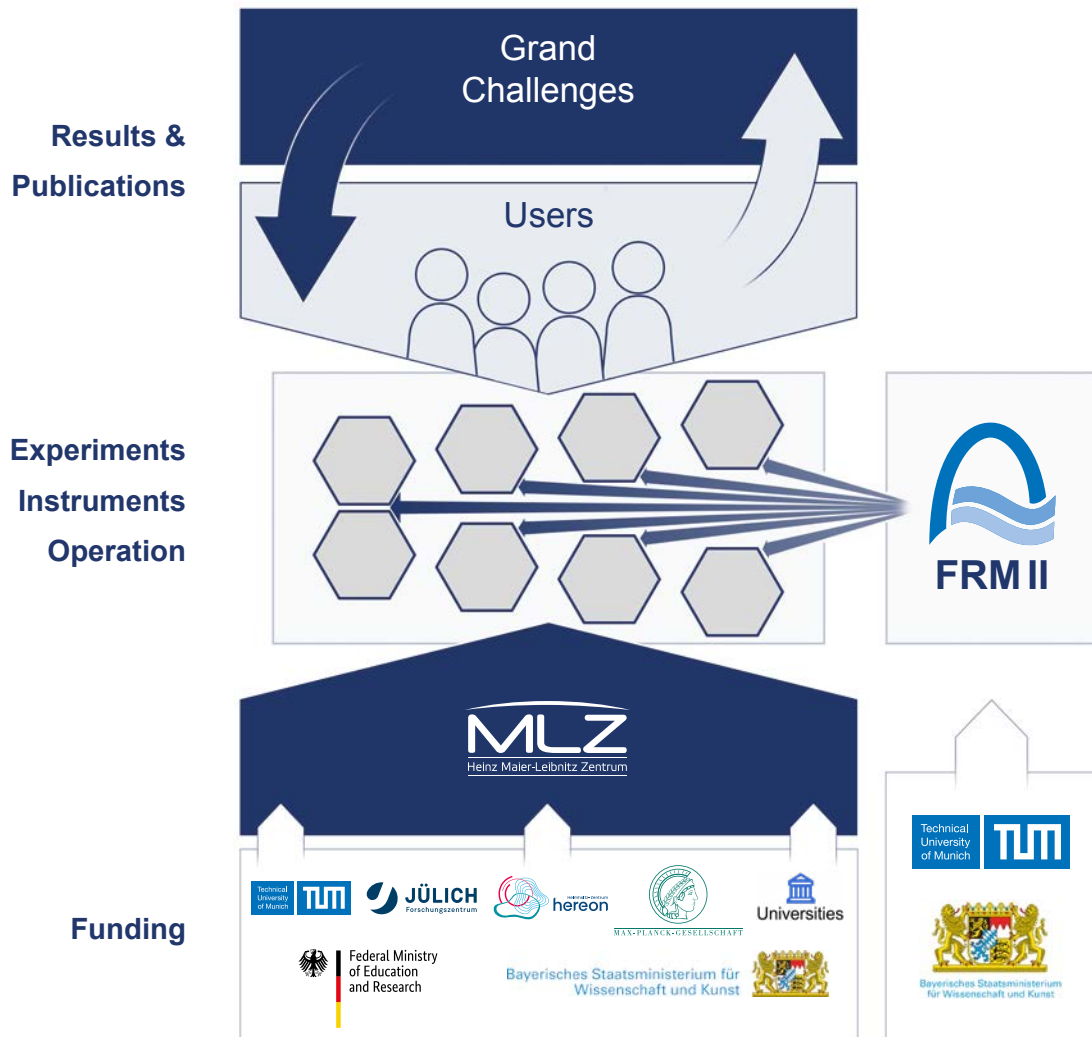


Fig. 1: The neutron source FRM II and the user facility MLZ.

Scientific Director MLZ, HGF

Prof. Dr. Martin Müller

Technical Director FRM II

Dr. Axel Pichlmaier

Scientific Director MLZ, FRM II

Prof. Dr. Peter Müller-Buschbaum

Administrative Director FRM II

Robert Rieck

Scientific Cooperation at the Heinz Maier-Leibnitz Zentrum (MLZ)

The Heinz Maier-Leibnitz Zentrum with its cooperating partners, the Technical University of Munich (TUM), Forschungszentrum Jülich GmbH (FZJ) and Helmholtz-Zentrum hereon GmbH is rooted in a network of strong partners including the Max Planck Society (MPG) and numerous university groups that benefit from scientific use of the Forschungs-Neutronenquelle Heinz Maier-Leibnitz. The organizational chart of the MLZ is shown below.

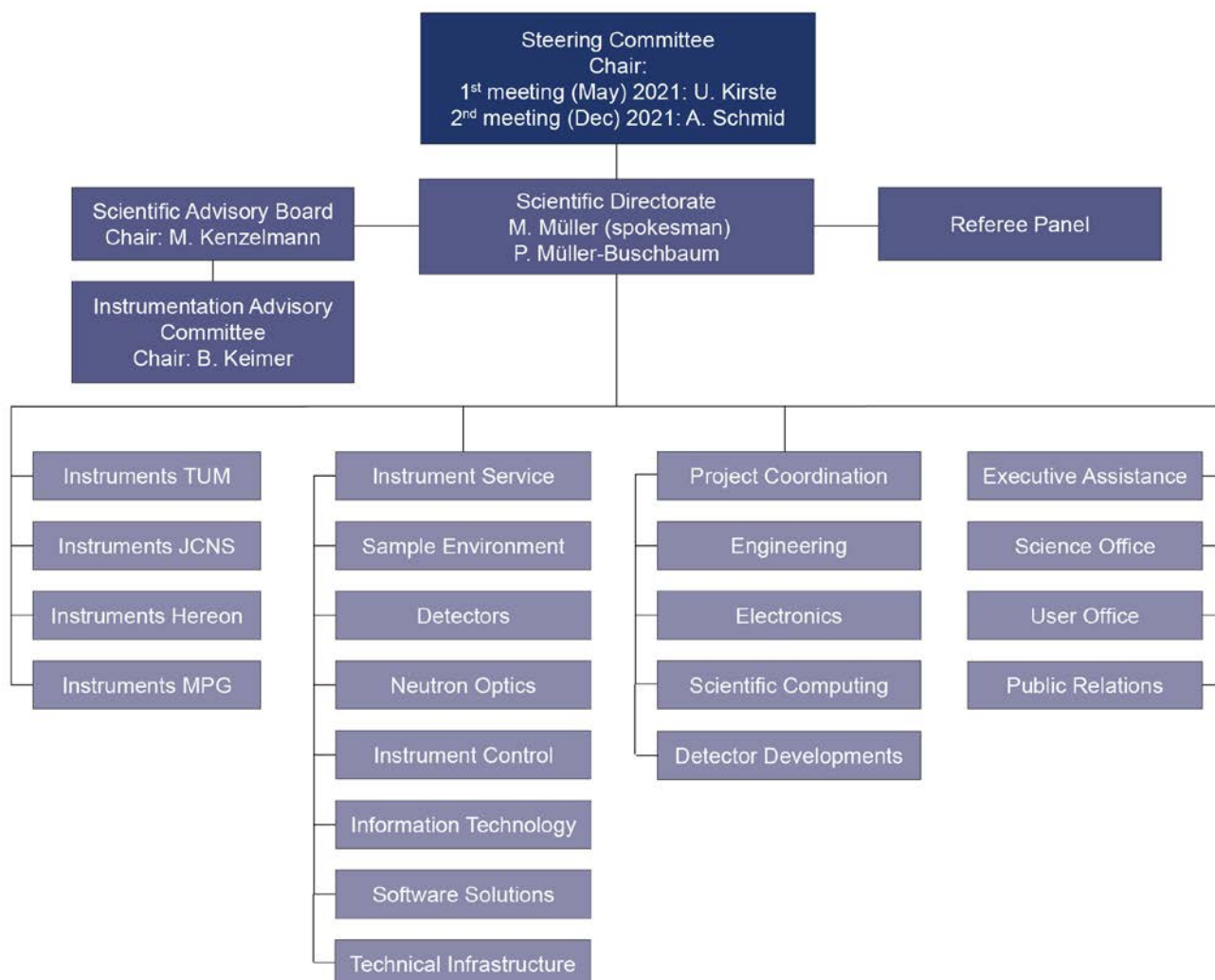
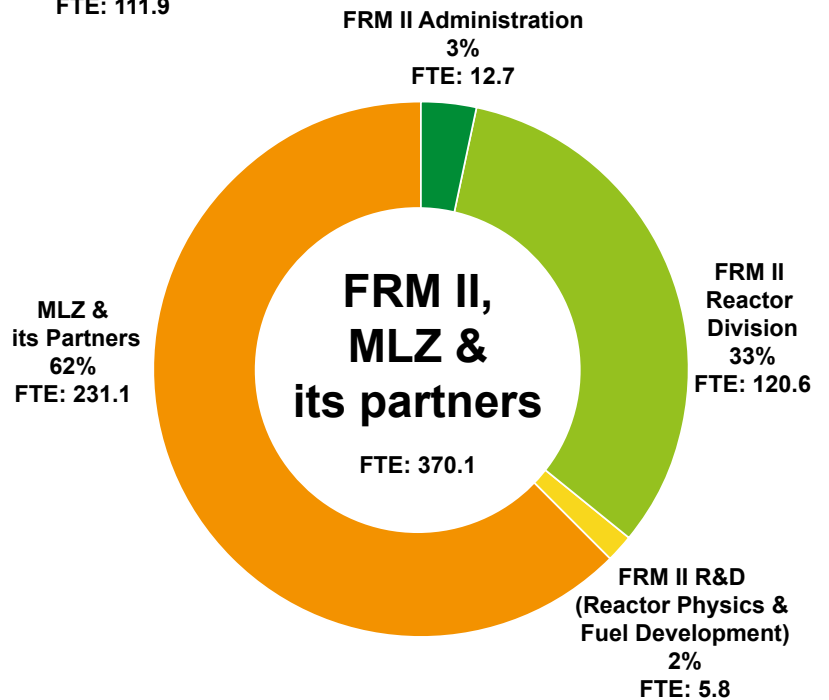
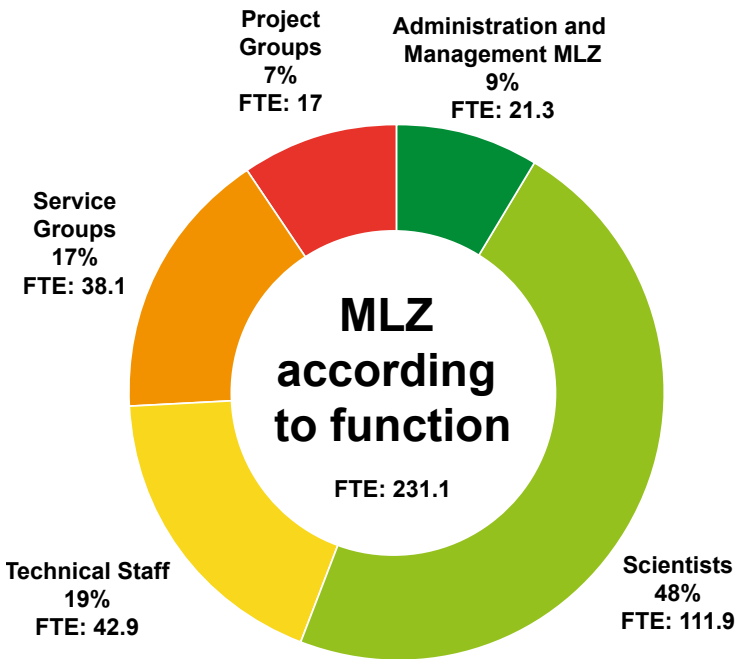
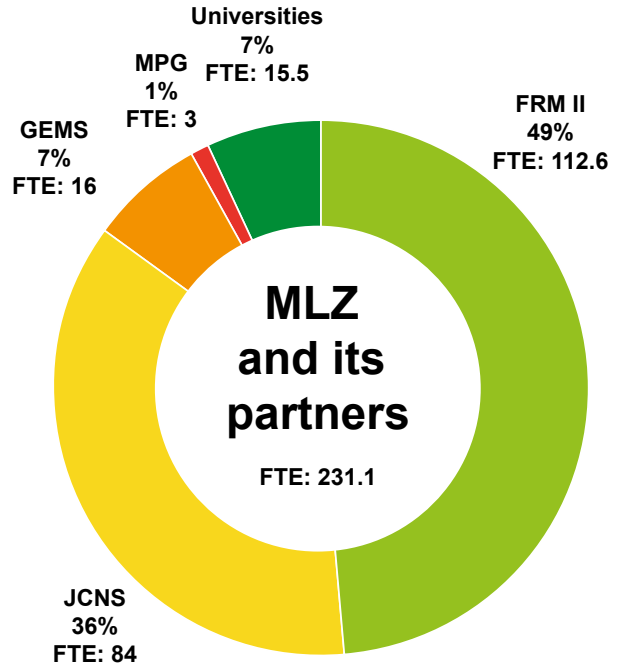


Fig. 2: Organizational chart MLZ.

Staff

The charts below show the staff of MLZ and FRM II. The staff of MLZ, as per their share among the partners with a detailed break-down of their function within the MLZ is also depicted.



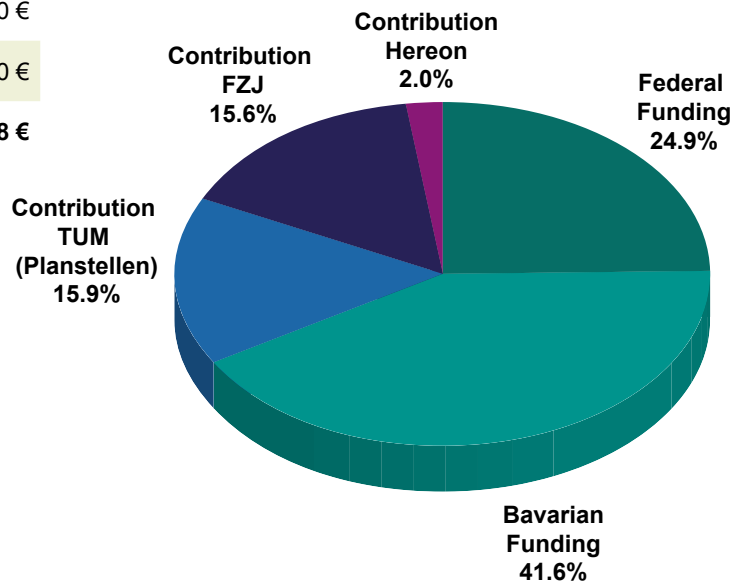
FTE = Full Time Equivalent

Budget

The tables and charts below show the revenue and expenses for 2021.

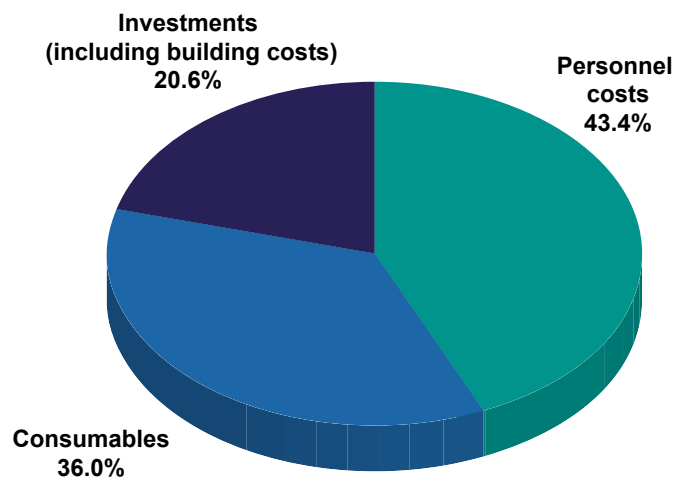
Revenue 2021

Federal Funding	16.700.000 €
Bavarian Funding	27.968.170 €
Contribution TUM (Planstellen)	10.683.368 €
Contribution FZJ	10.493.000 €
Contribution Hereon	1.320.000 €
Total	67.164.538 €



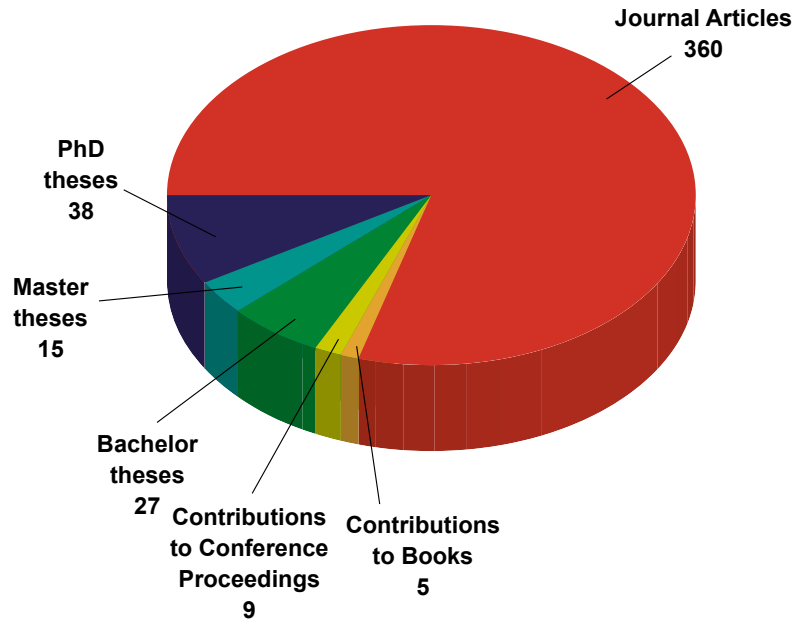
Expenses 2021

	TUM	FZJ	Hereon	Total
Personnel costs	19.094.100 €	9.520.000 €	1.423.000 €	30.037.100 €
Consumables	22.151.962 €	2.480.000 €	294.000 €	24.925.962 €
Investment (including building costs)	7.694.688 €	6.373.000 €	232.000 €	14.299.688 €
Total	48.940.750 €	18.373.000 €	1.949.000 €	69.262.750 €



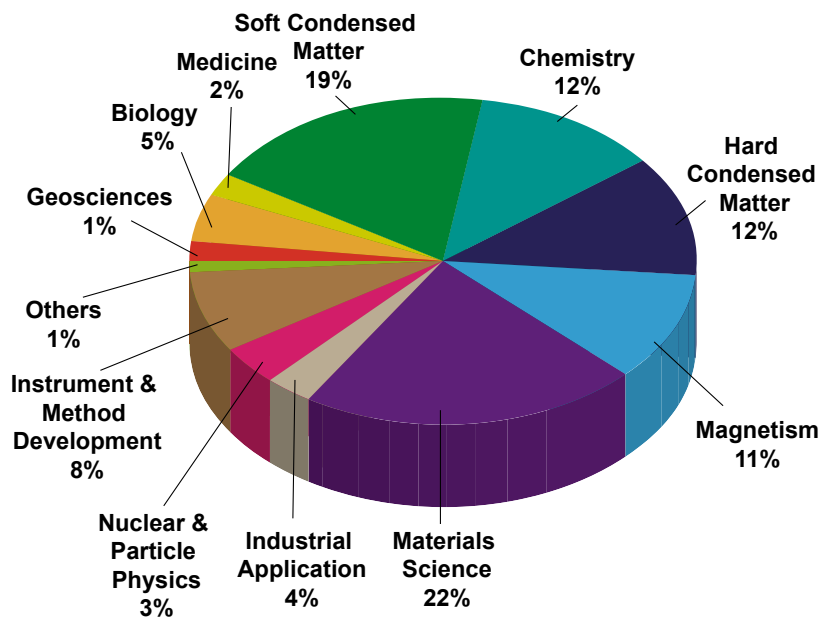
Publications & Theses

In 2021, we received notice of a total of 374 scientific publications, including journal articles, contributions to books and conference proceedings (<https://impulse.mlz-garching.de/> and figure below). Furthermore, in total 80 theses supervised by staff of the MLZ and its partner institutions were completed in 2021.

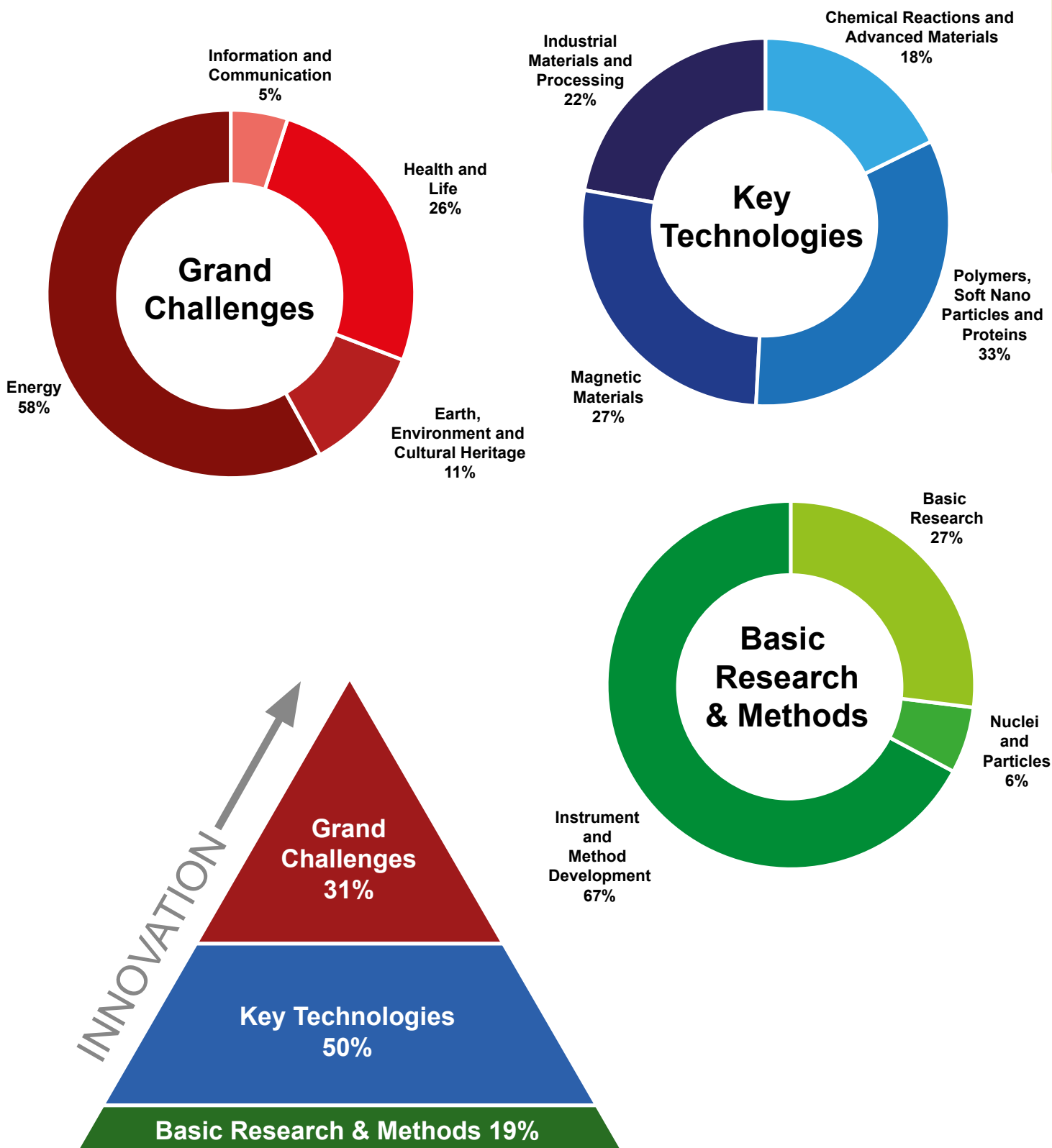


In 2021, 199 PhD theses, based on experiments at the MLZ or method and instrument developments for the MLZ, were either ongoing or completed. Of these, 143 are under the direct supervision of staff at the MLZ and its collaboration partners while the others involve external users. In total, 51 of the 199 PhD theses have been completed in 2021, including external users. Of all the doctoral students, around 86% come from German universities, 12% from other universities in Europe and 2% from the rest of the world.

The next figure shows the classification of the journal articles by Scientific Area (several tags per journal article are possible):

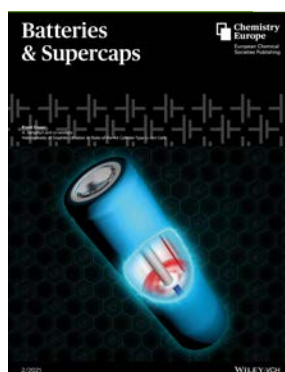


The journal articles at the MLZ can be pictured as a pyramid: Basic Research & Methods (19%) required to tackle the Key Technologies (50%) and articles that address directly the Grand Challenges of our society today (31%). The circular charts represent the individual subjects being dealt with within these three categories.

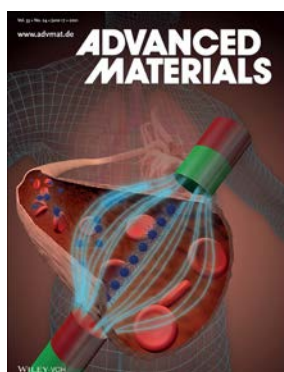


Cover pages

Research by MLZ scientists and at the FRM II made it to the cover pages of several journals in 2021 (see selection below).



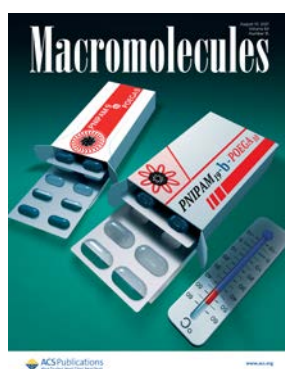
D. Petz, M. J. Mühlbauer, A. Schökel, K. Achterhold, F. Pfeiffer, T. Pirling, M. Hofmann, A. Senyshyn: Heterogeneity of Graphite Lithiation in State-of-the-Art Cylinder-Type Li-Ion Cells. *Batteries & Supercaps* 4 (2), 327-335 (2021)



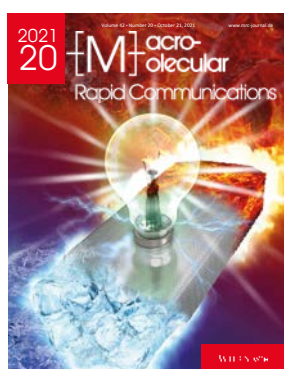
N. Nandakumar, L. Barnsley, A. Feoktystov, S. A. Ivanov, D. L. Huber, L. S. Fruhner, V. Leffler, S. Ehler, E. Kentzinger, A. Qdemat, T. Bhatnagar-Schöffmann, U. Rücker, M. T. Wharmby, A. Cervellino, R. E. Dunin-Borkowski, T. Brückel, M. Feygenson: Unravelling Magnetic Nanochain Formation in Dispersion for In Vivo Applications. *Adv. Mater.* 33, 2008683 (2021)



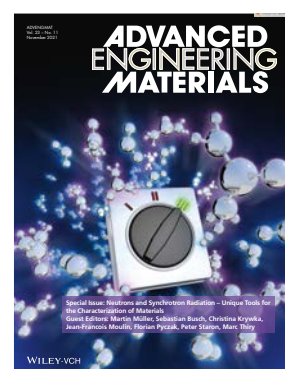
S. Yin, W. Cao, Q. Ji, Y. Cheng, L. Song, N. Li, C. L. Weindl, M. Schwartzkopf, S. V. Roth, P. Müller-Buschbaum: Multidimensional morphology control for PS-b-P₄VP templated mesoporous iron (III) oxide thin films. *Adv. Mater. Interf.* 8, 2100141 (2021)



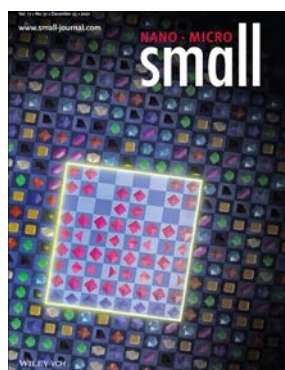
A. Vagias, A. Papagiannopoulos, L. P. Kreuzer, D. Giaouzi, S. Busch, S. Pispas, P. Müller-Buschbaum: Effects of polymer block length asymmetry and temperature on the nanoscale morphology of thermoresponsive double hydrophilic block copolymers in aqueous solutions. *Macromolecules* 54, 7298-7313 (2021)



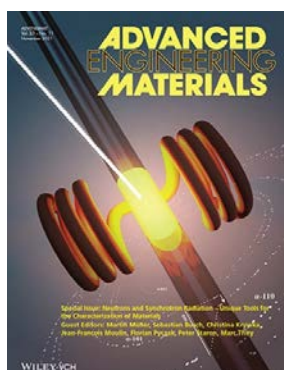
A. L. Oechle, J. E. Heger, N. Li, S. Yin, S. Bernstorff, P. Müller-Buschbaum: Correlation of thermoelectric performance, domain morphology and doping level in PEDOT:PSS thin films post-treated with ionic liquids. *Macromol. Rapid Com.* 42, 2100397 (2021)



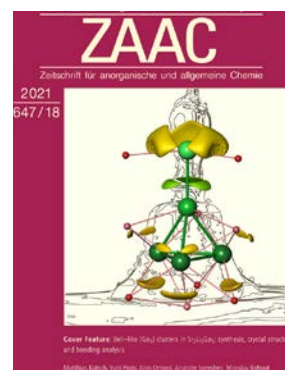
C. Geiger, J. Reitenbach, C. Henschel, L. P. Kreuzer, T. Widmann, P. Wang, G. Mangiapia, J.-F. Moulin, C. M. Papadakis, A. Laschewsky, P. Müller-Buschbaum: Ternary nanoswitches realized with multiresponsive PMMA-b-PNIPMAM films in mixed water/acetone vapor atmospheres. *Adv. Eng. Mater.* 23, 2100191 (2021)



L. Cao, O. Petravic, X.-K. Wei, H. Zhang, T. Duchoň, F. Gunkel, A. Koutsoubas, K. Zhernenkov, K. Z. Rushchanskii, H. Hartmann, M. Wilhelm, Z. Li, Y. Xie, S. He, M. L. Weber, K. Veltruská, A. Stellhorn, J. Mayer, S. Zhou, T. Brückel: Migration Kinetics of Surface Ions in Oxygen-Deficient Perovskite During Topotactic Transitions. *Small* 17 (51), 2104356 (2021)



X. H. Li, M. Hofmann, M. Landesberger, M. Reiberg, Y. D. Huang, L. J. Wang, E. Werner, W. M. Gan, X. Zhang: A Unique Quenching and Deformation Dilatometer for Combined In Situ Neutron Diffraction Analysis of Engineering Materials. *Adv. Eng. Mater.* 23, 2100163 (2021)



M. Kotsch, Y. Prots, A. Ormezi, A. Senyshyn, M. Kohout, Y. Grin: Bell-like [Ga₃] clusters in Sr₃Li₅Ga₃; synthesis, crystal structure and bonding analysis. *Z. Anorg. Allg. Chem.* 647, 1797-1803 (2021)

Committees

Steering Committee

Chair

1st meeting (May) 2021:

Dr. Ulrike Kirste

Bavarian State Ministry of Science and the Arts

2nd meeting (Dec) 2021:

Dr. Albert Schmid

Bavarian State Ministry of Science and the Arts

Members

Albert Berger

Technical University of Munich

Prof. Dr. sc. techn. Gerhard Kramer

Technical University of Munich

Dr. Jürgen Kroseberg

Federal Ministry for Education and Research

1st meeting (May) 2021:

Prof. Dr.-Ing. Harald Bolt

Forschungszentrum Jülich GmbH

2nd meeting (Dec) 2021:

Prof. Dr. Astrid Lambrecht

Forschungszentrum Jülich GmbH

Prof. Dr. Matthias Rehahn

Helmholtz-Zentrum hereon GmbH

Guests

Prof. Dr. Martin Müller

Helmholtz-Zentrum hereon GmbH

Prof. Dr. Peter Müller-Buschbaum

FRM II, Technical University of Munich

Prof. Dr. Stephan Förster

Forschungszentrum Jülich GmbH

Dr. Axel Pichlmaier

FRM II, Technical University of Munich

Robert Rieck

FRM II, Technical University of Munich

Dirk Schlotmann

Forschungszentrum Jülich GmbH



Fig. 1: Virtual Steering Committee meeting in December 2021 with A. Schmid, A. Pichlmaier, P. Müller-Buschbaum, A. Berger, M. Müller, A. Lambrecht, D. Schlotmann, G. Kramer, J. Kroseberg, M. Rehahn, and R. Rieck (from left to right and top to bottom)

Scientific Advisory Board

Chair

Prof. Dr. Michel Kenzelmann
Paul Scherrer Institute, Villigen

Prof. Dr. Thomas Hellweg
Bielefeld University

Members

Prof. Dr. Lise Arleth
University of Copenhagen

Prof. Dr. Bernhard Keimer
Max Planck Institute for Solid State Research, Stuttgart

Alejandro Javier Guirao Blank
Volkswagen AG, Wolfsburg

Prof. Dr. Rainer Niewa
University of Stuttgart

Dr. Werner Daum
Bundesanstalt für Materialforschung
und -prüfung (BAM), Berlin

Prof. Dr. Julian Oberdisse
Université de Montpellier

Prof. Dr. Martin Fertl
Johannes Gutenberg University, Mainz

Dr. Victoria Garcia Sakai
ISIS Neutron and Muon Source, Didcot

Prof. Dr. Helmut Schober
Institut Laue Langevin, Grenoble

Prof. Dr. Regine v. Klitzing
Technical University of Darmstadt



Fig. 2: Virtual meeting of the Scientific Advisory Board in April 2021 with M. Kenzelmann, J. Oberdisse, A. Guirao Blank, R. Niewa, H. Schober, R. v. Klitzing, W. Daum, V. Garcia Sakai, B. Keimer, T. Hellweg, M. Fertl, and L. Arleth (from left to right and top to bottom)



Fig. 3: Virtual Instrumentation Advisory Committee meeting in March 2021 with B. Keimer, M. Fernández-Díaz, U. Köster, E. Lehmann, F. Ott, C. Pappas, H. Rønnow, and M. Russina (from left to right and top to bottom)

Instrumentation Advisory Committee

Chair

Prof. Dr. Bernhard Keimer
Max Planck Institute for Solid State Research, Stuttgart

Members

Dr. Maria Teresa Fernández-Díaz
Institut Laue-Langevin, Grenoble

Dr. Ulli Köster
Institut Laue-Langevin, Grenoble

Dr. Eberhard Lehmann
Paul Scherrer Institute, Villigen

Dr. Frédéric Ott
Laboratoire Léon Brillouin, Saclay

Prof. Dr. Catherine Pappas
Delft University of Technology

Prof. Dr. Henrik Rønnow
Ecole Polytechnique Fédérale de Lausanne

Dr. Margarita Russina
Helmholtz-Zentrum Berlin für
Materialien und Energie

MLZ User Committee

Chair

Prof. Dr. Tommy Nylander
Lund University

Members

Dr. Andrea Scotti
RWTH Aachen University

Dr. Jens Gibmeier
Karlsruhe Institute of Technology

Dr. Ana Brás Würschig
University of Cologne

Dr. Sandra Cabeza
Institut Laue-Langevin, Grenoble

Prof. Dr. Holger Kohlmann (Observer on behalf of the KFN)
Leipzig University

Evaluation of Beam Time Proposals: Members of the Review Panels

Dr. Markus Appel
Institut Laue-Langevin, Grenoble

Prof. Dr. Lise Arleth
Niels Bohr Institute
University of Copenhagen

Dr. Mikhail Avdeev
Frank Laboratory of Neutron Physics
Joint Institute for Nuclear Research, Dubna

Prof. Dr. Piero Baglioni
University of Florence

Dr. Luis Fernández Barquín
University of Cantabria, Santander

Prof. Dr. Peter Battle
University of Oxford

Dr. Matthew Blakeley
Institut Laue-Langevin, Grenoble

Dr. Johann Bouchet
Commissariat à l'énergie atomique et
aux énergies alternatives, Arpajon

Dr. Philippe Bourges
Laboratoire Léon Brillouin, Saclay

Prof. Dr. William Brant
Uppsala University

Prof. Dr. Richard Campell
University of Manchester

Dr. Petr Čermák
Charles University, Prague

Dr. Robert Cubitt
Institut Laue-Langevin, Grenoble

Dr. Sabrina Disch
University of Cologne

Dr. Stephan Eijt
Delft University of Technology

Prof. Dr. Ulli Englert
RWTH Aachen University

Prof. Dr. Björn Fåk
Institut Laue-Langevin, Grenoble

Dr. Bela Farago
Institut Laue-Langevin, Grenoble

Prof. Dr. Rafael Omar Ferragut
L-NESS, Como

Dr. Anne-Caroline Genix
Laboratoire Charles Coulomb
Université Montpellier

Dr. Francesco Grazzi
National Research Council of Italy,
Florence Research Area

Dr. Christian Grünzweig
Paul Scherrer Institute, Villigen

Dr. Klaus Habicht
Helmholtz-Zentrum Berlin für
Materialien und Energie

Prof. Dr. Thomas Hellweg
Bielefeld University

Prof. Dr. Paul Henry
ISIS Neutron and Muon Source, Didcot

Dr. Ingo Hoffmann
Institut Laue-Langevin, Grenoble

Dr. Dirk Honecker
ISIS Neutron and Muon Source, Didcot

Dr. Christy Kinane
ISIS Neutron and Muon Source, Didcot

Dr. Joachim Kohlbrecher
Paul Scherrer Institute, Villigen

Dr. Reinhard Kremer
Max Planck Institute for
Solid State Research, Stuttgart

Prof. Dr. Christian Krempaszky
Technical University of Munich, Garching

Prof. Dr. Jeremy Lakey
University of Newcastle

Dr. Reidar Lund
Oslo University

Dr. Sandrine Lyonnard
Commissariat à l'énergie atomique et
aux énergies alternatives, Grenoble

Dr. Nicolas Martin
Laboratoire Léon Brillouin, Saclay

Dr. Gwilherm Nénert
PANalytical B.V., Almelo

Dr. Thomas Nitschke-Pagel
TU Braunschweig

Dr. Esko Oksanen
European Spallation Source, Lund

Prof. Dr. Andrea Orecchini
Università degli Studi di Perugia

Dr. Alessandro Paciaroni
Università degli Studi di Perugia

Prof. Dr. Christine Papadakis
Technical University of Munich, Garching

Dr. Oleg Petrenko
University of Warwick

Dr. Thilo Pirling
Institut Laue-Langevin, Grenoble

Prof. Dr. Radosław Przeniosło
University of Warsaw

Prof. Dr. Diana Lucia Quintero Castro
University of Stavanger

Dr. Navid Qureshi
Institut Laue-Langevin, Grenoble

Dr. Florin Radu
Helmholtz-Zentrum Berlin für
Materialien und Energie

Dr. Sarah Rogers
ISIS Neutron and Muon Source, Didcot

Dr. Emmanuel Schneck
Max Planck Institute of
Colloids and Interfaces, Potsdam

Prof. Dr. Roland Schwab
University of Tübingen

Dr. Romain Sibille
Paul Scherrer Institute, Villigen

Dr. Thorsten Soldner
Institut Laue-Langevin, Grenoble

Prof. Dr. Thomas Sottmann
University of Stuttgart

Dr. Andreas Stark
Helmholtz-Zentrum hereon GmbH

Dr. Johannes Sterba
Atominstytut Wien, TU Wien
Dr. Christopher Stock
University of Edinburgh

Dr. Pavel Strunz
Nuclear Physics Institute, Řez near Prague

Dr. Anne Stunault
Institut Laue-Langevin, Grenoble

Dr. László Szentmiklósi
Hungarian Academy of Sciences, Budapest

Dr. Kristiaan Temst
KU Leuven

Dr. Alexander Tsirlin
Augsburg University

Prof. Dr. Regine von Klitzing
Technical University of Darmstadt

Dr. Oksana Zaharko
Paul Scherer Institut, Villigen

Prof. Dr. Hongbin Zhang
Technical University of Darmstadt

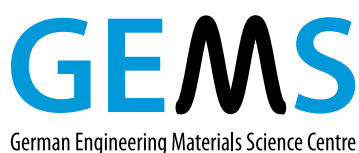
Partner institutions



Bavarian Research Institute of
Experimental Geochemistry and Geophysics
University of Bayreuth
www.bgi.uni-bayreuth.de



Georg-August-Universität Göttingen
• Geowissenschaftliches Zentrum
www.uni-goettingen.de/de/125309.html



German Engineering Materials Science Centre GEMS
Helmholtz-Zentrum hereon GmbH
www.hereon.de/central_units/gems/index.php.de



Jülich Centre for Neutron Science JCNS
Forschungszentrum Jülich GmbH
www.jcns.info



Karlsruhe Institute of Technology

- Institute for Applied Materials – Energy Storage Systems (IAM-ESS)
www.iam.kit.edu/ess/



Ludwig-Maximilians-University

- Section Crystallography
www.lmu.de/kristallographie
- Faculty of Physics
www.softmatter.physik.uni-muenchen.de



MAX-PLANCK-GESELLSCHAFT

Max Planck Institute for Solid State Research
Stuttgart

www.fkf.mpg.de



RWTH Aachen University

- Institute of Crystallography
www.xtal.rwth-aachen.de
- Institute of Inorganic Chemistry
www.iac.rwth-aachen.de/go/id/plnz/



Clausthal University of Technology

- Institute of Materials Science and Engineering
www.iww.tu-clausthal.de



Technische Universität Dresden

- Institute of Solid State and Materials Physics
www.tu-dresden.de/mn/physik/ifp



Technical University of Munich

Department of Physics

- E13 - Institute for Functional Materials
www.functmat.ph.tum.de
- E18 - Institute for Hadronic Structure and Fundamental Symmetries
www.e18.ph.tum.de
- E21 - Research area Strongly Correlated Electron Systems
www.sces.ph.tum.de

Department of Chemistry

- RCM - Radiochemie München
www.rcm.tum.de



Klinikum rechts der Isar

Technical University of Munich

- MRI - Klinikum rechts der Isar
www.mri.tum.de



Technical University of Munich

- Excellence Cluster ORIGINS
www.origins-cluster.de/



TECHNISCHE
UNIVERSITÄT
WIEN
Vienna University of Technology

Vienna University of Technology

- Neutron- and Quantum Physics
Research area at the Atominstitut Vienna
Abele Group
<https://ati.tuwien.ac.at/forschungsgruppen/nqp/home/>

der Bundeswehr
Universität München

Universität der Bundeswehr München

- Institute of Applied Physics and Measurement
Technology
www.unibw.de/Irt2

Universität zu Köln



University of Cologne

Faculty of Mathematics and
Natural Sciences

- Institute for Nuclear Physics
www.ikp.uni-koeln.de
- Institute of Physics II
www.ph2.uni-koeln.de

PHYSIKALISCHES
INSTITUT



UNIVERSITÄT
HEIDELBERG
ZUKUNFT
SEIT 1386

Universität Heidelberg

- Physikalisches Institut
www.physi.uni-heidelberg.de/

Imprint

Publisher

Technische Universität München
Forschungs-Neutronenquelle
Heinz Maier-Leibnitz (FRM II)
Lichtenbergstr. 1
85747 Garching
Germany

Phone: +49.89.289.14965
Fax: +49.89.289.14995
Internet: www.mlz-garching.de
www.frm2.tum.de
E-Mail: jahresbericht@frm2.tum.de

Editorial Office, Design and typesetting

Katharina Dietmann
Diana Fleischer
Anke Görg
Connie Hesse
Michael Hörmannsdorfer
Christoph Kreileder
Reiner Müller
Ramona Schurek
Andrea Voit

Editors

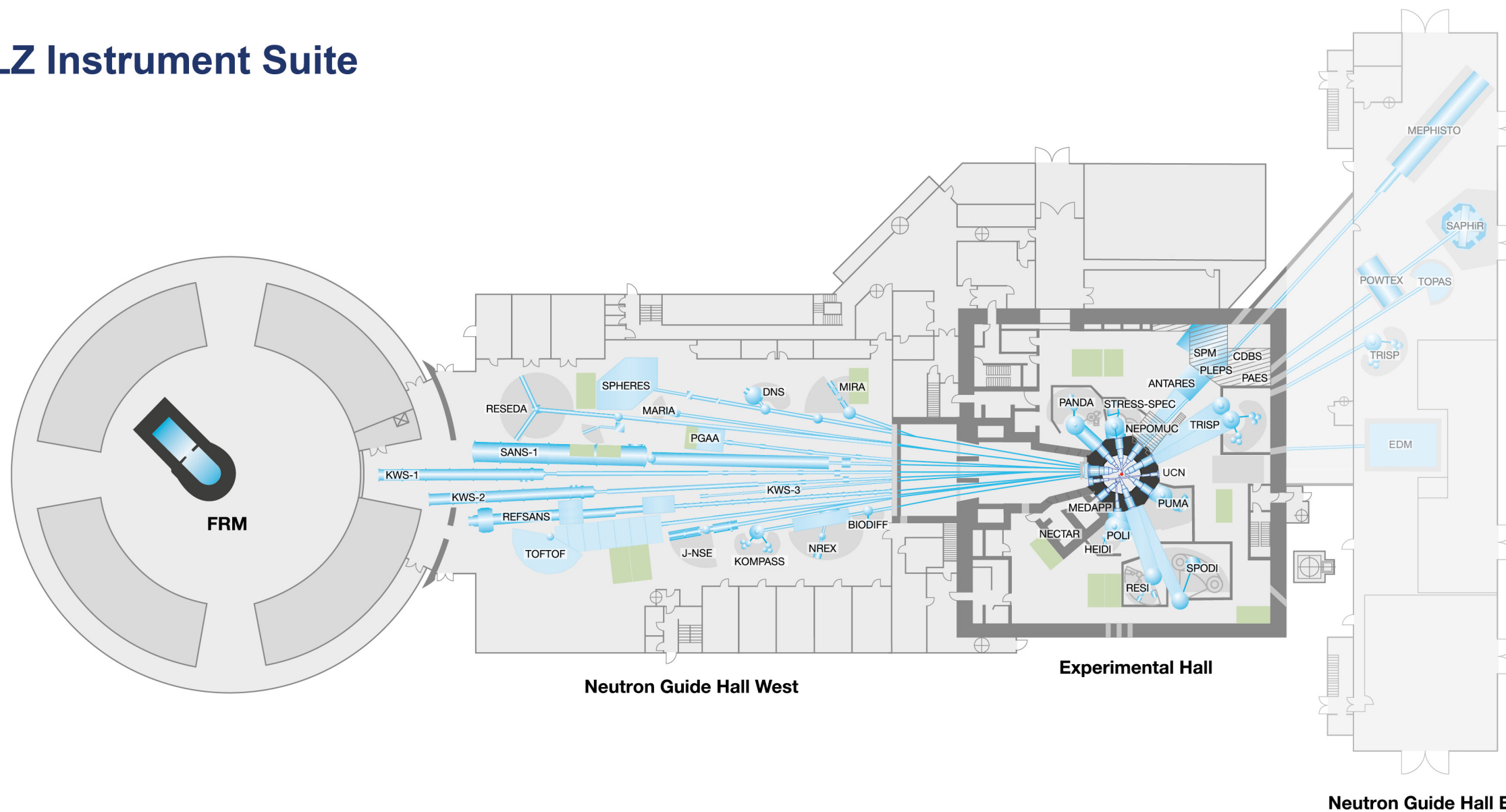
Henrich Frielinghaus
Robert Georgii
Markus Hölzel
Michael Hofmann
Olaf Holderer
Johanna Jochum
Peter Link
Martin Meven
Andreas Ostermann
Björn Pedersen
Zsolt Revay
Anatoliy Senyshyn
Christian Stieghorst
Yixi Su
Apostolos Vagias
Marcell Wolf

Photographic credits

p. 6 bottom left:
Andreas Heddergott (TUM)
bottom 2nd left:
Christian Schmid (hereon)
bottom 2nd right:
Alessandra Schellnegger
bottom right: Astrid Eckert (TUM)
Bernhard Ludewig (FRM II / TUM)
p. 8/9 Bernhard Ludewig (FRM II / TUM)
p. 12 Bernhard Ludewig (FRM II / TUM)
p. 15 Warwick Bromley
p. 17 Forschungszentrum Jülich GmbH
p. 20/21 Bernhard Ludewig (FRM II / TUM)
p. 22 Tobias Fritsch (Bundesanstalt für
Materialprüfung und Forschung)
p. 25 Markus Singer (TUM)
p. 26 Giacomo Costanzi (TUM)
p. 27 Bill Schmoker (PolarTREC 2010),
Courtesy of ARCUS
p. 29 Bernhard Ludewig (FRM II / TUM)
p. 31 Wenzel Schürmann (FRM II / TUM)
p. 32/33 Bernhard Ludewig (FRM II / TUM)
p. 37 Bernhard Ludewig (FRM II / TUM)
p. 76/77 Bernhard Ludewig (FRM II / TUM)
p. 82 /83 Bernhard Ludewig (FRM II / TUM)
p. 84 top: Christian Schmid (hereon),
middle:
Bernhard Ludewig (FRM II / TUM),
bottom: Deutsches Museum
Wenzel Schürmann
(FRM II / TUM) (3)
p. 85 Illustrations for the respective
journal covers as
quoted and pictured:
bottom left, Tomáš Duchoň,
Forschungszentrum Jülich GmbH
bottom middle: Liao Chia Lin,
liaochialin.de
bottom right: Max-Planck-Institut
für Chemische Physik fester Stoffe
(MPI CPfS)

Editors, authors or FRM II / TUM:
other images

MLZ Instrument Suite



Instrument	Description	Neutrons	Operated by	Funding	Instrument group at MLZ
ANTARES	Radiography and tomography	cold	TUM, GEMS	TUM, Hereon	FRM II, GEMS
BIODIFF	Diffractionmeter for large unit cells	cold	TUM, JCNS	TUM, FZJ	FRM II, JCNS
DNS	Diffuse scattering spectrometer	cold	JCNS	FZJ	JCNS
HEIDI	Single crystal diffractometer	hot	RWTH Aachen	FZJ	JCNS
J-NSE	Spin-echo spectrometer	cold	JCNS	FZJ	JCNS
KOMPASS	Three axes spectrometer	cold	Uni Köln, TUM	ErUM, TUM	FRM II
KWS-1	Small angle scattering	cold	JCNS	FZJ	JCNS
KWS-2	Small angle scattering	cold	JCNS	FZJ	JCNS
KWS-3	Very small angle scattering	cold	JCNS	FZJ	JCNS
MARIA	Magnetic reflectometer	cold	JCNS	FZJ	JCNS
MEPHISTO**	Instrument for particle physics, PERC	cold	TUM	TUM, DFG	FRM II
MIRA	Multipurpose instrument	cold	TUM	TUM	FRM II
MEDAPP	Medical irradiation treatment	fast	TUM	TUM	FRM II
NECTAR	Radiography and tomography	fast	TUM, GEMS	TUM, Hereon	FRM II, GEMS
NEPOMUC	Positron source, CDBS, PAES, PLEPS, SPM	-	TUM, UniBw München	TUM	FRM II
NREX	Reflectometer with X-ray option	cold	MPI Stuttgart	MPG	MPI Stuttgart
PANDA	Three axes spectrometer	cold	JCNS	FZJ	JCNS

Instrument	Description	Neutrons	Operated by	Funding	Instrument group at MLZ
PGAA	Prompt gamma activation analysis, Neutron activation analysis (NAA), Neutron depth profiling (NDP)	cold	Uni Köln	TUM	FRM II
PUMA	Three axes spectrometer	thermal	KIT	TUM	FRM II
POLI	Single-crystal diffractometer polarized neutrons	hot	RWTH Aachen	FZJ	JCNS
POWTEX*	Time-of-flight diffractometer	thermal	RWTH Aachen, Uni Göttingen, JCNS	ErUM, FZJ	JCNS
REFSANS	Reflectometer	cold	GEMS	Hereon	GEMS
RESEDA	Resonance spin-echo spectrometer	cold	TUM	TUM	FRM II
RESI/ERWIN*	Neutron diffractometer	thermal	LMU, KIT	TUM, ErUM	FRM II
SANS-1	Small angle scattering	cold	TUM, GEMS	TUM, Hereon	FRM II, GEMS
SAPHIR*	Six anvil press for radiography and diffraction	thermal	Uni Bayreuth	ErUM, TUM	FRM II
SPHERES	Backscattering spectrometer	cold	JCNS	FZJ	JCNS
SPODI	Powder diffractometer	thermal	KIT	TUM	FRM II
STRESS-SPEC	Materials science diffractometer	thermal	TUM, TU Clausthal, GEMS	TUM, Hereon	FRM II, GEMS
TOFTOF	Time-of-flight spectrometer	cold	TUM	TUM	FRM II
TOPAS*	Time-of-flight spectrometer	thermal	JCNS	FZJ	JCNS
TRISP	Three axes spin-echo spectrometer	thermal	MPI Stuttgart	MPG	MPI Stuttgart
UCN*	Ultra cold neutron source, EDM	ultra-cold	TUM	TUM, DFG	FRM II

*construction
 **reconstruction
 ErUM: instrument construction funded by ErUM-Pro (BMBF)

Front page:

How does the nanoparticle look like, that transports the mRNA as vaccine or therapeutic into the human body? Swedish researchers have studied this together with experts from the global biopharmaceutical company AstraZeneca using neutrons at the MLZ (see page 13).

Back page:

An impressionistically painted sky over the FRM and the new office buildings of the MLZ.



Heinz Maier-Leibnitz Zentrum (MLZ)

www.mlz-garching.de

DOI: 10.14459/2022md1639756